STRENGTH DEGRADATION OF GLASS FIBRE REINFORCED POLYMER SANDWICH COMPOSITES UNDER HYGROTHERMAL LOADING CONDITIONS

A
Thesis Report

submitted in partial fulfilment of the requirement for the award of degree

MASTER OF ENGINEERING
in
CAD/CAM & ROBOTICS

Submitted By
Sushma Singh
(Roll No. 800881020)

Under Guidance of

Dr. Abhijit Mukherjee
Director
Thapar University, Patiala

Dr. Rahul Chhibber
Assistant professor
Deptt. Of Mechanical Engg.
Thapar University, Patiala

DEPARTMENT OF MECHANICAL ENGINEERING
THAPAR UNIVERSITY
PATIALA-147004, INDIA

CERTIFICATE

This is to certify that the work done in this thesis report titled "**Strength Degradation of Glass Fibre Reinforced Polymer Sandwich Composites under Hygrothermal Loading Conditions**" submitted in partial fulfilment of requirement for the award of **Master of Engineering Degree in CAD/CAM/Robotics** in the Mechanical Engineering Department of Thapar University, Patiala, is an authentic record of work carried out by me under the guidance of **Dr. Abhijit Mukherjee, Director, Thapar University, Patiala and Dr. Rahul Chhibber, Assistant Professor, Mechanical Engineering Department, Thapar University, Patiala.**

The matter embodied in this report has not been submitted in part or full to any other university or institute for the award of any degree.

Dated: 15/07/10 **(Sushma Singh)**

This is to certify that above declaration made by the student concerned is correct to the best of my knowledge & belief.

Dr. Abhijit Mukherjee
Director
Thapar University, Patiala

Dr. Rahul Chhibber
Assistant Professor
Deptt. of Mechanical Engg.
Thapar University, Patiala

Dr. S.K. Mohopatra
Professor & HOD
Deptt. of Mechanical Engg.
Thapar University, Patiala

Dr. R.K. Sharma
Dean
Deptt. of Academic Affairs
Thapar University, Patiala

ACKNOWLEDGEMENT

I am highly grateful to the authorities of Thapar University, Patiala for providing this opportunity to carry out the seminar work.

I would like to express a deep sense of gratitude and thank profusely my thesis guide **Dr. Abhijit Mukherjee** & **Dr. Rahul Chhibber** for their sincere & invaluable guidance, suggestions and attitude which inspired me to submit seminar report in the present form.

I am highly thankful to **Dr. H. Bhunia**, assistant professor, Chemical Engg. Deptt. and **Mr. Gursewak Singh** (Ph.D Scholar in Chemical Engg. Deptt.) for his invaluable guidance & permission to work in his department.

I heartily thank to **Mr. Purshottam Kumar Singh** for his help in conducting the test on S.E.M. machine.

I am also thankful to other faculty members and all the workshop staff of Mechanical Department, Thapar University, Patiala for their l support.

I would also like to thank and acknowledge **BASF Construction Chemicals (India) Private Limited** for supplying us generously with MBrace E-Glass Fibre sheet, epoxy, saturant and hardener etc. for this experimentation.

My special thanks are due to my family members and friends who constantly encouraged me to complete this study.

Sushma Singh

ABSTRACT

Glass fibre-reinforced polymer (GFRP) have been used as an alternative to steel in concrete due to high strength-to-weight ratio, high stiffness-to-weight ratio, and corrosion and fatigue resistance.

The main environmental factors for the deterioration of GFRP sandwich composites are temperature, sunshine, water/moisture, alkalinity and load. Most of the early durability tests were carried out with reference to application of FRP (Fibre Reinforced Polymer) in aerospace industries.

In this thesis an experimental investigation has been carried out to study combined effect of chosen parameters moisture and temperature & also to study the rate & magnitude of damage of GFRP sandwich structure composites under hygrothermal loading conditions. For achieving this objective an experimental setup was prepared.

The sandwich structure composed of E-glass fibre, polystyrene (thermocol core) and epoxy resin were subjected to three point bending test to assess bending strength. Two thermocol cores with different thickness (8mm and 16mm) were investigated. The effect of core thickness and different bending pre-loads was assessed. It has been observed that the sandwich structure with higher core thickness withstand a higher bending load show less flexural stress and flexure modulus when compared with low core thickness. The bending pre-load also affect the degradation. Higher percent bending pre-loads lead to higher degradation in maximum flexure load as well as flexure modulus and flexure stress.

The macroscopic and microscopic behaviour of sandwich structure immersed in water has been examined. Moisture uptake was monitored for up to 50 days showing percentage weight gain curves for samples of pure epoxy and sandwich structure with different core thickness. The apparent diffusivity values extracted from the weight gain were significantly greater for initial days for higher core thickness sandwich structure. Micro hardness (Vickers's Hardness Number) is also found to be decreasing with respect to time for both pure epoxy and sandwich structures. An attempt to make relation between macroscopic and microscopic behaviour of sandwich structure has been made. Area fraction and circularity measurement of fibre using Image-J software on SEM-images have also been carried out.

TABLE OF CONTENTS

LIST OF FIGURES

LIST OF TABLES

CHAPTER 1 INTRODUCTION

1.1 COMPOSITE [2]

Composites are combination of two or more materials (reinforcing elements, fillers, and composite matrix binder), differing in form or composition on a macro scale. The constituents retain their identities, that is, they do not dissolve or merge completely into one another although they act in concert. The properties of a composite will be different from those of the constituents in isolation and set of performance characteristics is greater than that of the components taken separately.

Composite material is a material composed of two or more distinct phases (matrix phase and dispersed phase) and having bulk properties significantly different from those of any of the constituents.

- **MATRIX PHASE**

The primary phase, having a continuous character, is called matrix. Matrix is usually more ductile and less hard phase. It holds the dispersed phase and shares a load with it.

- **DISPERSED (REINFORCING) PHASE**

The second phase (or phases) is imbedded in the matrix in a discontinuous form. This secondary phase is called dispersed phase. Dispersed phase is usually stronger than the matrix, therefore it is sometimes called reinforcing phase.

1.2 CLASSIFICATION OF COMPOSITE

Composites can be broadly classified in to two groups. They are,

1.2.1 NATURAL COMPOSITES: Several natural materials can be grouped under natural composites (Fig 1.1). Example: bones, wood, shells, pearlite (steel which is a mixture of a phase and Fe_3C) etc.

Abalone shell ($CaCO_3$)

scallop shell

Fig.1.1 Natural Composite [2]

1.2.2 MAN-MADE COMPOSITES: Man-made composites (Fig 1.2) are produced by combining two or more materials in definite proportions under controlled conditions. e.g. Mud mixed straw to produce stronger mud mortar and bricks, Plywood, Chipboards, Decorative laminates, Fibre Reinforced Plastic (FRP), Carbon Composites, Concrete and RCC, Reinforced Glass etc.

Plywood

Bricks

Concrete

Fig.1.2 Man-made composites [2]

CLASSIFICATION OF MAN-MADE COMPOSITE MATERIALS [3]

1) METAL MATRIX COMPOSITES (MMC)

Metal Matrix Composite is composite material with at least two constituent parts, one being a metal.

2) CERAMIC MATRIX COMPOSITES (CMC)

Ceramic Matrix Composites are composed of a ceramic matrix and imbedded fibres of other ceramic material (dispersed phase).

3) POLYMER MATRIX COMPOSITES (PMC)

Polymer Matrix Composites are composed of a matrix from thermoset (Unsaturated Polyester (UP), Epoxy (EP)) or thermoplastic (Polycarbonate (PC), Polyvinylchloride, Nylon, Polystyrene) and embedded glass, carbon, steel or Kevlar fibres (dispersed phase).

4) PARTICULATE COMPOSITES

It consists of a matrix reinforced by a dispersed phase in form of particles.

1. Composites with random orientation of particles.
2. Composites with preferred orientation of particles. Dispersed phase of these materials consists of two-dimensional flat platelets (flakes), laid parallel to each other.

5) FIBROUS COMPOSITES

- Short fibre reinforced composites.
- Long-fibre reinforced composites.

6) LAMINATE COMPOSITES: When a fibre reinforced composite consists of several layers with different fibre orientations, it is called multilayer (angle-ply) composite.

1.3 PROPERTIES OF COMPOSITES

1. Composites possess excellent strength and stiffness
2. They are very light materials
3. They possess high resistance to corrosion, chemicals and other weathering agents.
4. They can be moulded to any shape and size with required mechanical properties in different directions.
5. High strength to weight ratio (low density high tensile strength)
6. High creep resistance
7. High tensile strength at elevated temperature
8. High toughness

1.4 COMPARISON OF COMPOSITES WITH OTHER METALS [6]

Figure 1.3 below shows the comparison of metals like steel & aluminium with composites. The reason for choosing the aluminium and steel is that they are widely used in industry. So one can figure out, composites are much lighter than other two metals in comparison by weight. Similarly in comparison of thermal expansion, the composites are low which is good for places where high temperature working is required. In case of stiffness & strength, the composites are ahead of the aluminium & steel.

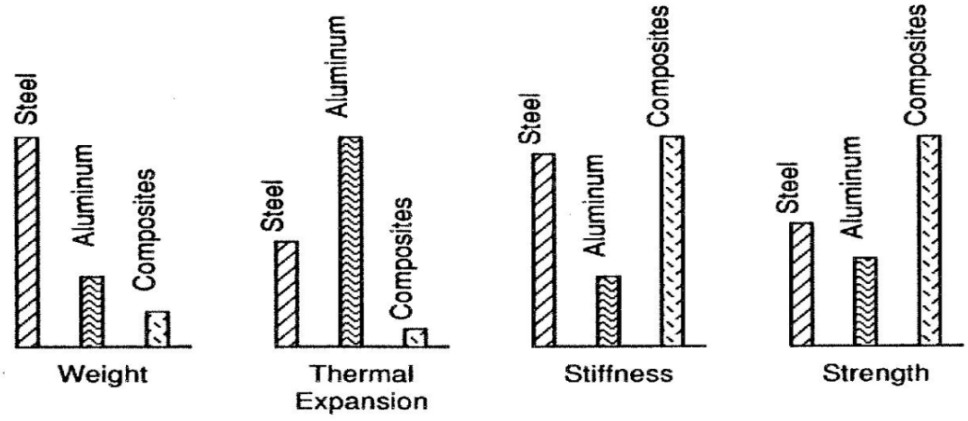

Fig.1.3 Comparison of performance of composites with other metals [6]

1.5 ADVANTAGES OF COMPOSITES [6]

1. Dimensional stability (e.g. Space based telescope)
2. Low dielectric
3. Corrosion resistance
4. Aero elastic Tailoring
5. Weight Saving

1.6 DISADVANTAGES OF COMPOSITES [6]

1. High production cost
2. Difficult to repair
3. Susceptible to damage

1.7 USES OF COMPOSITE MATERIALS [6]

1. Extensively used in space technology and production of *Aerospace components* (tails, wings, fuselages, propellers).
2. Used in the production of sport goods e.g. *racing car* bodies and *bicycle frames* etc.
3. Used for general industrial and engineering structures.
4. Used in high speed and fuel efficient transport vehicles.
5. The shell composed of CosmoLite, a thermoplastic fibre-reinforced composite and the exterior surface SpectraLite which incorporates DuPont Surlyn, an impact-resistant coating found on *golf balls.*
6. Carbon composite is a key material in today's launch vehicles and spacecraft. It is widely used in solar panel substrates, antenna reflectors and yokes of spacecraft. It is also used in payload adapters, inter-stage structures and heat shields of launch vehicles.

1.8 INTRODUCTION TO FRP [5]

A **fibre-reinforced polymer** (**FRP**) (also *fibre-reinforced plastic*) is a composite material comprising a polymer matrix reinforced with fibres. The fibres are usually fibreglass, carbon, or aramid, while the polymer is usually an epoxy, vinyl ester or polyester thermosetting plastic. FRP's are commonly used in the aerospace, automotive, marine, and construction industries.

Fig.1.4 Application of FRP to a Bridge [5]

The strength properties of FRP collectively make up one of the primary reasons for which civil engineers select them in the design of structures. A material's strength is governed by its ability to sustain a load without excessive deformation or failure. When an FRP specimen is tested in axial tension, the applied force per unit cross-sectional area (stress) is proportional

to the ratio of change in a specimen's length to its original length (strain). When the applied load is removed, FRP returns to its original shape or length. In other words, FRP responds linear-elastically to axial stress. The response of FRP to axial compression is reliant on the relative proportion in volume of fibres, the properties of the fibre and resin, and the interface bond strength. Application of FRP is shown in Fig 1.4.
FRP's response to transverse tensile stress is very much dependent on the properties of the fibre and matrix, the interaction between the fibre and matrix, and the strength of the fibre-matrix interface. Generally, however, tensile strength in this direction is very poor.

According to orientation of fibre (Fig 1.5) they can be categorized as:

1. Unidirectional
2. Bidirectional
   - Cross Ply
   - Angle Ply

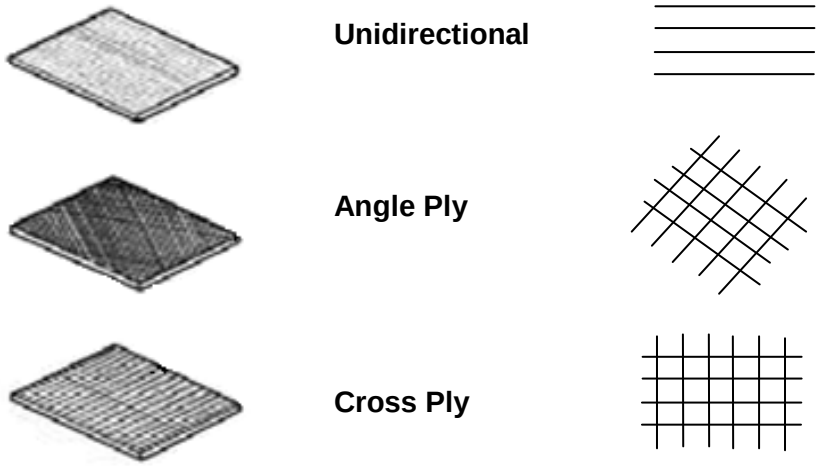

Fig.1.5 Orientation of fibre [7]

1.9 ADVANTAGES OF FRP:

1. High strength to weight ratio
2. Corrosion resistant
3. Can be tailored for the application (both shape and type of FRP)
4. FRP has a low cost considering other materials
5. Cost of installation versus replacement is low
6. Cost of installation time (both direct and indirect) is also low.

1.10 TYPES OF FIBRE [6]

A. CARBON FIBRE

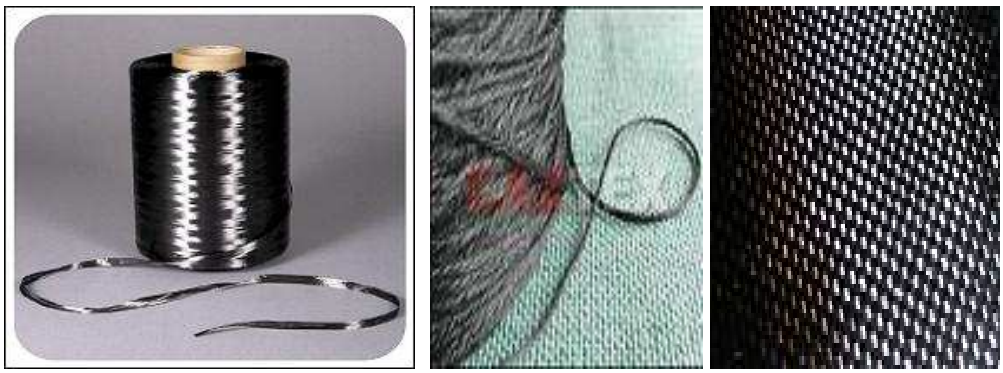

Fig.1.6 Carbon fibre [6]

Carbon fibre (Fig 1.6) is a material consisting of extremely thin fibres about 0.005–0.010 mm in diameter and composed mostly of carbon atoms. The carbon atoms are bonded together in microscopic crystals that are more or less aligned parallel to the long axis of the fibre. The crystal alignment makes the fibre very strong for its size.

Several thousand carbon fibres are twisted together to form a yarn, which may be used by itself or woven into a fabric. Carbon fibre has many different weave patterns and can be combined with a plastic resin and wound or moulded to form composite materials such as carbon fibre reinforced plastic (also referenced as carbon fibre) to provide a high strength-to-weight ratio material. The density of carbon fibre is also considerably lower than the density of steel, making it ideal for applications requiring low weight.

The properties of carbon fibre such as high tensile strength, low weight, and low thermal expansion make it very popular in aerospace, civil engineering, military, and motorsports, along with other competition sports. However, these enhanced features make it relatively expensive when compared to similar materials such as fibre glass or plastic.

B. GLASS FIBRE: Glass fibres are made of silicon oxide with addition of small amounts of other oxides. Glass fibres are characteristic for their high strength, good temperature and corrosion resistance, and low price.

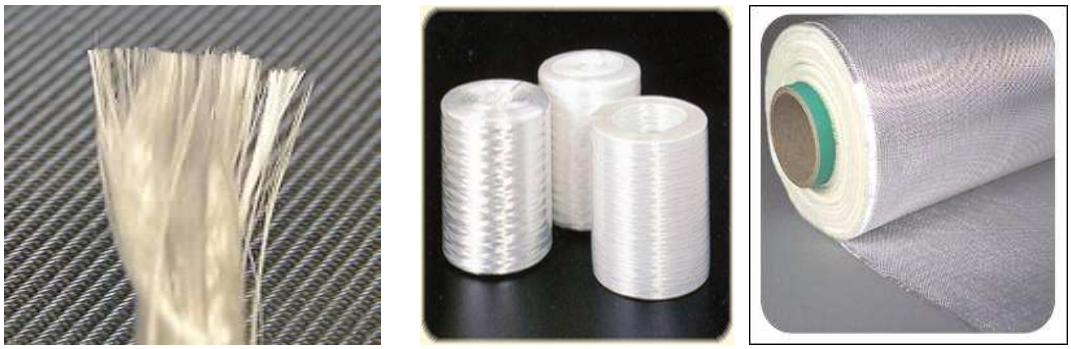

Fig.1.7 Glass fibre [8]

Glass fibre (Fig 1.7) is material made from extremely fine fibres of glass. It is used as a reinforcing agent for many polymer products; the resulting composite material, properly known as fibre-reinforced polymer (FRP) or glass-reinforced plastic (GRP).

By blending quarry products (sand, kaolin, limestone, colemanite) at 1,600 degrees C, liquid glass is formed. The liquid is passed through micro-fine bushings and simultaneously cooled to produce glass fibre filaments from 5-24um in diameter. The filaments are drawn together into a strand (closely associated) or roving (loosely associated), and coated with a "size" to provide filament cohesion and protect the glass from abrasion. By variation of the "recipe", different types of glass can be produced.

Glass Fibre Designation: Glass fibres are designated by the following internationally recognised terminology as shown in table T 1.1:

Table T 1.1: Designation of Glass Fibre [6]

Glass Type (example)	Yarn Type	Filament Diameter (μ)	Strand Weight (tex)	Single Strand Twist	No. Of Strands	Multi Strand Twit	No. of turns per metre
E	C	9	34	Z	X2	S	150
E = Electrical C = Continuous				Z = Clockwise S = Anticlockwise			

C. ARAMID (KEVLAR) FIBRE

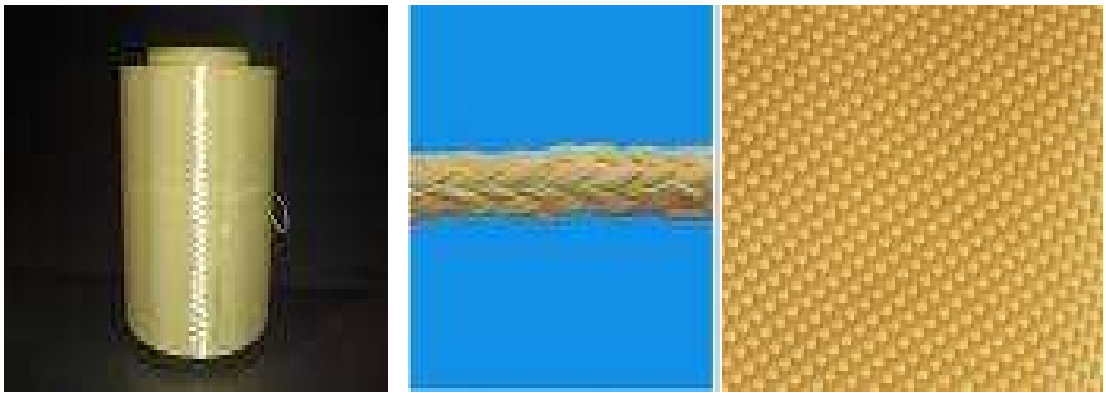

Fig.1.8 Aramid fibre [9]

Aramid fibre (Fig 1.8) is a man-made organic polymer (an aromatic polyamide) produced by spinning a solid fibre from a liquid chemical blend. The bright golden yellow filaments produced can have a range of properties, but all have high strength and low density giving very high specific strength. All grades have good resistance to impact, and lower modulus grades are used extensively in ballistic applications. Compressive strength, however, is only similar to that of E glass.

1.11 FIBRE TYPE COMPARISONS [6]

Comparing the properties of all of the fibre types with each other, shows that they all have distinct advantages and disadvantages. This makes different fibre types more suitable for some applications than others.
The following table (T 1.2) provides a basic comparison between the main desirable features of generic fibre types.
'A' indicates a feature where the fibre scores well
'C' indicates a feature where the fibre is not so good.

Table T 1.2: Comparison of different fibre [6]

Property	Aramid	Carbon	Glass
High Tensile Strength	B	A	B
High Tensile Modulus	B	A	C
High Compressive Strength	C	A	B
High Compressive Modulus	B	A	C
High Flexural Strength	C	A	B
High Flexural Modulus	B	A	C
High Impact Strength	A	C	B
High Interlaminar Shear Strength	B	A	A
High in-plane Shear Strength	B	A	A
Low density	A	B	C
High Fatigue Resistance	B	A	C
High Fire Resistance	A	C	A
High Thermal Insulation	A	C	B
High Electrical Insulation	B	C	A
Low Thermal Expansion	A	A	A
Low Cost	C	C	A

1.12 TYPES OF FIBRE REINFORCED POLYMERS:

- Carbon Fibre Reinforced Polymer (CFRP)
- Glass Fibre Reinforced Polymer (GFRP)
- Boron Fibre Reinforced Polymer (BFRP)
- Aramid Fibre Reinforced Polymer (AFRP)

Glass Fibre Reinforced Polymer (GFRP)

Glass fibre reinforced polymers sheets are being increasingly used in rehabilitation and retrofitting of concrete structures as an alternative to steel in concrete due to their high strength-to-weight ratio and corrosion and fatigue resistance. Ease of handling and application at site are added advantages.
It depends upon their properties and chemical composition. Of the different types of glass fibres, E-Glass is mostly used for reinforcement due to its high strength and electrical resistivity. Glass fibres have high strength and temperature resistance, but it is the low cost that makes GFRP the most popular.

1.13 COMMERCIALLY AVAILABLE GLASS FIBRE SPECIFICATIONS:

Table T 1.3: Detail of Commercially Available Fibre Glass Sheet (EU 900 & EU 750) [13]

MBrace G Sheet EU 900 & EU 750 – Unidirectional Glass fibre sheet		
Technical data of fibre	E-Glass, 900 gsm	E-Glass, 750 gsm
Modulus of elasticity	73 kN/mm²	73 kN/mm²
Tensile strength	3400 N/mm²	3400 N/mm²
Total weight of sheet	900 g/m² in main directions	750 g/m² in main directions
Density	2.6 g/cm³	2.6 g/cm³
ε Ultimate %	4.5	4.5
Thickness for static design weight / density	0.342 mm	0.285 mm
Safety factor for static design (manual lamination / woven product)	1.5 (recommended)	1.5 (recommended)

1.14 COMMERCIALLY AVAILABLE MATRIX RESIN SPECIFICATIONS:

MBrace Saturant resin (Table T 1.4) is the easy-to-apply. When cured with the fibre sheet, MBrace Saturant resin produces a high performance composite system for use in external structural repair or upgrade applications.

Table T 1.4: Details of commercially available MBrace Matrix Resin [13]

Aspect	Translucent blue liquid
Mixed density	1.13 ± 0.03 kg/litre
Volume solids	100 %
Mixing ratio, by weight	100 (Base): 40 (Hardener)
Mixed viscosity	3500 ± 500 cps at 25^{o}C
Coverage	
200 ~ 350 gsm fibre sheet	0.8 to 1.0 kg/m^2
350 ~ 450 gsm fibre sheet	0.9 to 1.2 kg/m^2
750 ~ 900 gsm fibre sheet	1.5 to 1.8 kg/m^2
Setting time	5 Hours at 25^{o}C
Over coating time	On setting
Full cure	7 Days
Compressive strength (ASTM C579)	> 40 MPa at 1 Day
	> 60 MPa at 7 Days
Tensile strength (BS:6319, pt 7)	> 23 MPa
Flexural strength(BS:6319, pt 3)	> 43 MPa

1.15 SANDWICH STRUCTURES OF GFRP [19]

INTRODUCTION

Sandwich structures provide an efficient method to increase bending rigidity without a significant increase in structural weight. Thin-gage face sheets (0.020″ to 0.045″) are co cured or bonded to honeycomb (aluminium or Nomex) or syntactic foam cores or polystyrene cores. These structures, based upon a minimum-gage thickness adequate to carry the in-plane loads, can carry out-of-plane loads and remain stable under compression without a significant weight penalty. The potential applications for sandwich structures are substantial. Transport aircraft components (e.g., control surfaces, engine cowlings, fairings, and fixed trailing edge wing panels), helicopter blades, optical benches for space applications, and nonferrous ship hulls are some of the current applications. In general aviation, skin/stiffener structures can be replaced with sandwich structures, where the design is based on several loading regimes including pressurization, gust, and landing loads.

SANDWICH STRUCTURED COMPOSITE

A **sandwich structured composite** is a special class of composite materials that is fabricated by attaching two thin but stiff skins to a lightweight but thick core. The core material is normally low strength material, but its higher thickness provides the sandwich composite with high bending stiffness with overall low density.

Metal composite material (MCM) (Fig 1.9) is a type of sandwich formed from two thin skins of metal bonded to a plastic core in a continuous process under controlled pressure, heat, and tension.

Fig.1.9 Metal composite material [19]

Sandwich construction (Fig 1.10) is a composite material structure combining low weight, high strength and good dynamic properties. Typically a sandwich composite consists of three main parts: two thin, stiff and strong facing layers separated by a thick, light and weaker inner core. The faces are adhesively bonded to the core to obtain a load transfer between the components. This way the properties of each separate component is utilized to the structural advantage of the whole assembly leading to a very high stiffness-to-weight and high bending strength-to-weight ratio. As a result sandwich components achieve the same structural performance as conventional materials with less weight.

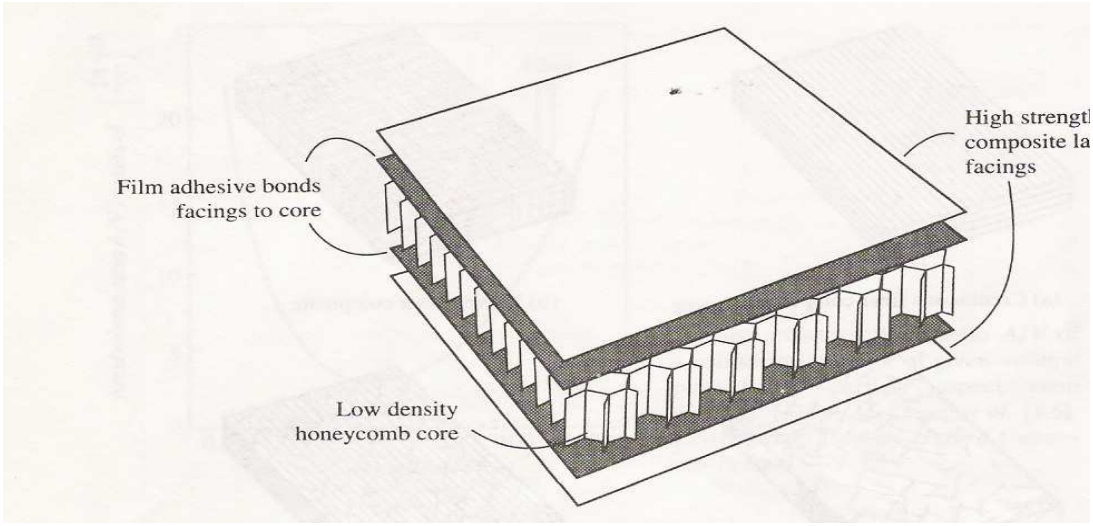

Fig.1.10 Honeycomb sandwich composite [10]

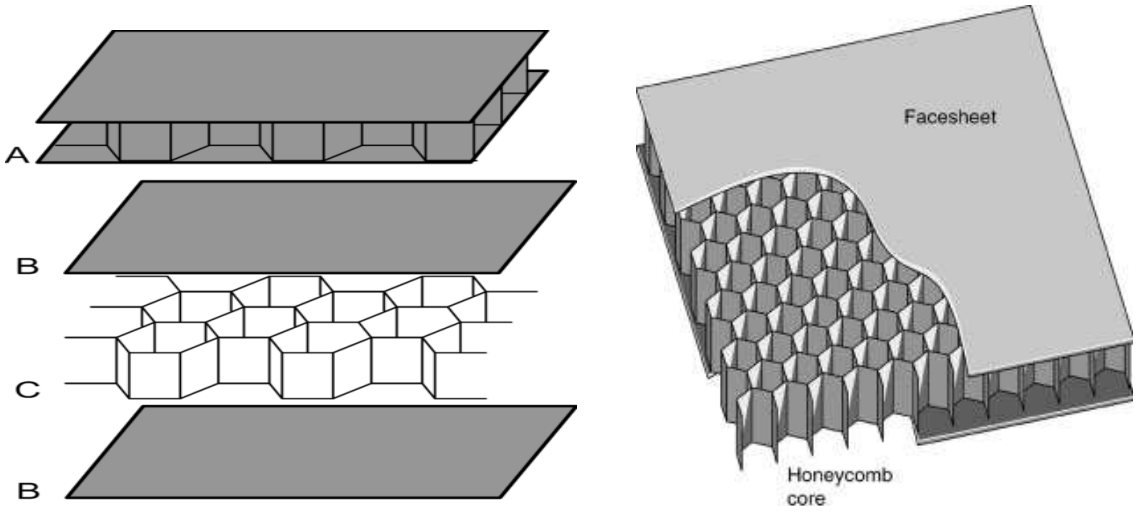

Fig.1.11 Diagram of an assembled composite sandwich (A), and its constituent face sheets or skins (B) and honeycomb core (C) [10]

Sandwich constructions (Fig 1.11) can be realised with a great variety of materials both for facing layers and inner core. The facing layers are typically realised by aluminium plates, high pressure laminates, glass fibre reinforced plastics etc. For the core material quite different realisations exist. The two most common ones are honeycombs and foams. Honeycombs have been used successfully for decades in airplanes. They are made from aluminium and more recently from glass or aramid fibre reinforced plastics. Typical foams used for sandwich cores are: chlorofluorocarbons (CFCs), halo-fluorocarbons (HFCs) and CO_2-foamed materials (the latter being the present lane of development).

MATERIALS USED FOR MAKING SANDWICH COMPOSITE [17]

- **HONEYCOMB**: Closed cell honeycomb structures (Fig 1.12(a)) are widely used for sandwich panel construction. Cell configurations of honeycomb are of different types for example hexagonal core, flex-core, ox-core, tube-core etc.

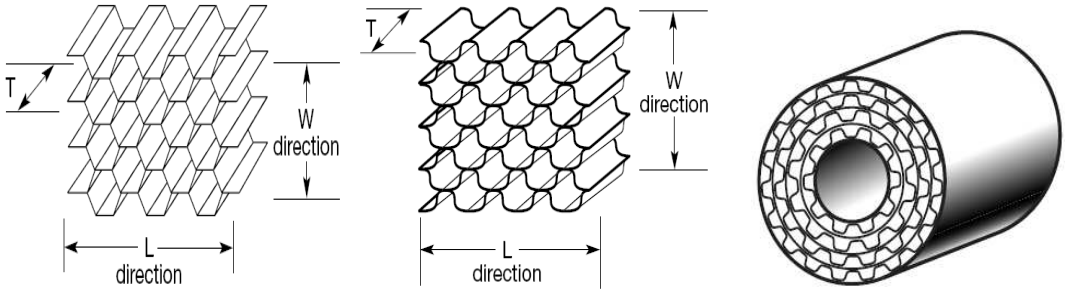

Hexagonal-core Flex-core Tube-core

Fig.1.12 (a) Configurations of honeycomb core [17]

- **PVC-FOAM:** PVC foam sheet (Fig 1.12(b)) is a closed-cell, lightweight, thermoplastic and hard foam material. It is a suitable core material for dynamically loaded and shock absorbing sandwich structures, which form 3-dimensional contour

Fig.1.12 (b) PVC-Foam [17]

- **POLYSTYRENE CORE:** polystyrene (Fig 1.12(c)) is a synthetic thermoplastic material obtained by polymerizing styrene; used as a white rigid foam (**expanded polystyrene**) for insulating and packing and as a glasslike material in light fittings and water tanks

Fig.1.12 (c) Thermocol (polystyrene) core [17]

BENEFITS OF SANDWICH STRUCTURE

The main advantages of sandwich structure are

- high rigidity combined with higher strength to weight ratio
- smoother exterior
- better stability
- high load carrying capacity
- increased fatigue life
- crack growth and fracture toughness characteristics are better compared to solid laminates
- thermal and acoustical insulation
- high bi-axial compression load bearing ability

FAILURE MODES OF SANDWICH STRUCTURE [18]

A variety of failure modes can occur in sandwich structures depending on the type of load, the constituent materials and clamping conditions (Fig 1.13). Local core crushing may occur due to impacting baggage corners, often leading to a face-to-core debonding, so that no more shear forces can be carried by the sandwich structure. High bending loads can lead to face fracture or core shear failure. Face wrinkling, shear crimping or global buckling failure can occur as a consequence of compressive loads in the sandwich plane. Further failure modes at load introduction points (inserts) and edge joints are possible.

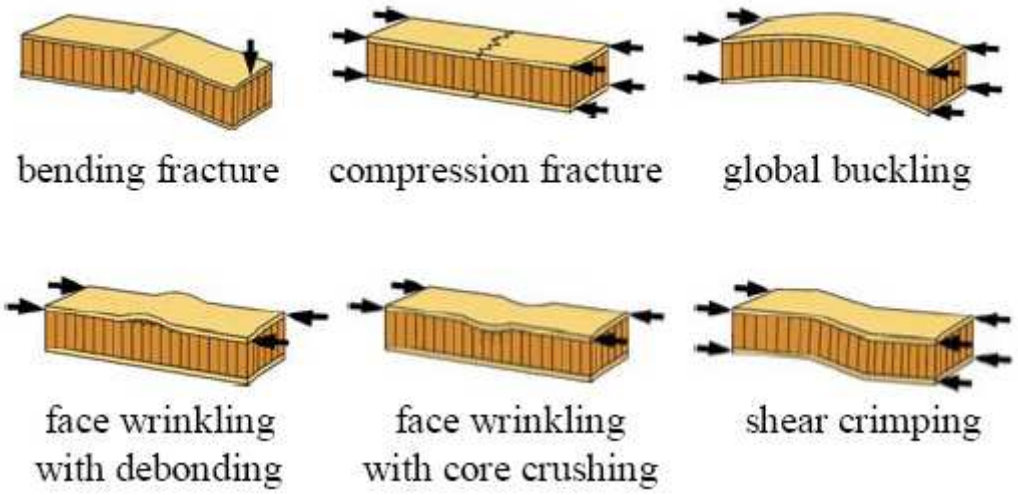

Fig.1.13 Sandwich structure failure modes [18]

APPLICATIONS [19]

The sandwich structures are used in aircraft wing construction (Fig 1.14(a)), hover craft construction (Fig 1.14(b)) and in electronic and communication radar dome (Fig 1.14(c)).

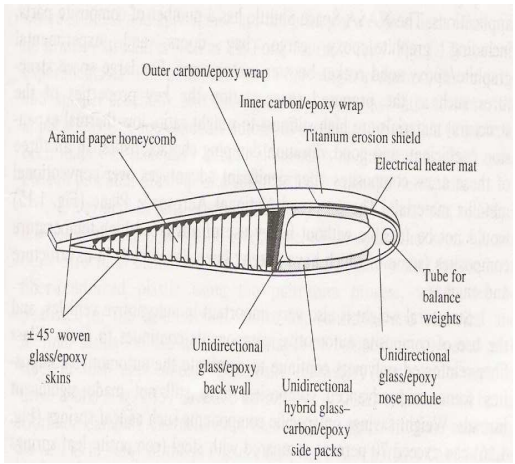

Fig.1.14(a) Wing has glass fibre main spar. Leading edge has composite (glass fibre) sandwich construction stabilized with polystyrene ribs [19].

Fig.1.14(b) The Cat190 is a motor powered oceanic luxury catamaran, with hulls and glass fibre structure with Sandwich of foam or polystyrene. [21]

Fig.1.14(c) FRP radar dome (25m diameter, factory made FRP sandwich panels are bolted together on site) [21]

1.14 ENVIRONMENTAL EFFECTS ON SANDWICH COMPOSITES:

Environmental factors such as humidity and temperature can limit the applications of sandwich structure composites by deteriorating the mechanical properties over a period of time. When a fibre-reinforced composite sandwich structure is exposed to a hygrothermal environment and mechanical loads, changes in material properties are expected. These changes in material properties are connected to irreversible material strength degradation. Exposure to water ambience induces environmental effects into both the core and the face sheet of sandwich structure. Effect of exposure to external temperature remains delimited to the outer facing of sandwich structure for a significant time due to the high thermal insulation provided by the core material. The hygrothermal environment effects induce an essentially one side expansion into the sandwich layup that tend to distort the shape, reduce the strength of the sandwich structure and produces the matrix cracking.

The moisture may affect the face sheet of sandwich structure through chemical changes such as relaxation and oxidation of the matrix material. A moisture environment exposed to a sandwich structure may cause damage such as *debonding* at fibre/matrix interfaces and continuous cracks. Other damage modes that can occur in a fibre-composite sandwich structures are transverse matrix cracks, delamination and fibre fracture. The results of chemical changes and mechanical damage in general affect the overall material properties, e.g. flexure modulus, micro-hardness, hygrothermal expansion coefficients, diffusion coefficients. In sandwich structure the delamination cracks propagates close to the interface in the water environment whereas it stays within the core material in natural environment.

If the face sheet has cracks or small pin holes then the moisture uptake will be more which leads to reduction in mechanical properties of sandwich structure because faster moisture uptake results faster material degradation.

CHAPTER 2 LITERATURE REVIEW

1) A. Mukherjee, S.J. Arwikar (ACI Structural Journal) Part1-Title No. 102-S76 [2006]
A set of accelerated aging and natural environment tests has been carried out to evaluate performance of glass fibres reinforced polymer (GFRP) sheets bonded on concrete in tropical environment. Plain concrete beams were cast and externally reinforced by bonding with E-glass GFRP sheets. The beams were immersed in a 60^{o}C water bath for varying durations. The novelty of the experiment was that the environmental exposure was given while they were subjected to service loads. This load helped in seeping sheet exposed to hot water under stressed condition. Thus field environment very similar to tropical climate was simulated. The loaded specimen were also subjected to natural weathering for 6 and 12 months duration. The sheets were removed from the specimen and the tensile strength and modulus were determined to assess the degradation, if any. In the first part of the paper the structural level studies are discussed. In Part 2 the micro structural investigation is reported.

2) A. Mukherjee, S.J. Arwikar (ACI Structural Journal) Part2- Title No. 102-S82 [2006]
In the first part of the paper the structural scale tests on the synergistic effects of moisture, temperature, alkalinity and stress level on the performance and durability of GFRP sheet bonded externally on concrete have been discussed. This part describes the micro structural studies to find out the nature, quantum and mechanism of deterioration in the conditioned sheets. Micrographic investigations were carried out using a scanning electron microscope (SEM) to visualize the changes in the microstructure. The other tests are energy dispersive X-ray analysis (EDX) and inductively coupled plasma mass spectrometry (ICP-MS) to determine the chemical changes in the composite.

3) Abhijit Mukherjee and S. J. Arwikar-Part1(Composite Structures 81 (2007) 21–32) [2007] A set of accelerated aging and natural environment tests has been carried out to evaluate performance of glass fibre-reinforced polymer (GFRP) reinforcing bar in a tropical environment. Beams were cast with the GFRP reinforcing bars as internal reinforcement. They were immersed in a 60 °C water bath for varying durations. The novelty of the experiment was that the environmental exposure was given to the beams while they were subjected to service loads. These loads kept the cracks open for reinforcing bars to remain exposed to hot water. Thus, a field environment very similar to a tropical climate was created. The loaded specimen were also subjected to natural weathering for 18 and 30 months duration. The reinforcing bars were removed from the specimen and investigated at both structural and micro structural scale to assess the degradation, if any.

4) Abhijit Mukherjee and S. J. Arwikar-Part 2 (Composite Structures 81 (2007) 33–40) [2007] In the first part of this study, the structural scale tests on the synergistic effects of moisture, temperature, alkalinity, and stress level on the performance and durability of glass fibre-reinforced polymer (GFRP) reinforcing bars in concrete have been discussed. In this part, investigations on micro structural studies, carried out to find out the nature, quantum, and mechanism of deterioration in the conditioned reinforcing bars, are reported. Micrographic investigations were carried out using a scanning electron microscope (SEM) to

visualize the changes in the microstructure. The other tests that have been carried out are energy-dispersive x-ray analysis (EDX) and inductively coupled plasma mass spectrometry (ICPMS) to determine the chemical changes in the composite. Observations of the fracture surfaces by optical and scanning electron microscopes showed typical damage mechanisms for laminates [0/0]s and [0/90]s.

5) A. Bezazi, A. El Mahi, J.-M. Berthelot and B. Bezzazi (Volume 39, Number 2 / March, 2007) [2007] In this paper the analysis of stiffness and the identification of rupture mechanisms during and after static tests of sandwich panels and their components have been investigated. The sandwich panels, having cross-ply laminates skins made of glass fibre and epoxy resin were manufactured by vacuum moulding and subjected to three-point bending tests. Two polyvinyl chloride cores of similar type but with differing densities were investigated. The effect of core density and its thickness on the behaviour and the damage was highlighted. In terms of stiffness and load at failure, the sandwich structure has better mechanical characteristics compared to its components.

6) A. Bezazi, A. El Mahi, J.-M. Berthelot and B. Bezzazi (Volume 41, Number 3 / May, 2009)[2009] In this paper the analysis of stiffness degradation and the identification of damage mechanisms during and after fatigue tests of sandwich panels with PVC foam cores have been performed. The sandwich panels with cross-ply laminates skins made of glass fibre and epoxy resin were manufactured by vacuum moulding and subjected to three-point bending tests. Two PVC cores of similar type but with differing densities were investigated. The effect of core density and thickness on the damage behaviour was highlighted. Using the cyclic life criterion, fatigue curves were plotted according to two models and compared with those of the literature. It has been demonstrated that the sandwich SD 2, with the higher core density, withstands a higher load and possesses greater rigidity in static tests, combined with an enhanced fatigue resistance, when compared to sandwich SD 1 which has a lower core density.

7) Akawut Siriruk, Y. Jack Weitsman and Dayakar Penumadu (Volume 69, Issue 6, pages 814-820) [2008] In this paper effect of sea environment on interfacial delamination behaviour of polymeric sandwich structures is described. Sandwich structures are utilized in naval craft and thereby are exposed to sea water environment and temperature fluctuations over extended periods. The sandwich layup consists of a closed cell polymeric foam layer placed between thin carbon or glass fibre reinforced polymeric composite facings. Attention in this paper is focused on sea water effects on the interfacial mechanical response between foam and facing due to sustained sea water exposure using carefully controlled laboratory conditions. Pre-cracked sandwich composite specimen are soaked in sea water for extended periods and interfacial fracture behaviour compared against dry specimen. Results indicate that the delamination crack propagates close to the interface in the wet case, while it stays within the foam in the dry case. Significant reduction in fracture toughness due to sea water exposure is observed and needs to be considered in the design of ship structures. The effect of sea water on values of energy release rate are determined experimentally and predicted using the J-integral concept. A good agreement between data and predictions is achieved, indicating a reduction in fracture toughness by 30% due to sustained exposure to sea water.

8) Akawut Siriruk, Y. Jack Weitsman and Dayakar Penumadu (Volume 69, Issue 6, pages 821-828) [2008] Marine composite sandwich structural materials, comprising of low density PVC foam core and carbon fibre reinforced vinyl ester based resin composite facings, are studied for associated degradation in mechanical behaviour caused by sea water. This paper presents experimental and analytical results concerning the properties and response of closed cell polymeric foams (PVC H100) and their sandwich composites. Data regarding the elastic properties of foam (shear and Young's modulus) are collected by means of novel custom made devices and interpreted by means of displacement based analytical models. Emphasis is placed on environmental effects and a novel approach of using expansion strain analogy to study the effects of both sea water and temperature are proposed. It is shown that the custom made shear testing apparatus employed here in offers a significant improvement over the device recommended by ASTM. Using torsion testing, the value of shear modulus in the water-saturated outer shell of soaked foam specimen are obtained and show a degradation of 72% with long-term exposure to sea water.

9) A. R. Bezazi, A. El Mahi, J.M. Berthelot and B. Bezzazi (Vol. 35, No. 2) [2003] In this paper mechanical behaviour of different resin-epoxy laminates reinforced with cross-ply Kevlar and glass fibres under conditions of static and cyclic three-point bending is described. In static tests, we consider the effect of stacking sequence, the thickness of 90°-oriented layers, reinforcement type on the mechanical behaviour of laminates under loading and on realization of various damage modes leading to rupture. Cyclic loading studies have been performed in two steps. In the first stage, we inquire into the dependence of the behaviour and durability of four glass fibre-reinforced laminate-types on the stacking sequence; the second stage is devoted to studying the dependence of cyclic strength and fatigue behaviour of laminates on the reinforcement type. Fatigue tests are carried out in load-control regime for glass and hybrid (Kevlar + glass) fibre laminates. Fatigue curves are constructed in coordinates "stress – number of cycles until fracture" from the criteria corresponding to a drop in stiffness by 5 and 10%. Analysis of the results obtained permit evaluation of the effect of the stacking sequence and the reinforcement type on the behaviour of cross-ply laminates in cyclic loading. The presence of Kevlar fibres accounts for nonlinear behaviour of laminates in static tests and for low cyclic strength in fatigue tests under three-point bending.

10) Ashcroft, I. A., Abdel Wahab, M. M., and Crocombe, A. D. (Mechanics of Advanced Materials and Structures, Volume 10, Number 3, Jul-Sep 2003 , pp. 227-248(22)) [2003] In this paper, a method of predicting failure in bonded composite joints subjected to combined mechanical loading and environmental degradation is described. The technique is based on a coupled mechanical-diffusion finite-element analysis combined with an appropriate failure criterion. The method is evaluated by predicting the fatigue thresholds of epoxy-CFRP lap-strap joints preconditioned and tested in dry and wet environments. The coupled stress-diffusion method was shown to be capable of predicting correctly the effect that different environments would have on the fatigue resistance of the joints. Both elastic and elastoplastic fracture criteria were then used to quantitatively predict the fatigue thresholds. The elastoplastic fracture criterion was the most suitable when moisture was encountered at elevated temperatures and was capable of predicting fatigue thresholds within

the experimental scatter range. It is concluded that the technique described is a powerful and flexible way to predict failure in bonded joints subjected to a wide variety of loads and environmental conditions. The method does, however, rely on material data not commonly available, and reasonable simplifying assumptions should be made to make the method cost effective.

11) Baley, C., Davies, P., Grohens, Y., and Dolto, G. (Volume 11, Number 2) [2004] This paper gives an overview of the characterization of the inter laminar properties of composites used for marine structures. Composites to be used in marine applications have particular requirements due to their environment, their large dimensions, mechanical loading and cost constraints. Under certain loading conditions (insert loading, impact) there is a risk of delamination as interlaminar strength of these materials is limited. This paper presents an overview of the tests available to measure delamination resistance. The parameters which influence this property, including the constituents (fibre, matrix and interface), specimen geometry, fabrication route and the resulting defects and aging are reviewed here.

12) Botelho, E. C., Pardini, L. C., and Rezende, M. C (Volume 41, Number 21) [2006] The environmental factors, such as humidity and temperature, can limit the applications of composites by deteriorating the mechanical properties over a period of time. Environmental factors play an important role during the manufacture step and during composite's life cycle. The degradation of composites due to environmental effects is mainly caused by chemical and/or physical damages in the polymer matrix, loss of adhesion at the fibre/matrix interface, and/or reduction of fibre strength and stiffness. Composite's degradation can be measure by shear tests because shear failure is a matrix dominated property. In this work, the influence of moisture in shear properties of carbon fibre/epoxy composites (laminates [0/0]s and [0/90]s) have been investigated. The interlaminar shear strength (ILSS) was measured by using the short beam shear test, and Iosipescu shear strength and modulus (G12) have been determined by using the Iosipescu test. Results for laminates [0/0]s and [0/90]s, after hygrothermal conditioning, exhibited a reduction of 21% and 18% on the inter laminar shear strength, respectively, when compared to the unconditioned specimen. Shear modulus follows the same trend. A reduction of 14.1 and 17.6% was found for [0/0]s and [0/90]s, respectively, when compared to the unconditioned specimen. Micro structural observations of the fracture surfaces by optical and scanning electron microscopes showed typical damage mechanisms for laminates [0/0]s and [0/90]s.

13)Craig A. Steeves and Norman A. Fleck (Volume 46, Issue 4**) [2004]** This paper focuses on the competing collapse mechanisms for simply supported sandwich beams with composite faces and a PVC foam core subjected to three point bending. The faces comprise Hexcel Fibredux 7781-914G woven glass fibre-epoxy prepreg, while the core comprises closed cell Divinycell PVC foam of relative density 6.6% and 13.3%. The mechanical properties of the face sheets and core are measured independently. Depending upon the geometry of the beam and the relative properties of the constituents, collapse is by core shear, face sheet micro buckling or by indentation beneath the middle loading roller. A systematic series of experiments and finite element simulations have been performed in order to assess the

accuracy of simple analytic expressions for the strength. In general, the analytic expressions for peak load are adequate; however, simple beam theory becomes inappropriate and the analytic models are inaccurate for stubby beams with thick faces relative to the core thickness. A failure mechanism map is constructed to reveal the dependence of the dominant collapse mechanism upon the geometry of the beam.

14) David R. Veazie, Kito R. Robinson and Kunigal Shivakumar (Volume 35, Issues 6-8) [2004] An experimental study was undertaken to investigate the face sheet/core interfacial fracture toughness of E-Glass/Vinylester face sheet, closed-cell polyvinyl chloride (PVC) core, sandwich composites. To determine the effects of a marine environment (temperature and sea-water) on conditioned specimen with a crack present, an interfacial crack was induced prior, as well as subsequent to, 5000 h of elevated temperature (80 °C), elevated temperature and moisture (80 °C, 90%+ relative humidity), and sea-water (submersed) conditioning. The interfacial fracture toughness from room temperature double cantilever beam tests for each environmental condition was then compared using the critical strain energy release rate, G_C. The G_C was reduced considerably (greater than 50%) in specimen submerged in sea-water, and significantly (approximately 90%) due to 5000 h of the 'hot/wet' and hot/dry exposure. Results showed that elevated temperature exposure contributes greatest to the PVC core degradation, whereas sea-water exposure mostly degrades the face sheet/core interface. Exposure to elevated temperatures, along with inducing cracks between the face sheet and a PVC core degraded by elevated temperature exposure, appear to be the most detrimental to interfacial fracture toughness.

15) F. Aviles and M. Augilar-Montero (**Volume 92, Issue 1) [2009]** Sandwich specimen composed of E-glass/polyester face sheets bonded to a PVC foam core were exposed to high moisture (95% RH) and immersed in sea-water for extended periods of time. Degradation of mechanical properties of the face sheets, foam core and face/core interface were progressively evaluated using flexural testing of the laminates, through-thickness tension of the foam core and interfacial sandwich DCB fracture testing. Testing reveals substantial flexural stiffness and strength reductions for the laminated composites, and only minor reduction in the tensile stiffness and strength of the foam. Degradation of the interfacial face/core fracture toughness is weak for specimen subjected to elevated moisture and more pronounced for sandwich specimen immersed in sea-water. After 30 days of exposure to high moisture, foam damage is visible in the form of cracks and pits on the cell walls. Optical examinations of expansional strains show that moisture absorbed by the foam penetrates only about to 2–3 mm from the core free surface for the 95% RH condition, while penetrates deeply for the immersed condition.

16) G. Caprino, P. Iaccarino , and A. Lamboglia (Volume 88, Issue 3)[2008] Three-point bending tests in the elastic domain were carried out on unidirectional laminates made of T800H/3900-2 laminae, holding the fibre direction coincident with the longitudinal axis of the beam. The slenderness ratio was varied in the range 10–65, in order to highlight the contribution of the shear deformation to the structural response. Local rigidity tests were also performed, to ascertain the influence of the indentation at the loading points on the rigidities measured. From the results obtained, the effect of the local deformation on the apparent

flexural rigidity was the higher, as the slenderness ratio was reduced, with errors as large as 18% for the shorter spans adopted.
Using Timoshenko's beam theory and finite element analyses, a prediction of the rigidity in flexure was attempted. The theoretical results and the experimental data showed an excellent correlation, provided an unexpectedly low value of the through-thickness shear modulus was assumed in the calculations. Possible reasons for this occurrence were pointed out, involving the role played by the epoxy/polyamide interleaves in the behaviour of the material, as well as the actual shear correction factor to be used to take into account the shear effect.

17) Jilin Yu, Erheng Wang, Jianrong Li and Zhijun Zheng (Volume 35, Issue 8) [2008] In this paper, the response and failure of sandwich beams with aluminium-foam core are investigated. Quasi-static and low-velocity impact bending tests are carried out for sandwich beams with aluminium-foam core. The deformation and failure behaviour is explored. It is found that the failure mode and the load history predicted by a modified Gibson's model agree well with the quasi-static experimental data. The failure modes and crash processes of beams under impact loading are similar to those under quasi-static loading, but the force-displacement history is very different. Hence the quasi-static model can also predict the initial dynamic failure modes of sandwich beams when the impact velocity is lower than 5 m/s.

18) J. S. Earl , J. M. Dulieu-Barton and R. A. Shenoi (Volume 63, Issue 2) [2002] In this paper typical marine sandwich construction composite tee joints have been exposed to a hygrothermal ageing environment and were simultaneously subjected to one of three loading conditions: free standing, static compression and cyclic compression. The joints were removed from their environment for experimental evaluation after 60 and 144 days of ageing. The experimental approach adopted for this work was thermoelastic stress analysis (TSA), using the DeltaTherm equipment to obtain full-field thermoelastic data from the region of interest in the structural specimen. Readings from the aged joints have been obtained and compared to reference readings taken from an un-aged joint. The implications of the changes in thermoelastic signal in specific regions of the joints have been discussed. The work shows the potential for using TSA to detect material changes due to hygrothermal ageing and for establishing damage severity levels resulting from mechanical loading during hygrothermal exposure.

19) L.W. Davies, R.J. Day, D. Bond, A. Nesbitt, J. Ellis, E. Gordon (Volume 67, No.9) [2007] This paper assesses the use of the Quickstep method for the processing of an epoxy/carbon fibre aerospace material and compares this to equivalent composites produced using an autoclave process. Higher process ramp rates, achievable using Quickstep, have been shown to reduce resin viscosity thus facilitating void removal. Manipulation of the Quickstep cure cycle, while the resin is at low-viscosity, has significant effects on the mechanical properties of the product whilst simultaneously reducing the cure cycle time. Using Quickstep curing, specimen were produced exhibiting comparable interlaminar properties but lower flexural strength as compared to those produced using the autoclave. However, normalisation of the data to a common fibre volume fraction showed that better interlaminar shear strengths could be obtained using Quickstep. This improvement in specific

interlaminar shear strength was postulated to be due to the lowering of the resin viscosity over the duration of the cure, resulting in better wet through of fibres by resin and improved interfacial adhesion between fibre and matrix. This study identifies key parameters associated with the Quickstep process, providing a basis for further optimisation.

20) M. Dawood, E. Taylor and S. Rizkalla (Volume 92, Issue 4) [2010] This paper presents the details of a research program that was conducted to evaluate the two-way bending behaviour of 3-D glass fibre reinforced polymer (GFRP) sandwich panels. The panels consist of GFRP skins with a foam core and through-thickness fibre insertions. While the behaviour of these panels under one-way bending is relatively well understood the behaviour under two-way bending has not yet been investigated. An experimental program was conducted to evaluate the effect of the fibre insertion pattern and the panel thickness on the two-way bending behaviour under the effect of a concentrated load. The experimental results were used to verify a non-linear, static finite element model which was used to introduce a simplified method to predict the behaviour. The measured and predicted responses indicate that at lower deflections the panel behaviour is dominated by plate bending action while for higher deflections membrane action dominates. The finite element analysis was extended to study the effect of different parameters which were not tested in the experimental program. The parametric study indicates that increasing the relative flexural or shear rigidities of the panel alters the behaviour towards the plate bending mechanism thereby reducing the percentage of load carried by membrane action.

21) Pavankiran Vaddadi, Toshio Nakamura, Raman P. Singh (Volume 41, No.3) [2002] A new approach has been developed, based on an inverse analysis technique, to determine critical moisture diffusion parameters for a fibre-reinforced composite. This technique incorporates two distinct features: direct experimental observations of the weight gained by a composite material exposed to a humid environment, and highly detailed computational analyses that capture the actual heterogeneous microstructure of the composite. The latter feature was carried out by modelling more than 1000 individual carbon fibres that are randomly distributed within an epoxy matrix. The verification and efficacy of this technique was established by conducting an experiment on a high-grade IM7/997 carbon fibre-reinforced epoxy to determine the maximum moisture content at saturation and the moisture diffusivity of epoxy. With the inverse analysis, the time duration required to estimate these moisture diffusion parameters could be drastically reduced as compared to conventional procedures. Subsequently, the established models were employed to characterize transient moisture absorption process within the composite. Here, it was demonstrated that modelling the heterogeneous microstructure of the composite is critical for obtaining accurate diffusion parameters, and an analytical model with effective properties does not produce correct transient moisture absorption behaviour. Furthermore, the evolution of stress fields due to moisture induced volumetric expansion was quantified. It was observed that high stress concentrations develop in regions of fibre concentration. These regions then act as potential failure initiation sites that can lead to lower damage tolerance.

22) Pavankiran Vaddadi, Toshio Nakamura, Raman P. Singh (Volume 34, No. 8) [2003] Transient hygrothermal stresses induced in fibre-reinforced composites are studied in detail by adopting a novel heterogeneous characterization approach. This approach incorporates two distinct features: transient moisture absorption analysis of actual composite materials exposed to a humid environment, and highly detailed computational analyses that capture the actual heterogeneous microstructure of the composite. The latter feature is carried out by modelling a uniaxial laminate having more than one thousand individual carbon fibres that are randomly distributed within an epoxy matrix. Results indicate that these computational models are essential in capturing the accurate moisture absorption process of the actual specimen. In the analysis, the evolutions of thermal residual stresses and moisture-induced stresses within the humidity and thermal exposed composites have been analyzed. It was observed that high stress concentration develops in the epoxy phase where high fibre density or fibre clustering exists and its magnitude increases as the moisture content saturates. Large stresses can potentially initiate epoxy damage or delamination of epoxy and fibres. Furthermore, due to opposing effects of thermal and moisture exposure, lower stresses are found in the laminate when both are considered simultaneously.

23) V. Crupi and R. Montanini (Volume 34, Issue 3) [2005] In this paper static and dynamic three-point bending tests were carried out in order to investigate the structural response (collapse modes, energy dissipation, strain rate sensitivity) of two different typologies of aluminium foam sandwich (AFS) panels, consisting of a closed-cell aluminium foam core with either two integral (Schunk) or two glued (Alulight) faces. Impact measurements were performed by a bi-pendulum testing machine designed by the authors. It was found that different collapse modes can be obtained for specimen with identical nominal dimensions, depending on the support span distance and on the own AFS properties. Simplified theoretical collapse models were introduced to explain the observed experimental behaviour, showing good agreement between predicted and experimental limit loads. As far as energy dissipation is concerned, no strain rate sensitivity was found for initial impact velocity up to about 1.2 m/s.

24) W.Steven Johnson and C.Kyle Berkowitz (Volume 39, Number 16) [2005] In this paper a composite sandwich system is investigated. Quasistatic fracture toughness and fatigue crack growth experimental and analytical approaches are the focus. The particular system studied is comprised of a Nomex (aramid fibre) honeycomb core with graphite/epoxy face sheets (skins). A modified version of the double cantilever beam (DCB) specimen geometry is used for experimentation. The critical strain energy release rate, Gc, is used to characterize the fracture toughness of the face sheet–core joint. Fatigue crack growth testing is also performed. Novel analytical and experimental techniques are coupled and utilized to address challenges presented by the material system, especially difficult crack visualization. Crack length and growth can be estimated with an empirical approach, employing a compliance calibration. Experiments can also be simulated once several constants are estimated, aiding design. Many of these techniques can be generalized to other adhesive DCB experimentation. Results show that cold tests result in higher fracture toughness and slightly slower fatigue crack growth rates than room temperature tests.

CHAPTER 3 PROBLEM FORMULATION

The use of sandwich structures with composite face sheets in commercial aviation is increasing since they offer great energy absorption potential and increase in flexural inertia without significant weight penalties. The purpose of the core is to maintain the distance between the laminates and to sustain shear deformation. Bye varying the core, the thickness and the material of the face sheet of sandwich structures, it is possible to obtain various properties and desired performance.

From the literature survey related to glass fibre sandwich structures the following gaps were identified:

- Experimentation data related to mechanical behaviour in sandwich structure using polystyrene (thermocol sheet) as a core material is not available.
- Environmental effects under hygrothermal conditions on sandwich structure for a long time period have not been studied so far.

From the gaps in the literature survey the problem to be studied was formulated. It was decided to study the effect of moisture, heat (i.e. hygrothermal effect) and loading conditions on **sandwich structure of Glass Fibre Reinforced Polymer (GFRP) woven fabric (E Glass) and thermocol (polystyrene) of different thickness for** a specified time period. The change in physical & mechanical properties at macroscopic and microscopic levels was to be analysed. It was decided to attempt to further relate the macroscopic behaviour and microscopic behaviour shown by the sandwich structures under exposure to environmental conditions.

CHAPTER 4 EXPERIMENTAL SETUP

4.1 INTRODUCTION:

A set of accelerated aging and natural environment tests has been carried out to evaluate performance of glass fibres reinforced polymer (GFRP) sandwich sheets in tropical environment. The specimen are to be immersed in a 45°C water bath for varying durations. The novelty of the experiment was that the accelerated environmental exposure was given while they were subjected to different levels of bending pre-loads. Thus field environment very similar to tropical climate was simulated.

Fig. 4.1 Work setup

4.2 SETUP FABRICATION:

The setup (Fig 4.1) basically consists of following main elements:

	ITEM NAME	QUANTITY.
1	Water Tank	- 01
2	Heating Elements	- 01
3	RTD Sensors	- 01
4	Temperature Controllers	- 01
5	Solid State Relays	- 01

1) Water Tanks:

The experimental setup consists of well insulated hot water bath to avoid heat loss to environment. The specimen are to be kept fully immersed into the bath below a plate. Different specimen are subjected to different levels of bending pre-loads as discussed before. The specimen are numbered numerically and kept in bath for the respective time as decided

previously. After the time of exposure of respective specimen was over the specimen were taken out and the tests were performed on them to check the degradation.

Fig 4.2 Water Tanks (at 45°C)

Fig 4.3 Water Tank (Natural Degradation)

2) Heating Element:

The setup was heated with help of commercially available heating rod elements (Fig 4.4). Each bath was having its own heating rod connected via temperature controller (Fig 4.5). The wattage of rod was 1000KW with single phase connection. As the temperature reaches the required value the power supply of rods were cut off by controllers.

Fig. 4.4 Heating Element and RTD sensor in a tank

3) RTD (Resistance temperature detector) Sensors: Each of the tanks was provided with separate RTD sensors (Fig 4.3). It senses process value of temperature (value at given time) of the bath and input was send to the controller which controlled the system as per set value.

4) Temperature Controller:

The objective of this set up was to maintain the bath temperature at specified value till the duration of experiment for day and night on daily basis. So a temperature controller (Fig 4.5) was connected with water tank along with relays cut off.

The controller used the proportional-integral-derivative (PID) control to maintain the temperature. On the controller display we had to feed the “Set Value” of temperature indicated in green and the “Process Value” of temperature would be indicated in the red (refer Fig 4.5), which was the output from the RTD sensor. For the very first time we had to set the controller to auto-tune mode so that it could adjust itself according to the input variables. Once the bath had attained the set value the controller cuts off its supply and after sometime it senses the temperature had gone below set value it again starts heating to obtain set value.

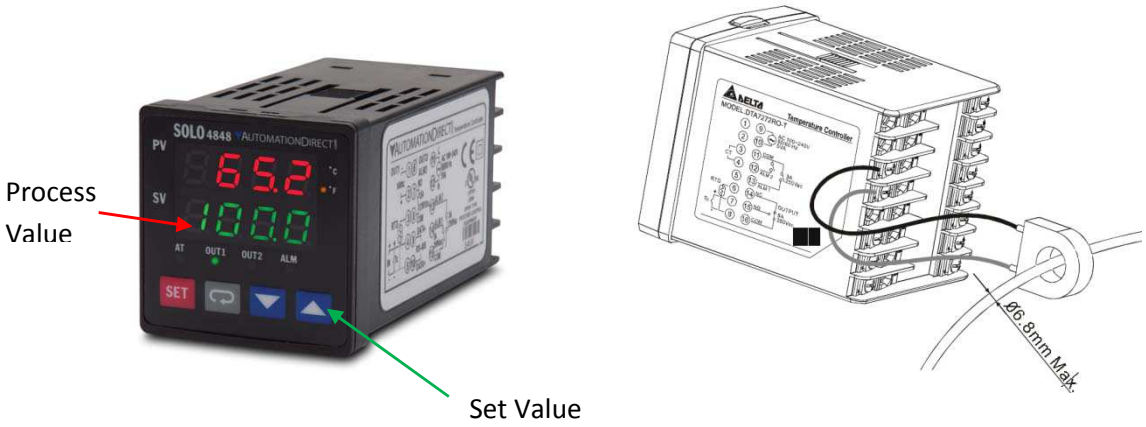

Fig. 4.5 Actual image of the temperature controller showing front and back side of it [14]

The connections of controller are shown below in the Fig 4.5 as given by its maufacturer. It consists of terimanls named with different numbers. Each terminal is having specific input or output requirements. Terminal 1 and 2 here were connected to the power supply of 220Volts with live at 1 and neutral at 2. The relay was connected to the terminals at 3 & 4 with respective positive and negative connections. The live terminal of the heating element was connected to the T1 terminal of the relay and neutral was connected to the power input.The RTD Sensor was connected to the terminals 7, 8 & 9 as shown in circuit diagram (Fig 4.6).

TERMINAL CONNECTIONS

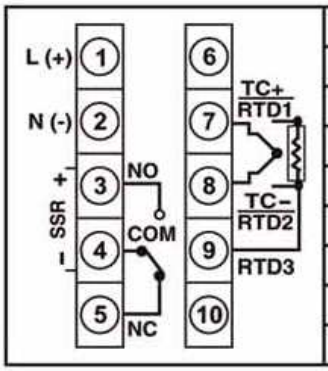

TERMINAL DESCRIPTION	NO.
L (Live)	1
N (Neutral)	2
NO	3
COM	4
NC	5
+ve of TC or RTD1	7
-ve of TC or RTD2	8
3rd wire of RTD (PT100)	9

Fig. 4.6 Circuit diagram of the connections made in the controller [14]

The temperature controller was needed to be secured at some place so we fabricated a display panel out of wood (Fig 4.8). The front face was provided with four holes of the size of the controller outer cover specifications i.e. 48 X 48mm (Fig 4.7). The difference of about 200mm was kept within back of controller and the wall it was attached. The distance was kept more so as to provide accessibility as well as good air circulation to dispose of heat generated.

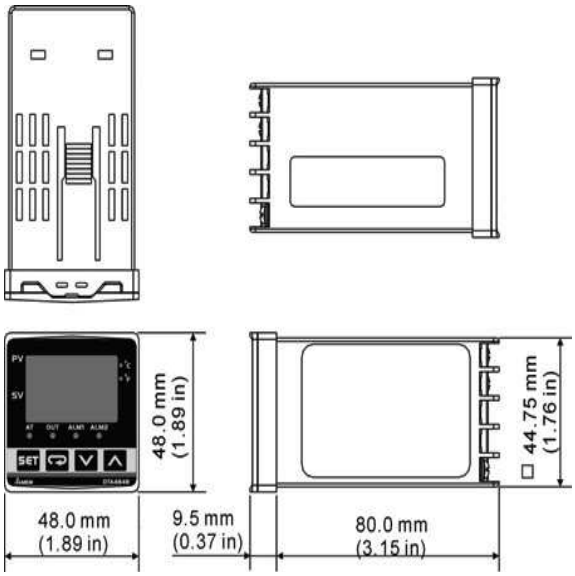

Fig. 4.7 Dimensions of controller [14]

Fig. 4.8 Temperature display panel with controllers

5) Solid State Relays (SSR):

The solid state relay (Fig 4.9) was required to break the circuit in case of overloading. It controlled the switching of the heating element and acted as a switch. It helped in protecting controller for any kind of overload or short circuiting.

Fig. 4.9 Solid State Relay used in setup [15]

4.3 SPECIMEN SPECIFICATIONS

The following were the specifications of the specimen:

Length of specimen : 300 mm

Breadth of specimen : 40 mm

Thickness of specimen : t+2h mm (approx.)

Where t is thickness of thermocol sheet and h is thickness of glass fibre sheet. For this experimentation thickness of specimen are 12mm and 20mm for 8mm and 16mm core respectively.

Dimensions of the specimen (Fig 4.10) had been taken according the ASTM Standard C-393 as a reference [16].

Fig.4.10 Dimensions of the Specimen

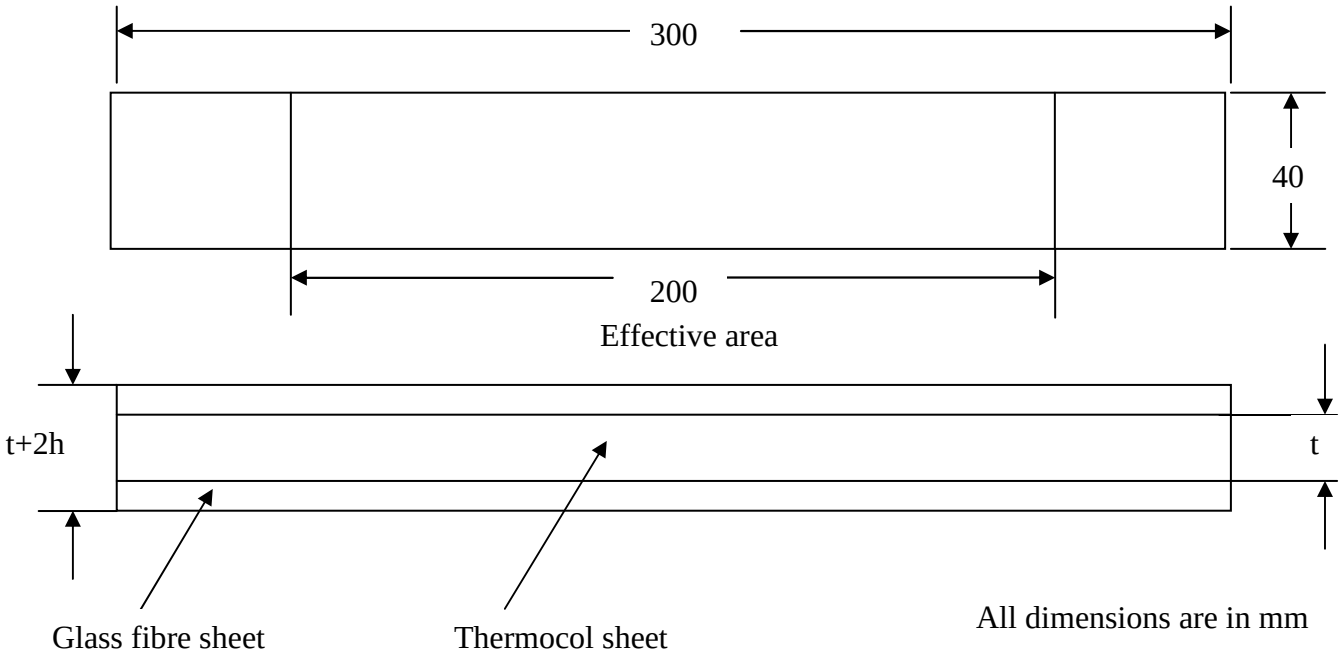

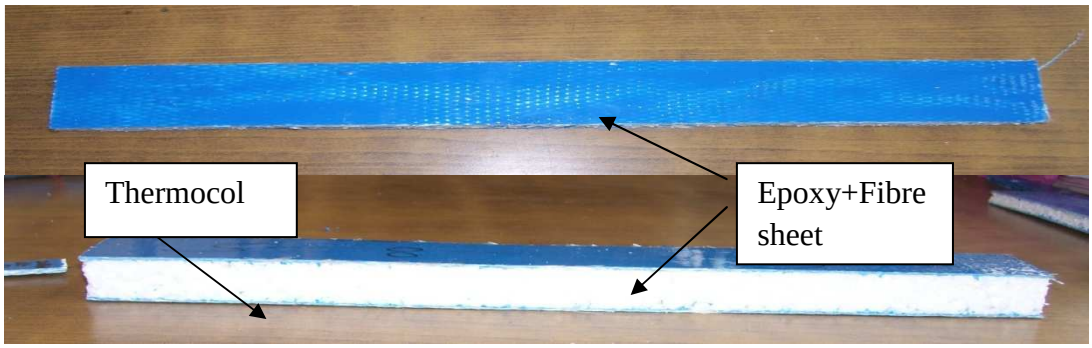

Fig.4.11 Actual image of specimen

The actual image of the final specimen is shown in Fig 4.11. The specimen were hung fully immersed into the bath over a hanger stick with help of thread. Permanent marker was used for numbering the specimen to recognise different pre-loading specimen. After the exposure time of respective specimen was over the specimen were taken out & the bending tests were performed on them in order to check their degradation. A SEM image of the specimen was also taken in order to see the microscope degradation of specimen.

4.4 SPECIMEN PREPARATION

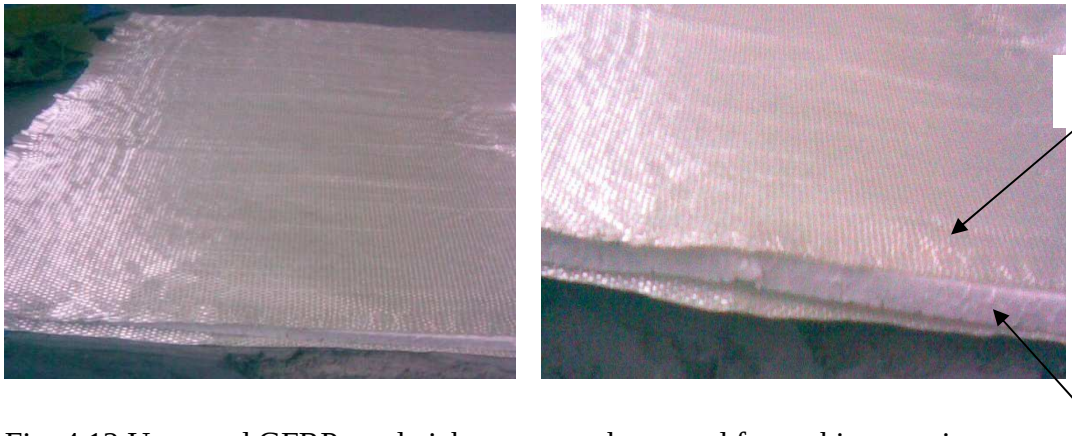

Fig. 4.12 Uncoated GFRP sandwich structure sheet used for making specimen

A) Cutting GFRP Sheet

For the experimentation we had purchased the unidirectional woven fabric roll of GFRP of 50cm width having 0^o fibre orientation woven with polymer fibres. The sheets were initially cut from roll in length of 350mm (i.e. 50mm more than actual sample length). The reason for overcutting was that after its curing we had to trim of the edges in order to remove flaws at end. Then put the thermocol sheet between the two sheets of glass fibre sheets to make it like sandwich (Fig 4.12) and then compress this structure in hydraulic press to make thin sheet of sandwich.

B) Mixing of Epoxy

The sheets were epoxy coated in order to make a composite sandwich material. I epoxy resin (by M Brace) was used which basically consists of two parts (Fig 4.13):

a) Base

b) Hardener

Base is thick blue liquid which was considered as main ingredient and orangish coloured hardener was added to it to help it in settling down by starting the exothermic reactions. Both base and hardener were mixed (by weight) in a container in ratio of 100: 40 respectively.

Fig.4.13 Base (blue colour container) and Hardener (white bottle) used for coating

Fig.4.14 Hand mixing of both base and hardener

After putting the base and hardener in required quantity, the mixture was stirred continuously by manual process (Fig 4.14) so that the mixing takes place in proper manner. If mixing was not done properly the material would not settle well. Also if the ratio of the hardener was more than the pot life of the material would have been lesser. Amount was prepared in a quantity which was consumed in 20-30 min, otherwise epoxy would have settled in container itself.

C) Applying resin on sheet

The epoxy was applied on sheet using a steel scrapper by carefully spreading it evenly on all sides of sheet. It was made sure that there is no air bubbles present entrapped inside the epoxy applied on sheet otherwise it would create a flaw there. After applying epoxy the sheet took overnight to dry and now the coat could be applied on other side if required. The full curing of sheet (Fig 4.15) was done by leaving it under ambient temperature for at least seven days before processing further.

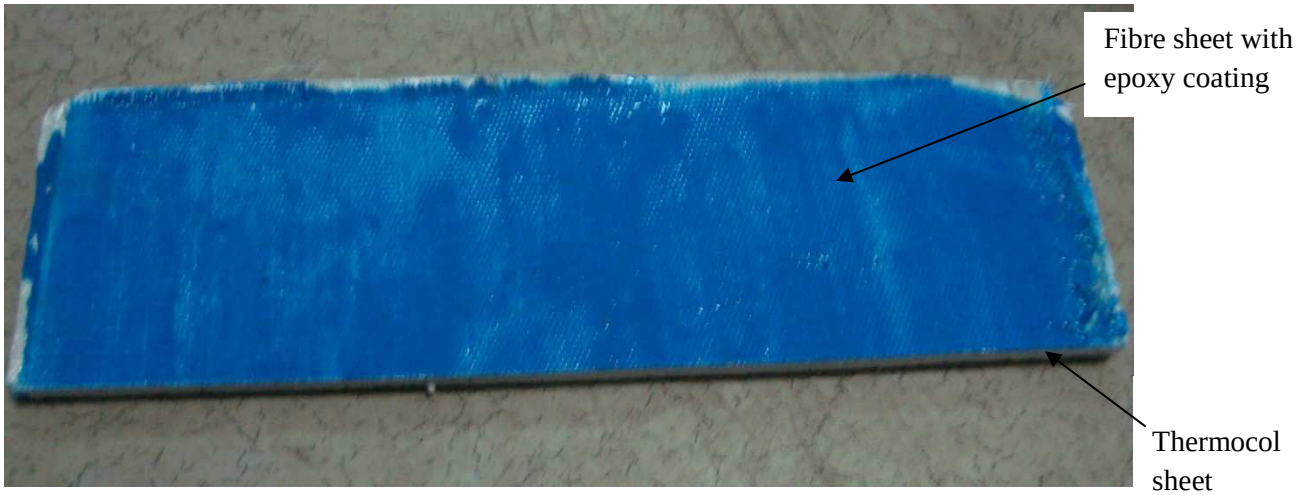

Fig. 4.15 Fully cured sandwich structure sheet with epoxy coating

D) Sizing of sheet for specimen

Once the epoxy was fully cured, the sheet was cut to actual specimen size using the hand saw which would cut it into required size of 300mm x 40mm.

Fig.4.15 Cutting of specimen with the help of Hand Saw

The process of specimen preparation is shown in the form of flow diagram in Fig 4.16

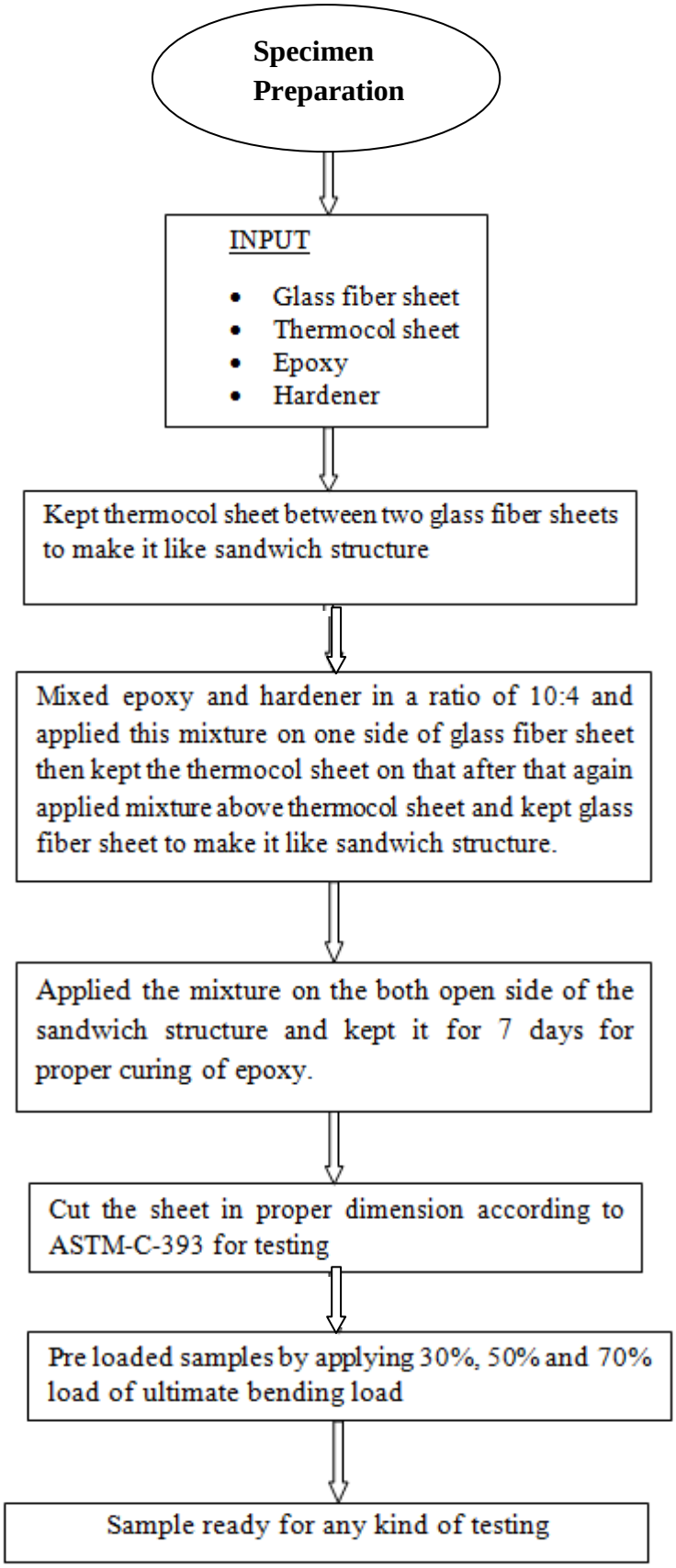

Fig.4.16 Flow Chart of specimen preparation

4.5 TEST MATRICES:

Matrices of number of specimen for different type of testing are shown below. One test matrix is made for accelerated degradation, another is for natural degradation and one is made for weight gain testing

Table T 4.1: Test matrix Details (For Accelerated Degradation)

Sandwich type	Bath Temperature (°C)	Holding Time (days)	No. of specimen pre stressed at % Load at failure (N)			No. of specimen for final testing	Total Specimen
			30%	50%	70%	Tension test & Micrograph (two specimen from each loading)	
Sandwich with thermocol (8mm thick)	45	30	2	2	2	6	6
Sandwich with thermocol (16mm thick)	45		2	2	2	6	9
Sandwich with thermocol (8mm thick)	45	60	2	2	2	6	6
Sandwich with thermocol (16mm thick)	45		2	2	2	6	6
Total pieces at particular load			8	8	8	**Total specimen**	**24**

Table T 4.2: Test matrix Details (For Natural Degradation)

Sandwich type	Holding Time (days)	No. of specimen pre stressed at % Load at failure (N)				Total Specimen
		Without load	**30%**	**50%**	**70%**	
Sandwich with thermocol (8mm thick)	30	1	1	1	1	4
Sandwich with thermocol(16mm thick)		1	1	1	1	4
Sandwich with thermocol (8mm thick)	60	1	1	1	1	4
Sandwich with thermocol (16mm thick)		1	1	1	1	4
Total specimen						**16**

Table T 4.3: Test Matrix Details (For weight gain)

Sandwich type	**Bath Temperature (°C)**	**Holding Time (days)**	**No. of specimen pre stressed at % Load at failure (N)**				**Total Specimen**
			Without load	**30%**	**50%**	**70%**	
Sandwich with thermocol (8mm thick)	45	10	1	1	1	1	4
		20	1	1	1	1	4
		30	1	1	1	1	4
		40	1	1	1	1	4
		50	1	1	1	1	4
Sandwich with thermocol (16mm thick)	45	10	1	1	1	1	4
		20	1	1	1	1	4
		30	1	1	1	1	4
		40	1	1	1	1	4
		50	1	1	1	1	4
Total specimen							**40**

- One sample of each loading and of each core thickness is used for analysing different properties after interval of each 3 day which amount to total 8 specimen.

***Total specimen immersed in water = 24+16+40+8=88**

In above experiment according to the planned test matrix (refer Table T 4.1, Table T 4.2 and Table T 4.3) overall numbers of specimen were estimated initially as 88.
The bending test of initial unexposed sample was first conducted on a Universal Testing Machine to determine the actual ultimate load (peak load) of the sample at a particular deformation. On basis of that ultimate load the loading weight for specimen was calculated. The first set of specimen which would be loaded to 30%, 50%, & 70% of ultimate flexure load of both the core thickness and at temperature of 45^{o}C would be taken out of bath after a time of 1 & 2 months and were checked for its ultimate bending strength. Three specimen for each varied load were tested for their bending strength. One failed sample under each load was tested for micrograph and compositional details.

There were 16 specimen to be studied for the natural degradation & would be kept at normal water for a period of 1 & 2 months. After that they would also be tested in similar manner.

There were 40 specimen for testing of weight gain and micro hardness. 5 specimen of each loading and each core thicknesses are kept into the water at 45^{o}C. After each 10 days, 1 sample of each loading of both the core thickness would be taken out and tested for percentage weight gain and micro hardness. Moisture diffusivity of these specimen is also calculated manually.

One sample of each core thickness and each loading was kept at 45^{o}C in water to study apparent moisture diffusivity after intervals of each three day each up to 12 days.

4.6 Graphs for loading values of specimen (percentage of Ultimate Bending Load):

The following table T 4.4, T 4.5 and graphs (Fig 4.17 to Fig 4.18) show the values at which specimen were subjected different percentage bending load as mentioned earlier.

Table T 4.4: loading values (percentage of ultimate bending load) for 8 mm core thickness specimen

Loading Value (%) of Ultimate bending load at 5% deformation	Actual Values of Force (N)
30%	12
50%	20
70%	28

Area of cross-section considered is 480mm^2 and failure load for calculating percentage loading values for 8mm core thickness was considered as 40N (Ultimate failure load).

Table T 4.5: loading values (percentage of ultimate bending load) for 16 mm core thickness specimen

* Loading Value (%) of Ultimate bending load at 5% deformation	Actual Values of Force (N)
30%	16.5
50%	27.5
70%	38.5

*Area of cross-section considered is 800mm^2 and failure load for calculating percentage loading values for 16mm core thickness was considered as 55N (Ultimate failure load).
** Actual values are the loading value shown by bending testing machine.

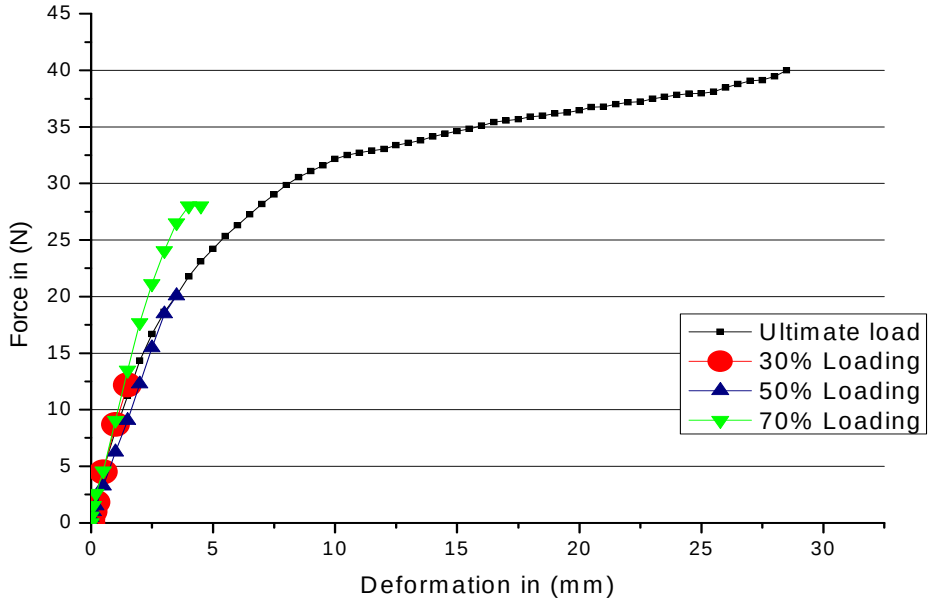

Fig.4.17: Graphs of specimen (8mm core thickness) which were subjected to **ultimate bending load,** 3**0%, 50% and 70% loading of U.B.L.**

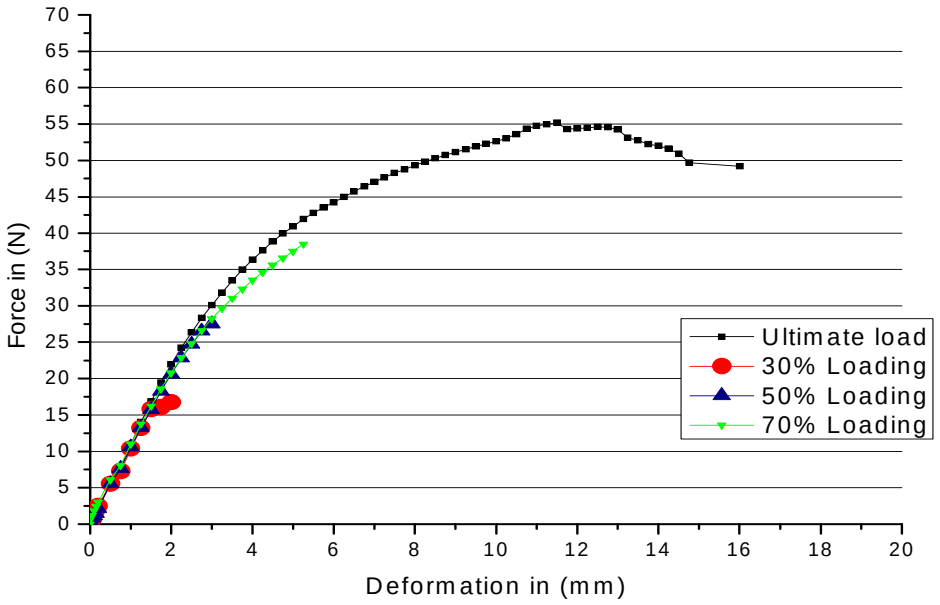

Fig.4.18: Graphs of specimen (16mm core thickness) which were subjected to **ultimate bending load,** 3**0%, 50% and 70% loading of U.B.L.**

4.7 TESTING METHODS USED IN THE EXPERIMENTATION:

4.7.1 Three Point Bending or Flexural Testing

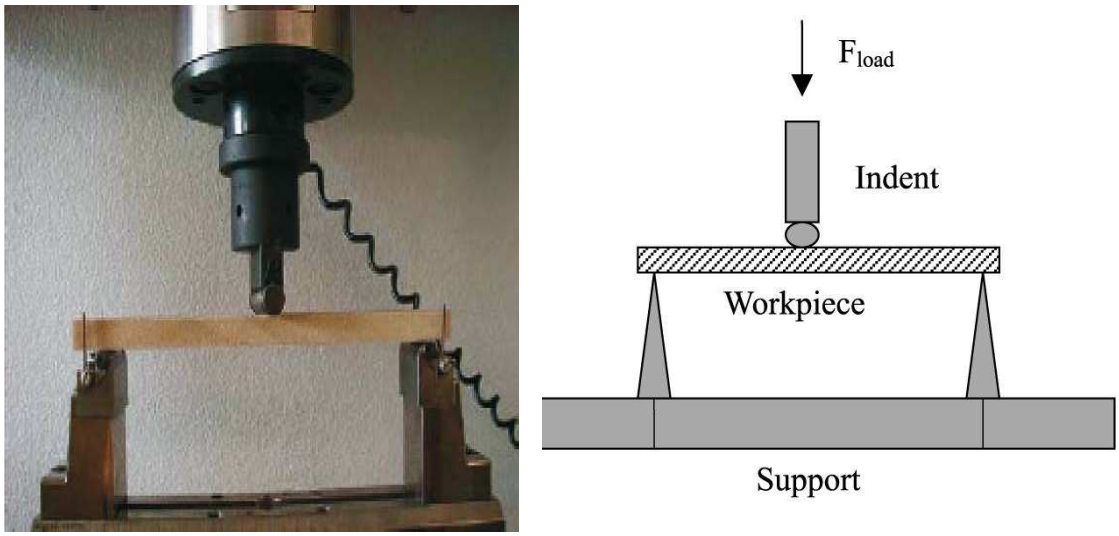

Fig.4.19 Three-point bending experimental setup [22]

The Three Point Bending flexural test provides values for the modulus of elasticity in bending E_f, flexural stress σ_f, flexural strain ε_f and the flexural stress-strain response of the material. The main advantage of a three point flexural test is the ease of the specimen preparation and testing.

For rectangular cross section

Flexural stress

$$\sigma_f = \frac{3PL}{2bd^2} \quad \text{.....(4.1)}$$

Where-

σ_f = Stress in outer fibres at midpoint, (MPa)
ε_f = Strain in the outer surface, (mm/mm)
E_f = flexural Modulus of elasticity,(MPa)
P = load at a given point on the load deflection curve, (N)
L = Support span, (mm)
b = Width of test beam, (mm)
d = Depth of tested beam, (mm)
D = maximum deflection of the center of the beam, (mm)
m = the gradient (i.e., slope) of the initial straight-line portion of the load deflection curve, (N/m)

Flexural strain

$$\epsilon_f = \frac{6Dd}{L^2} \quad \text{.....(4.2)}$$

Flexure modulus

$$E_f = \frac{L^3 m}{4bd^3} \quad \text{.....(4.3)}$$

Flexural stress (σ_f) of sandwich structure can be calculated as:

$$\sigma_f = {}^{M}/_{Z} \quad \text{..... (4.4)}$$

For simply supported beam M can be calculated as:

$$M = \frac{Pl}{4} \qquad \text{..... (4.5)}$$

Where,

M - Bending moment
Z - Section modulus
P - Maximum force applied in the beam
l- Effective length of beam

For the calculation of section modulus Z, the section of composite sandwich is considered as I section. Section modulus can be found as:

..... (4.6)

$$Z = \frac{\text{moment of inertia about the neutral axis}}{\text{Distance of the most distant point of the dection from the neutral axis}}$$

Thickness of thermocol is converted into the thickness equivalent to thickness of fibre/epoxy sheet with the help of following equation

$$b_t = \frac{E_t}{E_F} \times b_f \qquad \text{..... (4.7)}$$

Where,

b_t - thickness of thermocol equivalent to thickness of fibre/epoxy sheet
b_f - thickness of fibre/epoxy sheet of sandwich structure
E_t - Young's modulus of thermocol of sandwich structure
E_f - Young's modulus of fibre/epoxy sheet of sandwich structure

Fig. 4.20 Universal Testing machine


Fig. 4.21 Flexural Testing setup

A Universal Testing machine (Fig 4.20, Fig 4.21) was used for the performing flexural test on GFRP composite sandwich structure specimen and to calculate maximum flexural stress, flexure modulus and maximum applied force. All specimen were tested (Fig 4.22) at a predefined fixed deformation (5%) and peak load and different stress and strength (Fig 4.23) were found after and before exposure.

Fig.4.22 Gripped specimen on the machine

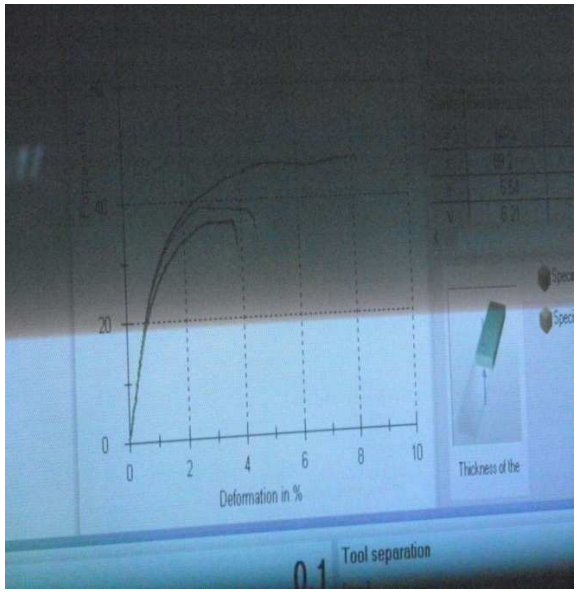

Fig.4.23Simultaneous display of output as test was conducted

4.7.2 Micro Hardness Testing

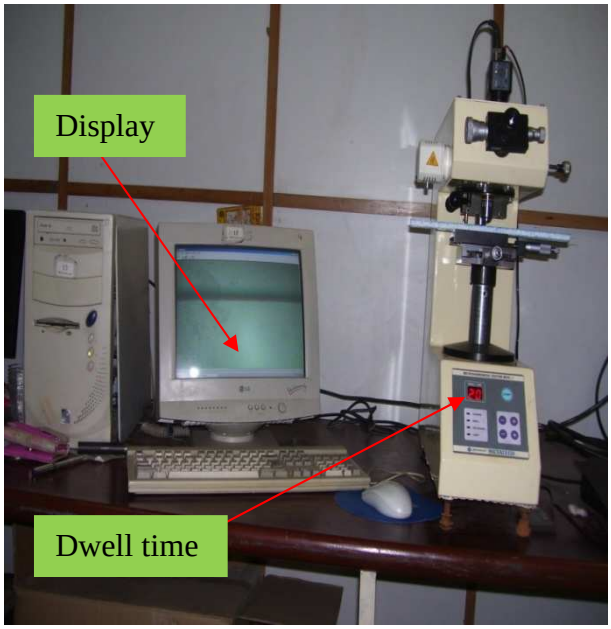

Fig.4.24 Vickers's Hardness Testing Machine

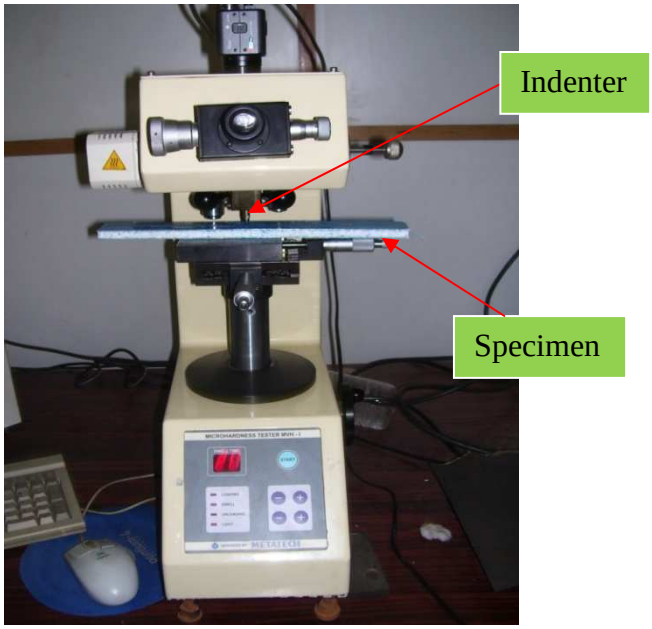

Fig.4.25 Specimen positioning on machine

Vickers's hardness testing machine (Fig 4.24) was used to find Vickers's Hardness Number (VHN) of GFRP sandwich structure specimen. First of all initial VHN reading of each loading i.e. 30%, 50%, 70% and without loading, and of each core thickness (8mm and 16mm) has been taken. After that the specimen were kept in water at 45°C and then again taken readings of VHN after interval of 10 days.

4.7.3 Scanning Electron Microscope Testing

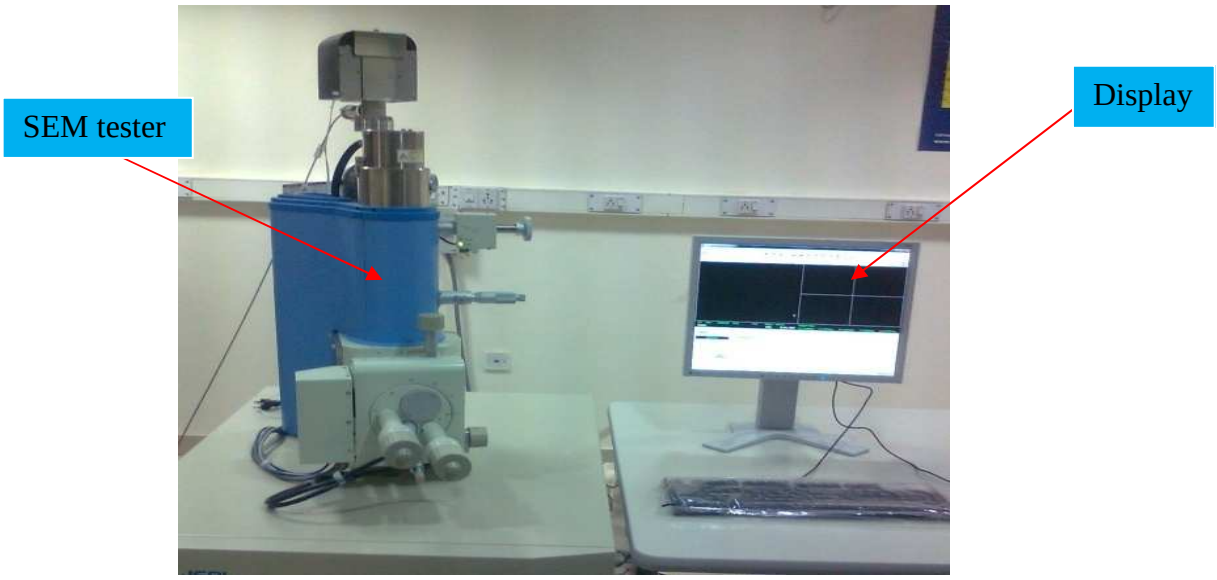

Fig.4.26 Scanning Electron Microscope (SEM) machine

A Scanning Electron Microscope (Fig 4.26) was used to study the condition of fibre and matrix after the specified time period.

CHAPTER 5 RESULTS AND DISCUSSION

5.1 MACROSCOPIC BEHAVIOUR

5.1.1 MACROSCOPIC VISUAL OBSERVATION OF SPECIMEN

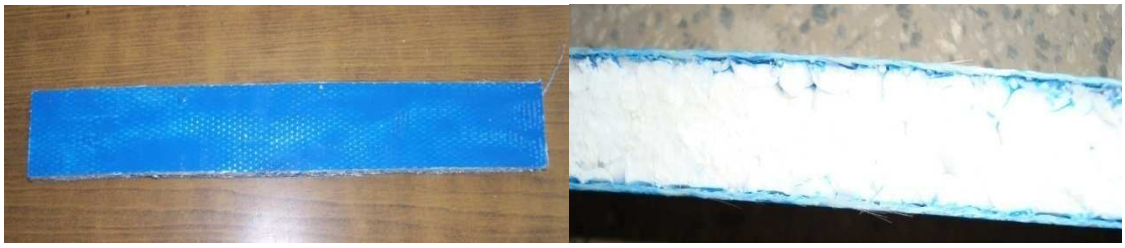

Fig.5.1 Specimen (Surface and Longitudinal view) before the exposure

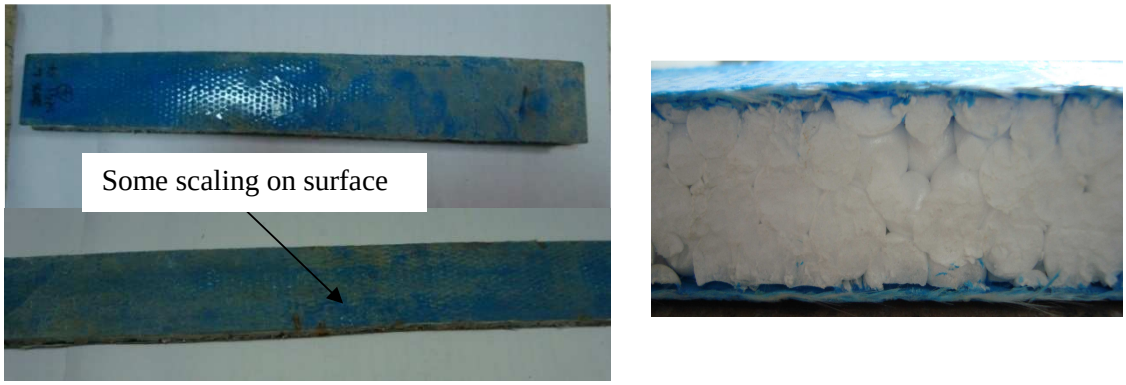

Fig.5.2 Condition of specimen (Surface and Longitudinal view) after 1 month of exposure

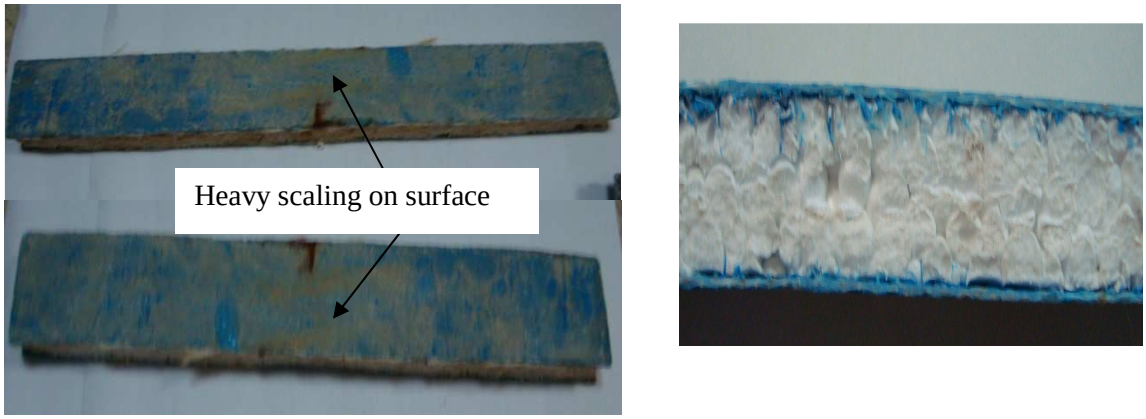

Fig.5.3 Condition of specimen (Surface and Longitudinal view) after 2 month of exposure

As per the visual observation the initial sample (Fig 5.1) had fine shiny epoxy coating.

After 1 month (Fig 5.2) there was some scale formation on the specimen, with water immersed specimen. Surface observation showed that due to scale formation the epoxy had lost some shine on outer edges on either side. But still after bending (by hands) the epoxy showed considerable strength and flexibility. After 2 months (Fig 5.3) scale formation throughout the specimen was noted. There was considerable decrease in strength of the composite and its flexibility.

Pictorial longitudinal view of specimen after one month of exposure

Following figures are showing pictorial longitudinal view of specimen of 8mm and 16mm core after failure.

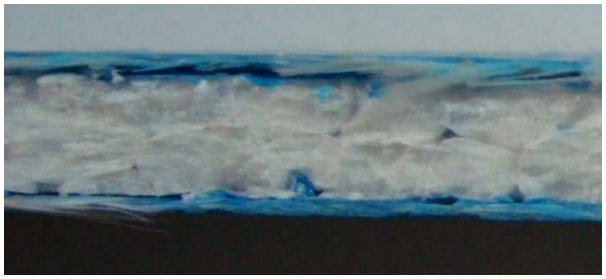

Fig.5.4 Shows condition of specimen of 8mm core thickness at 30% UFL

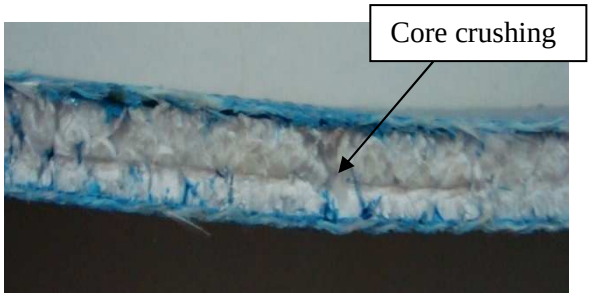

Fig.5.5 Shows condition of specimen of 8mm core thickness at 50% UFL

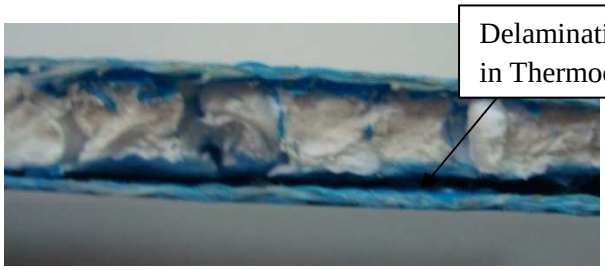

Fig.5.6 Shows condition of specimen of 8mm core thickness at 70% UFL

Fig.5.7 Shows condition of specimen of 16mm core thickness at 30% UFL

Fig.5.8 Shows condition of specimen of 16mm core thickness at 50% UFL

Fig.5.9 Shows condition of specimen of 16mm core thickness 30% UFL at natural degradation

Above figures (Fig 5.4 to Fig 5.9) are showing longitudinal view of specimen of different core thicknesses and different loading after 1 month. As per visual observation of specimen, it was observed that core cracking and delamination occurred in thermocol sheet during the flexural testing. Degradation in thermocol was observed which is clearly visible in above figures also core defects like shear cracks and core crushing were observed. These defects affect the strength and durability of sandwich composite structures.

Pictorial longitudinal view of specimen after two month of exposure

Following figures are showing pictorial longitudinal view of specimen of 8mm and 16mm core after failure

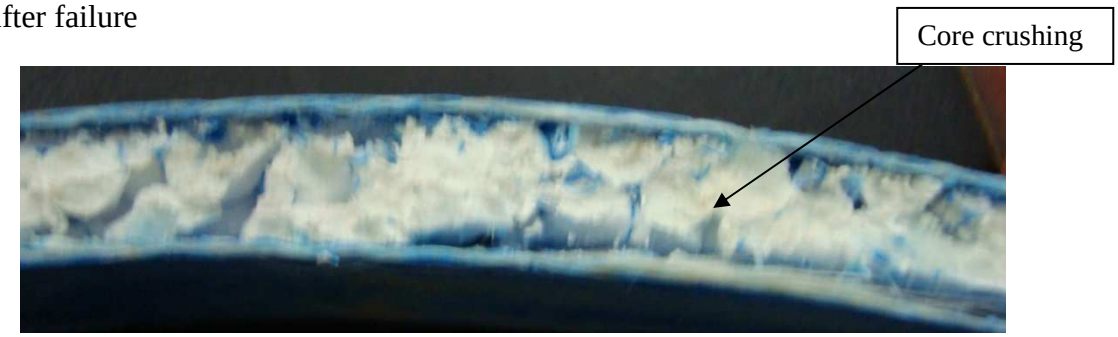

Fig.5.10 Shows condition of specimen of 8mm core thickness at 50% UFL

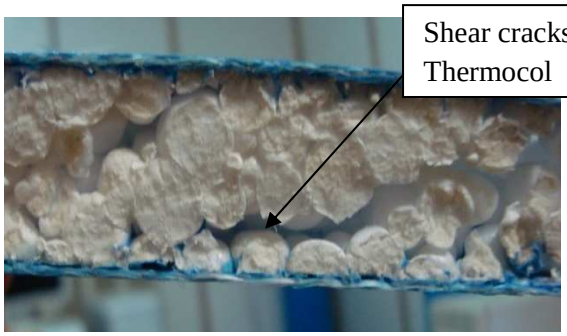

Fig.5.11 Shows condition of specimen of 16mm core thickness at 30% UFL

Fig.5.12 Shows condition of specimen of 16mm core thickness at 50% UFL

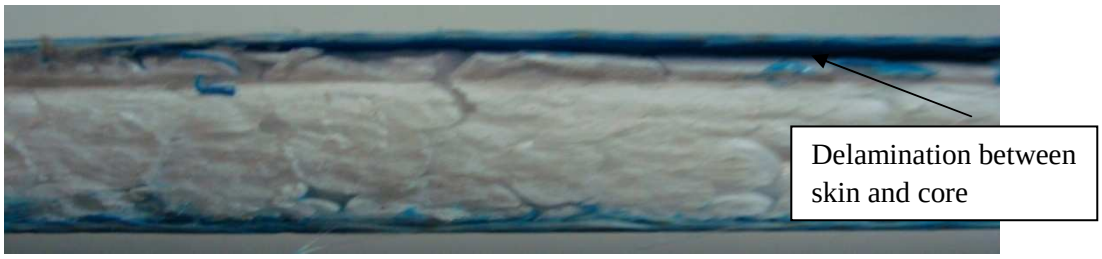

Fig.5.13 Shows condition of specimen of 16mm core thickness at 70% UFL

Fig.5.14 Shows condition of specimen of 16mm core thickness 30% UFL at natural degradation

Above figures (Fig 5.10 to Fig 5.14) are showing longitudinal view of specimen of different core thicknesses and different loading after 2 month. Cracking in thermocol and delamination was observed in specimen after two month of exposure. Epoxy cracking was also observed in some portions. Debonding between core (thermocol) and skin (fibre/epoxy sheet) were found is clearly visible in above figures.

Pictorial transverse view of specimen after oneo month of exposure

Following figures are showing pictorial transverse view of specimen of 8mm and 16mm core after failure

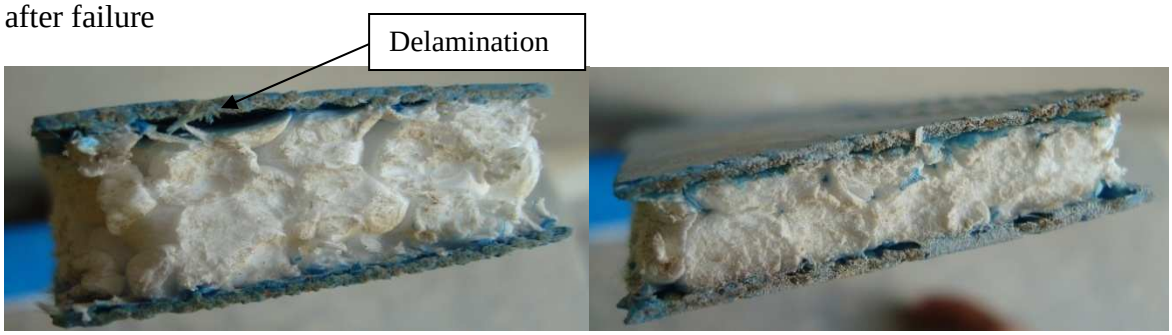

Fig.5.15 Shows condition of specimen of 8mm core thickness at 30% UFL

Fig.5.16 Shows condition of specimen of 8mm core thickness at 50% UFL

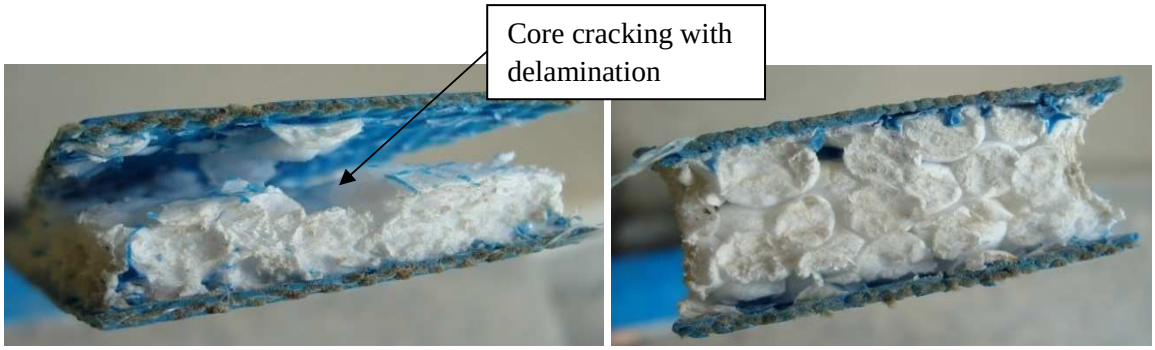

Fig.5.17 Shows condition of specimen of 8mm core thickness at 70% UFL

Fig.5.18 Shows condition of specimen of 16mm core thickness at 30% UFL

Fig.5.19 Shows condition of specimen of 16mm core thickness at 70% UFL

Fig.5.20 Shows condition of specimen of 16mm core thickness at without UFL

Above figures (Fig 5.15 to Fig 5.20) are showing transverse view of specimen of different core thicknesses and different loading after 1 month. Core cracking with delamination was observed in specimen of 8mm core thickness (70% loading). Specimen without bending preload was not showing any defect in 1 month. Delamination was observed in some portions in all specimen.

Pictorial transverse view of specimen after two month of exposure

Following figures are showing pictorial transverse view of specimen of 8mm and 16mm core after failure

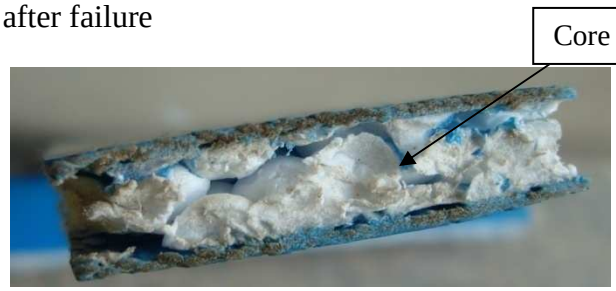

Fig.5.21 Shows condition of specimen of 8mm core thickness at 30% UFL

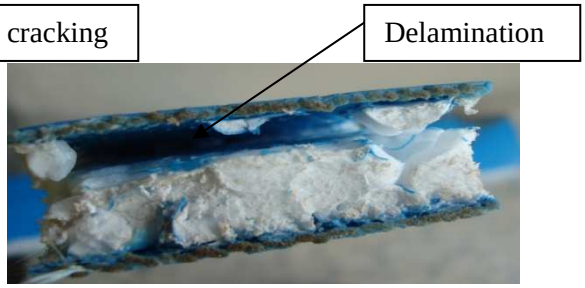

Fig.5.22 Shows condition of specimen of 8mm core thickness at 50% UFL

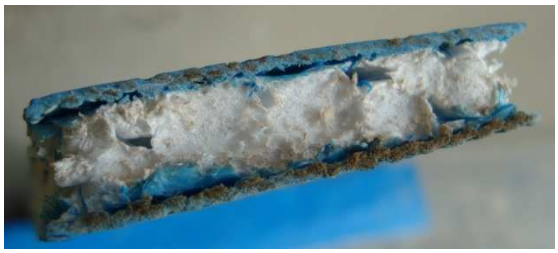

Fig.5.23 Shows condition of specimen of 8mm core thickness at 70% UFL

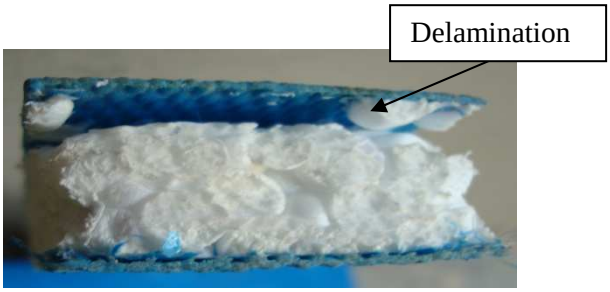

Fig.5.24 Shows condition of specimen of 16mm core thickness at 30% UFL

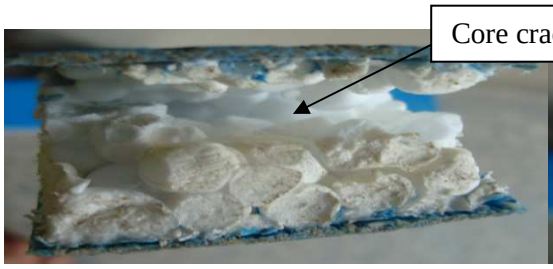

Fig.5.25 Shows condition of specimen of 16mm core thickness at 50% UFL

Fig.5.26 Shows condition of specimen of 16mm core thickness at 70% UFL

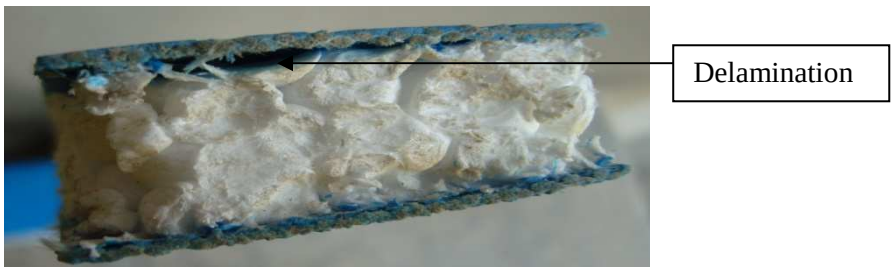

Fig.5.27 Shows condition of specimen of 16mm core thickness at without loading

Above figures (Fig 5.21 to Fig 5.27) are showing transverse view of specimen of different core thicknesses and different loading after 2 month. As per visual observation it was observed that core cracking and delamination occurred in thermocol sheet during the flexural testing almost in all bending preload specimen.

5.1.2 DETAILS OF RESULTS OF ALL SPECIMEN WITH RESPECT TO TIME AT EACH LOAD PERCENTAGE OF ULTIMATE FLEXURAL LOAD:

The results of bending load of all the specimen are shown as follows:-

5.1.2.1 Result for maximum flexure load after one month (Water at 45°C)

Holding parameters:

Plain water bath

Time: 1 month

Temperature: 45°C

A) Results of the specimen of 8mm core thicknesses which were subjected to 30%, 50% and 70% bending pre-loads after one month are shown below:

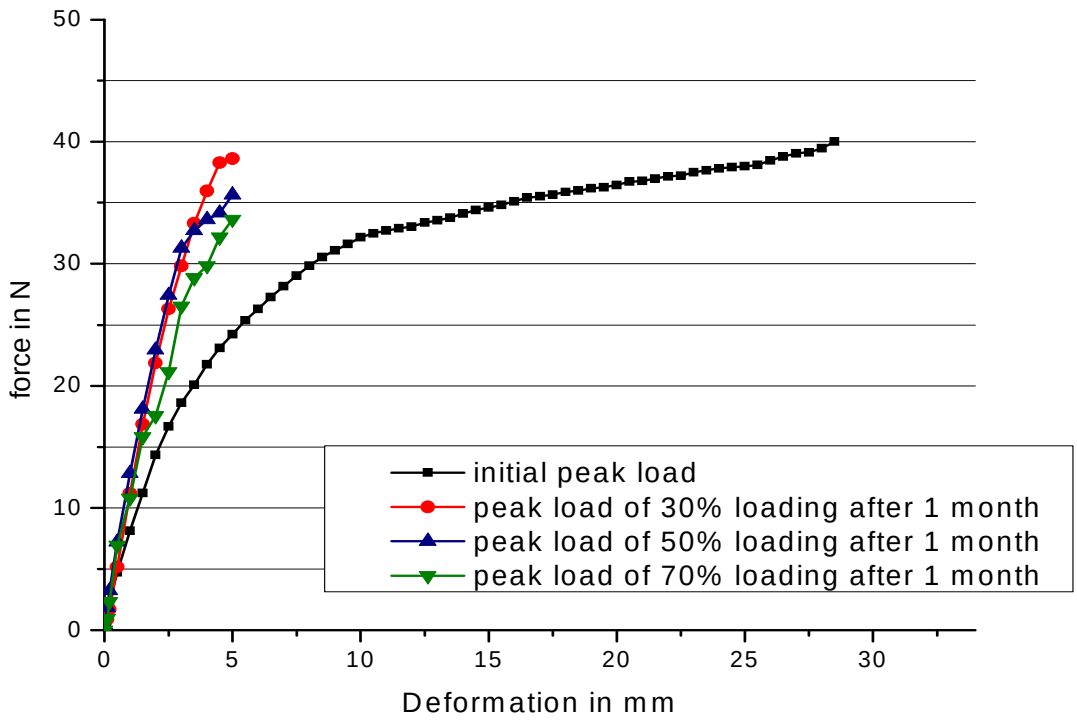

Fig.5.28 Graph showing peak load values of 30%, 50% and 70% loading **after 1 month** and initial peak load for 8mm core thickness specimen at 45°C

B) Results of the specimen of 16mm core thicknesses which were subjected to 30%, 50% and 70% bending pre-loads after one month are shown below:

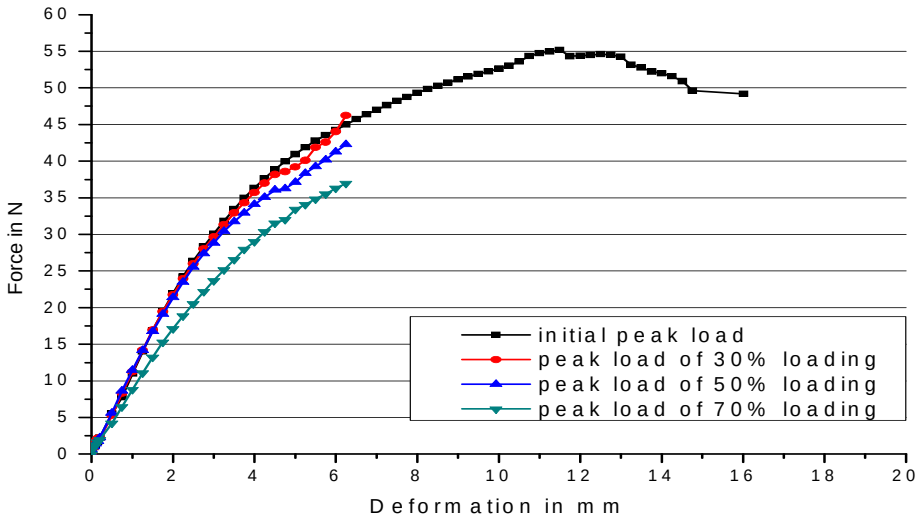

Fig.5.29 Graph showing peak load values of 30%, 50% and 70% loading **after 1 month** and initial peak load for 16mm core thickness specimen at 45°C

5.1.2.2 Result for maximum flexure load after one month (Normal water)

Holding parameters:

Plain water bath

Time: 1 month

Temperature: Normal water (Room temperature)

A) Results of the specimen (after one month) of 8mm core thicknesses which were subjected to 30%, 50% and 70% bending pre-loads are shown below:

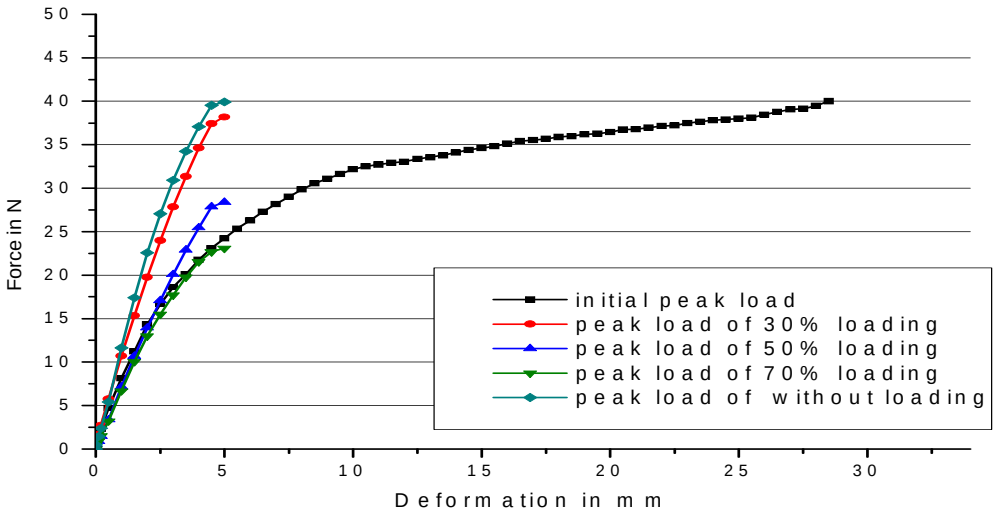

Fig.5.30 Graph showing peak load values of 30%, 50% and 70% loading **after 1 month** and initial peak load for 8mm core thickness specimen (Normal water at room temperature)

B) Results of the specimen (after one month) of 16mm core thicknesses which were subjected to 30%, 50% and 70% bending pre-loads are shown below:

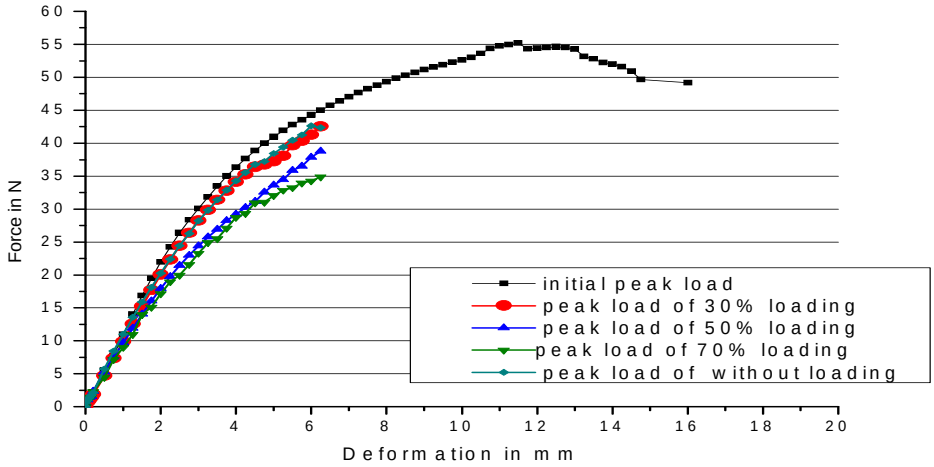

Fig.5.31 Graph showing peak load values of 30%, 50% and 70% loading **after 1 month** and initial peak load for 16mm core thickness specimen (Normal water at room temperature)

5.1.2.3 Result for maximum flexure load after two month (Water at 45°C)

Holding parameters:

Plain water bath

Time: 1 month

Temperature: 45°C

A) Results of the specimen (after 2 month) of 8mm core thicknesses which were subjected to 30%, 50% and 70% bending pre-loads are shown below:

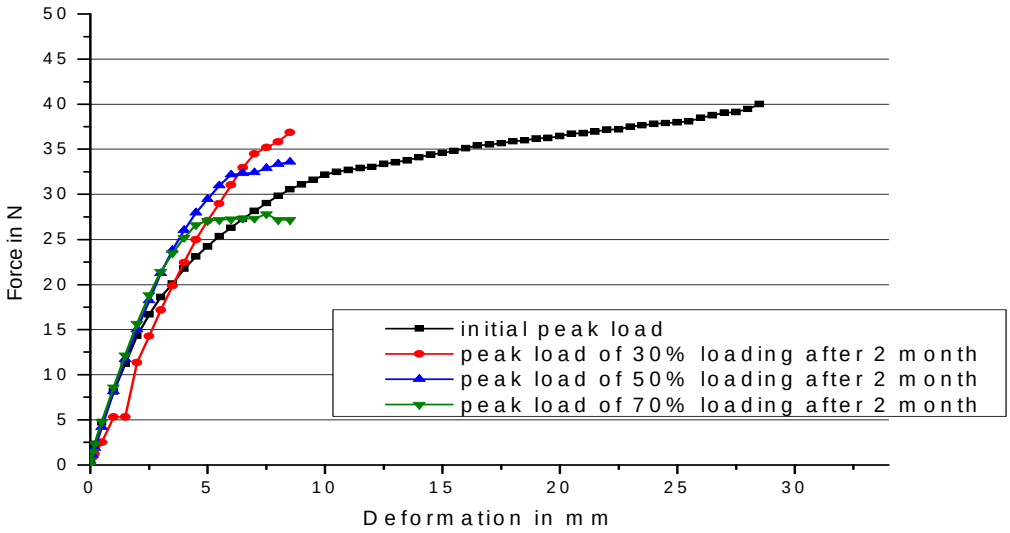

Fig.5.32 Graph showing peak load values of 30%, 50% and 70% loading **after 2 month** and initial peak load for 8mm core thickness specimen at 45°C

B) Results of the specimen (after 2 month) of 16mm core thicknesses which were subjected to 30%, 50% and 70% bending pre-loads are shown below:

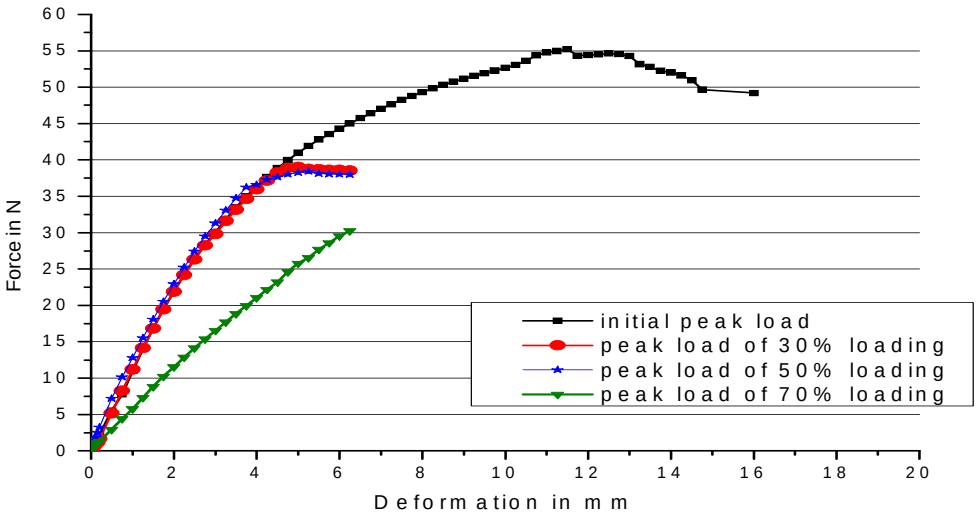

Fig.5.33 Graph showing peak load values of 30%, 50% and 70% loading **after 2 month** and initial peak load for 16mm core thickness specimen at 45°C

5.1.2.4 Result for maximum flexure load after two month (Normal water)

Holding parameters:

Plain water bath

Time: 1 month

Temperature: Normal water (Room temperature)

A) Results of the specimen (after one month) of 8mm core thicknesses which were subjected to 30%, 50% and 70% bending pre-load are shown below:

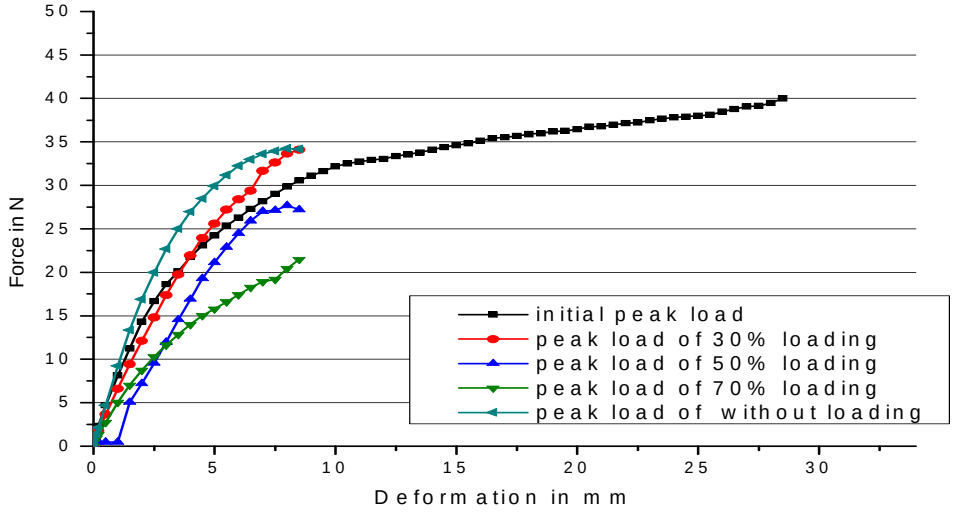

Fig.5.34 Graph showing peak load values of 30%, 50% and 70% loading **after 2 month** and initial peak load for 8mm core thickness specimen (Normal water at room temperature)

B) Results of the specimen (after 2 month) of 16mm core thicknesses which were subjected to 30%, 50% and 70% bending pre-loads are shown below:

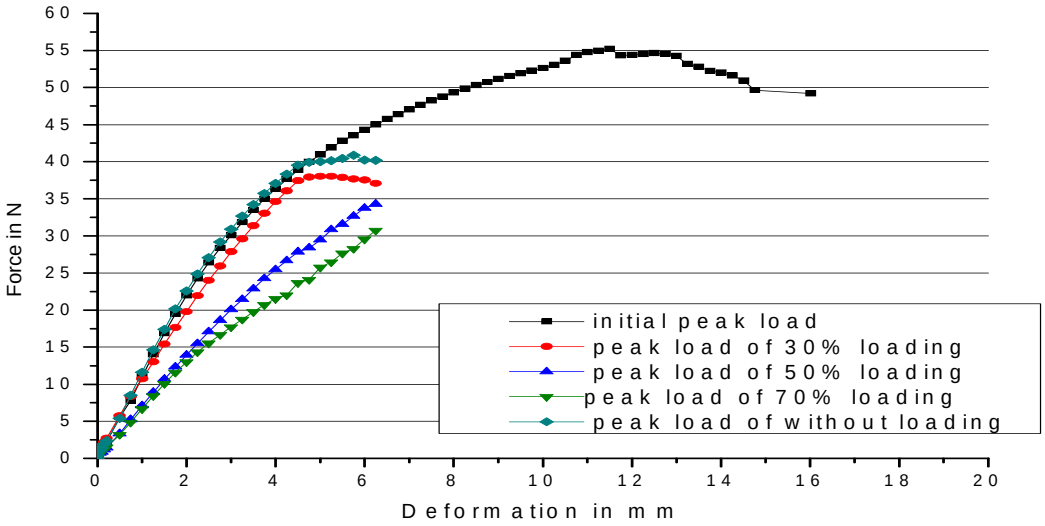

Fig.5.35 Graph showing peak load values of 30%, 50% and 70% loading **after 2 month** and initial peak load for 16mm core thickness specimen (Normal water at room temperature)

5.1.2.5 Comparison of Maximum flexure load after 1 and 2 month (specimen at 45°C)

1) 8mm core thickness specimen:

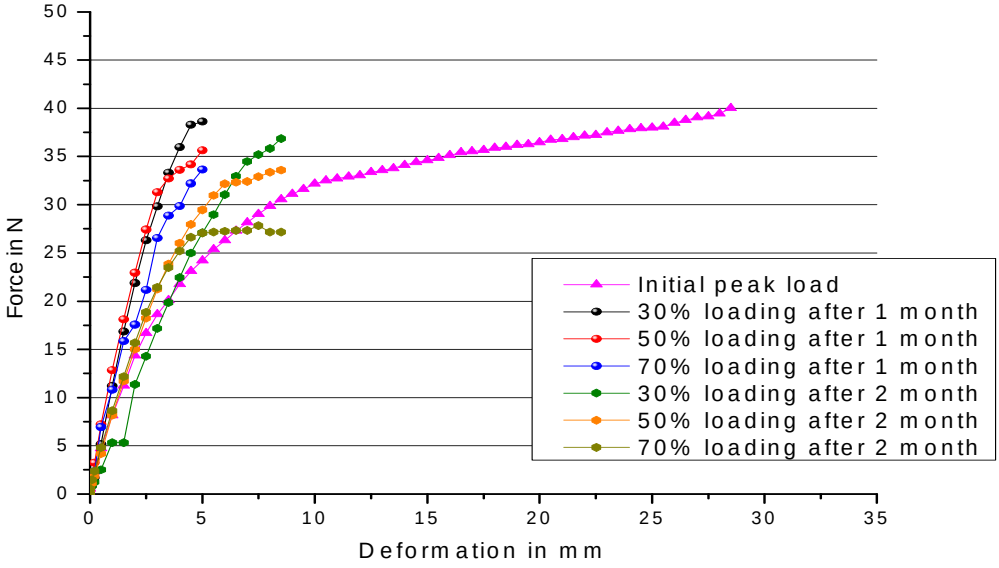

Fig.5.36 Graph showing initial peak load and ultimate load of 8 mm core thickness specimen of different loading with variation of time i.e. 1month and 2 month

2) 16mm core thickness specimen:

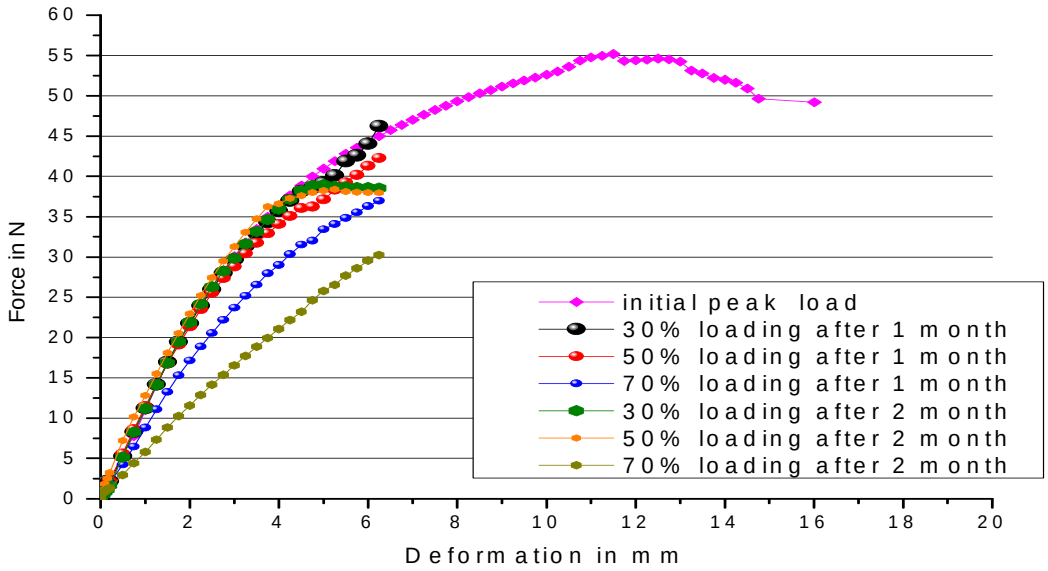

Fig.5.37 Graph showing initial peak load and ultimate load of 16 mm core thickness specimen of different loading with variation of time i.e. 1month and 2 month

5.1.2.6 Comparison of Maximum flexure load after 1 and 2 month (Specimen at room temperature)

1) 8mm core thickness specimen:

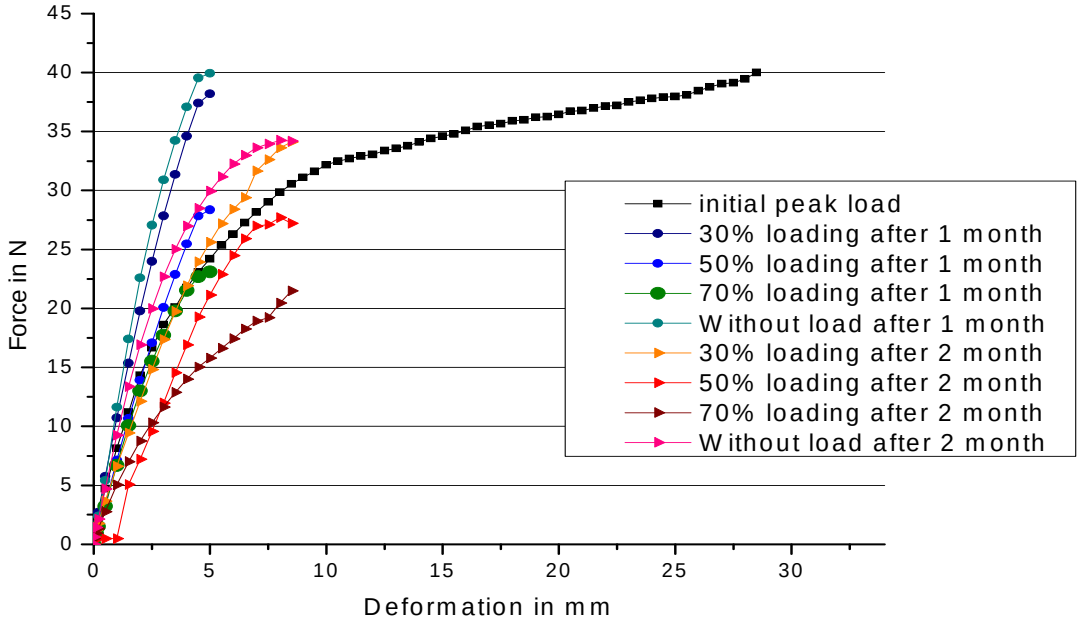

Fig.5.38 Graph showing initial peak load and ultimate load of 8 mm core thickness specimen of different loading with variation of time i.e. 1and 2 month (At room temperature)

2) 16mm core thickness specimen:

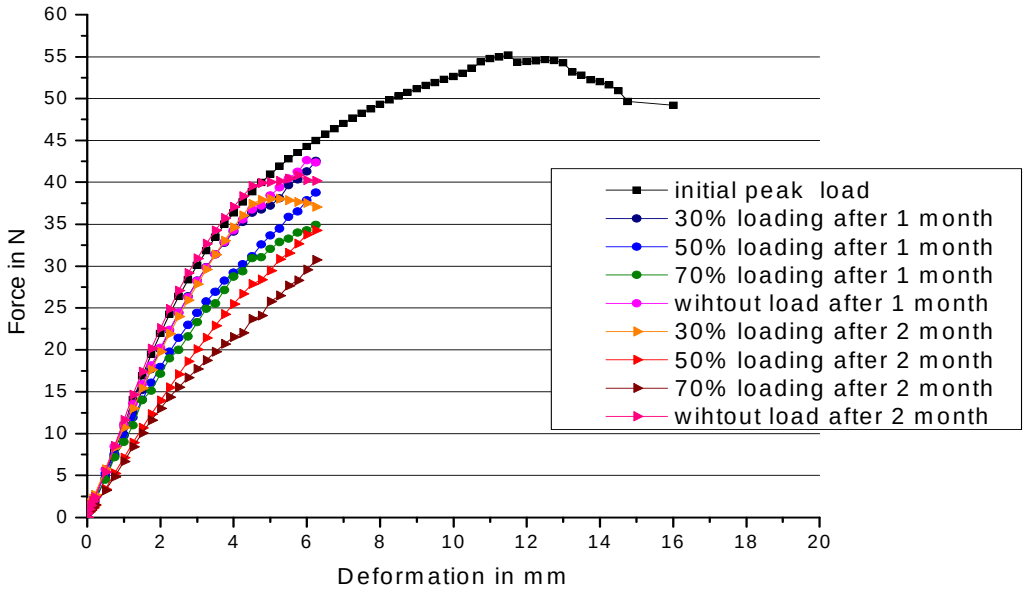

Fig.5.39 Graph showing initial peak load and ultimate load of 16 mm core thickness specimen of different loading with variation of time i.e. 1and 2 month (At room temperature)

5.1.3 EVALUATION AND DISCUSSION OF ALL RESULTS:

5.1.3.1 RESULTS OF MAXIMUM FLEXURE LOAD BEFORE AND AFTER EXPOSURE

Comparison of maximum flexure load applied in different loading specimen with respect to time is as follows:

Table T 5.1: Average maximum flexure load of different loaded specimen (8mm core thickness) with respect to time and water temperature

8mm core thickness specimen					
Loading	**Initial maximum Flexure load in (N)**	**Maximum Flexure load (Water at 45^0C) in (N)**		**Maximum Flexurel load (Water at room temperature) in (N)**	
		1 month	**2 month**	**1month**	**2month**
30%loading	40.000113	38.60891	36.1376305	38.19859	34.1093
50%loading	40.000113	35.62849	33.5877762	28.37029	27.2079
70%loading	40.000113	33.64071	27.8294182	23.10035	21.4892
without load	40.000113	--	--	39.92628	34.1747

Table T 5.2: Average maximum flexure load of different loaded specimen (16mm core thickness) with respect to time and water temperature

16mm core thickness specimen					
Loading	**Initial maximum Flexure load in (N)**	**Maximum Flexure load (Water at 45^0C) in (N)**		**Maximum Flexure load (Water at room temperature) in (N)**	
		1 month	**2 month**	**1month**	**2month**
30%loading	55.168911	46.23962	38.994321	42.54316	37.0624
50%loading	55.168911	42.27462	37.9945621	38.76243	34.2853
70%loading	55.168911	36.9624	30.23794312	34.89654	30.7236
without load	55.168911	--	--	42.37862	40.1678

WATER AT 45^0c

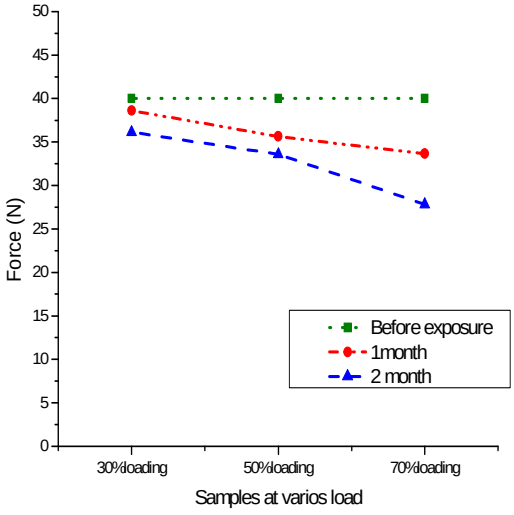

Fig.5.40 Comparison of maximum force at different loading after 1 and 2 month (8mm core)

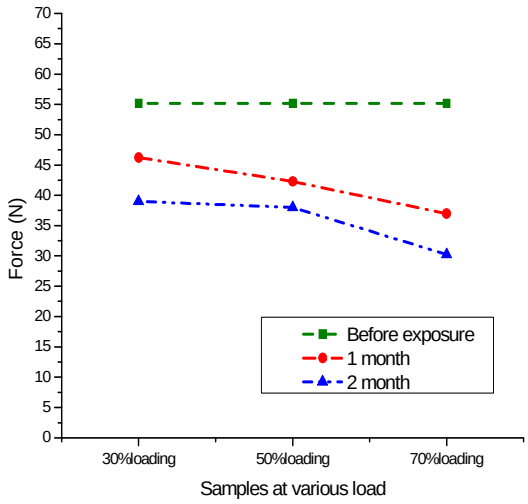

Fig.5.41 Comparison of maximum force at different loading after 1 and 2 month (16mm core)

WATER AT ROOM TEMPERATURE

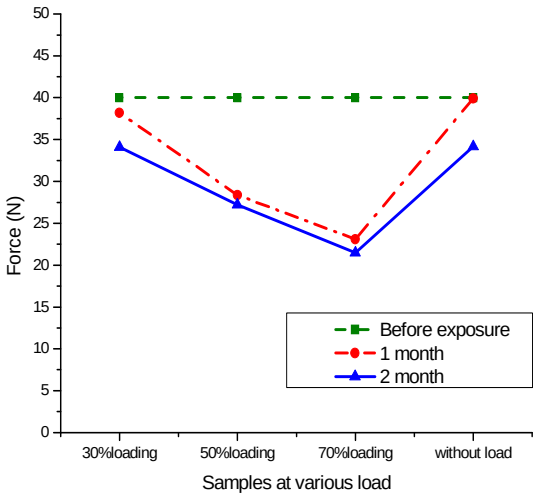

Fig.5.42 Comparison of maximum force at different loading after 1 and 2 month (8mm core)

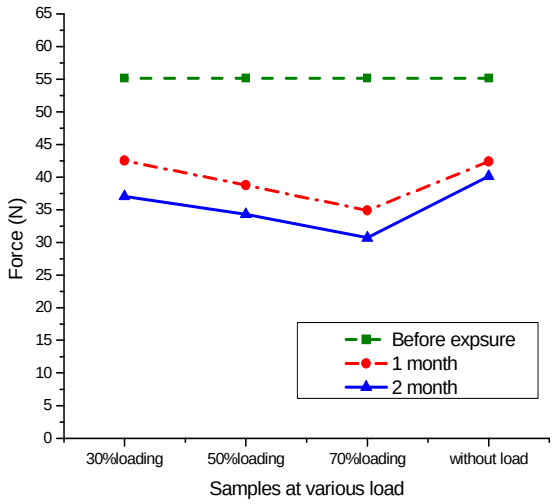

Fig.5.43 Comparison of maximum force at different loading after 1 and 2 month (16mm core)

DISCUSSION

A) **Effect of core thickness on maximum flexure load:**

The above graphs (Fig 5.40 to Fig 5.43) and table (T 5.1, T 5.2) show that maximum flexural load is more in 16mm core thickness as compared to 8mm core thickness specimen. It is also observed that the maximum flexure load is decreasing in both the core thickness specimen but drop in maximum flexure load in 16 mm core thickness specimen is more when compared with 8mm core thickness specimen immerged in water at both the temperatures (45°C and room temperature) with some exceptions. The drop in maximum force in 8mm core thickness after 2 month is 13N where as drop in 16mm core thickness is 25N.

B) **Effect of bending pre-loads on maximum flexure load:**

The drop in maximum flexure load is increasing with increase in bending preloads in both core thickness specimen. Above graphs are showing that decrease in maximum force in 70% bending pre-load in both the core thickness specimen is much higher than other bending pre-loaded specimen.

C) **Effect of time on maximum flexure load:**

The drop in maximum flexure load is increasing with respect to time period. Above graphs shows that decrease in maximum flexure load for each bending pre-load specimen of each core thickness is more in 2 month as compared to 1 month. Average drop in force in 8mm core after 1 and 2 month is 5N and 8.25N respectively whereas average drop in force for 16mm core after 1 and 2 month is 13.33N and 19.33N respectively.

Reason for the degradation in maximum force may be hygrothermal load becauce all the specimen were kept in water at 45°C for a specified time period, this results in softening of epoxy and degrdation in maximum force.

5.1.3.2 RESULTS OF ULTIMATE FLEXURAL STRENGTH (U.F.S.) AND PERCENTAGE CHANGE IN U.F.S.

WATER AT 45°C

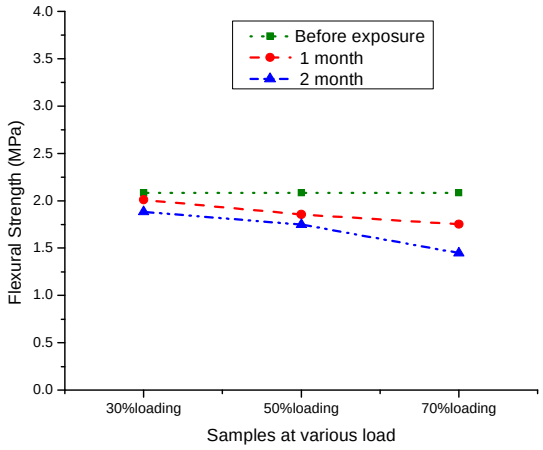

Fig.5.44 Graph showing flexural strength of 8mm core thickness specimen after 1 and 2 month

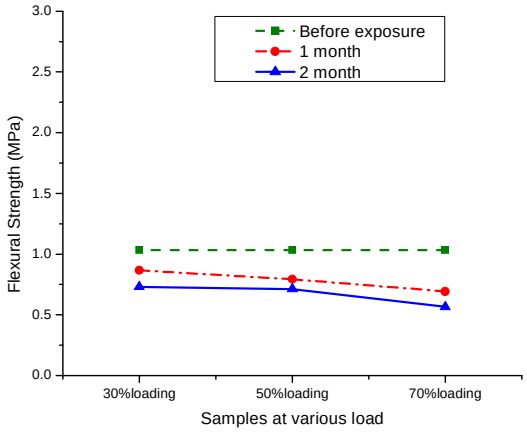

Fig.5.45 Graph showing flexural strength of 16mm core thickness specimen after 1 and 2month

WATER AT ROOM TEMPERATURE

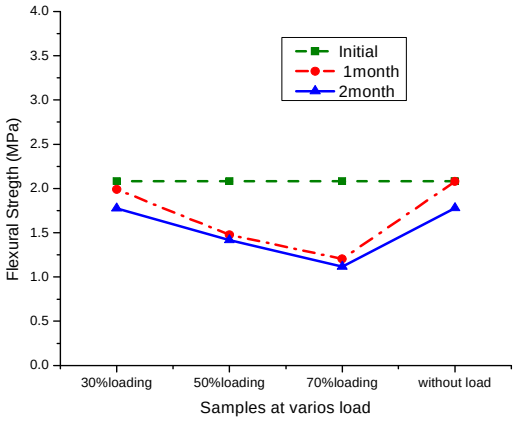

Fig.5.46 Graph showing flexural stress of 8mm core thickness specimen after 1 and 2 month

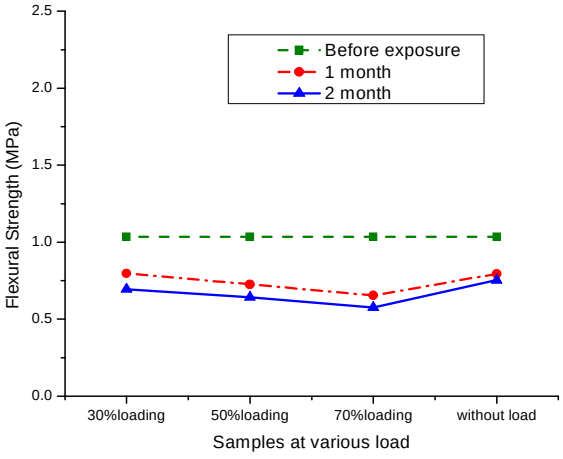

Fig.5.47 Graph showing flexural strength of 16mm core thickness specimen after 1 and 2 month

DISCUSSION

A) **Effect of core thickness on ultimate Flexural Strength:**

The above graphs (Fig 5.44 to Fig 5.47) show that the flexural strength of 16mm core thickness specimen is less as compared to 8mm core thickness specimen. It was also observed that there was marginal decrease in flexural strength of the specimen immersed in water at 45°C and room temperature for one month compared to that of Initial value. Further after two months drop in flexural Strength was less as compared to 1 month specimen in both the core thickness specimen.

B) **Effect of bending pre-loads on ultimate Flexural Strength:**

It was observed from above graph (Fig 5.44 to Fig 5.47) that decrease in strength in 70% bending pre-load specimen was more as compared to 30% and 50% bending pre-load specimen in both core thicknesses. Flexural strength was decreasing due to decrease in maximum applied force. Average decrease in flexural strength in 70% loading in 8mm core thickness was 16MPa whereas in 50% and 30% bending pre -load it was 11MPa and 3.35MPa. In 16mm core thickness average decrease in flexural strength for 70% loading was 33.5N whereas for 50% and 30% bending pre-load it was 23.23MPa and 15.86MPa. It was also observed that degradation in flexural strength was less in without loading specimen as compared to bending pre-loaded specimen. The drop in strength was increasing with increase in bending pre-loads in 8mm core specimen where as in 16mm core drop was similar.

C) **Effect of time on Flexural Strength:**

It was observed from the above graphs that flexural stress in both the core thicknesses and each bending pre-load specimen is decreasing with increasing time. Decrease in flexure strength after 2 month of exposure is more as compared to 1 month and before exposure values.

PERCENTAGE DECREASE IN FLEXURAL STRENGTH:

For calculation of bending strength refer section 4.7.1. Bending moment of 16mm core thickness and 8mm core thickness specimen are shown in table T 5.3 and T 5.4.

Value of Section Modulus (Z) for 16mm core thickness specimen is $2.76*10^{-6}$ N/m^3
Value of Section Modulus (Z) for 8mm core thickness specimen is $0.962*10^{-6} N/m^3$

Table T 5.3: Bending moment of 16mm core specimen at 45°C and room temperature

Bending moment M in (N.m) (16mm core thickness)					
loading	Initial	Water at 45°C		Water at room temperature	
		1 month	2 month	1 month	2 month
30% loading	2.76	2.312	1.952	2.127	1.853
50% loading	2.76	2.113	1.9025	1.9382	1.714
50% loading	2.76	1.848	1.512	1.7448	1.536
Without load	2.76			2.118	2.008

Table T 5.4: Bending moment of 8mm core specimen at 45°C and room temperature

Bending moment M in (N.m) (8mm core thickness)					
loading	Initial	Water at 45°C		Water at room temperature	
		1 month	2 month	1 month	2 month
30% loading	2	1.9304	1.806	1.909	1.705
50% loading	2	1.7442	1.679	1.418	1.36
50% loading	2	1.682	1.391	1.155	1.074
Without load	2			1.996	1.708

Table T 5.5: Decrease in flexural strength in 8mm core specimen at 45°C

8mm core thickness specimen					
Loading	Initial flexural stress (MPa)	Flexural strength after 1month (MPa)	percentage decrease in flexural strength (1 month)	Flexural strength after 2month (MPa)	Percentage decrease in flexural strength (2 month)
30%loading-1	2.08	2.01	3.48	1.88	9.66
30%loading-2	2.08	2.01	3.36	1.87	10.07
50%loading-1	2.08	1.86	10.93	1.75	16.03
50%loading-2	2.08	1.85	11.11	1.74	16.66
70%loading-1	2.08	1.75	16.18	1.44	30.75
70%loading-2	2.08	1.75	15.90	1.45	30.43

Table T 5.6: Decrease in flexure strength in 16mm core specimen time at 45°C

16mm core thickness specimen					
Loading	Initial flexural strength (MPa)	Flexural strength after 1month (MPa)	Percentage decrease in flexural strength (1 month)	Flexural strength after 2month (MPa)	Percentage decrease in flexural strength (2 month)
30%loading-1	1.03	0.87	16.19	0.73	29.61
30%loading-2	1.03	0.87	15.47	0.73	29.32
50%loading-1	1.03	0.79	23.37	0.72	30.73
50%loading-2	1.03	0.78	24.26	0.71	31.13
70%loading-1	1.03	0.69	33.00	0.55	46.49
70%loading-2	1.03	0.67	34.98	0.57	45.19

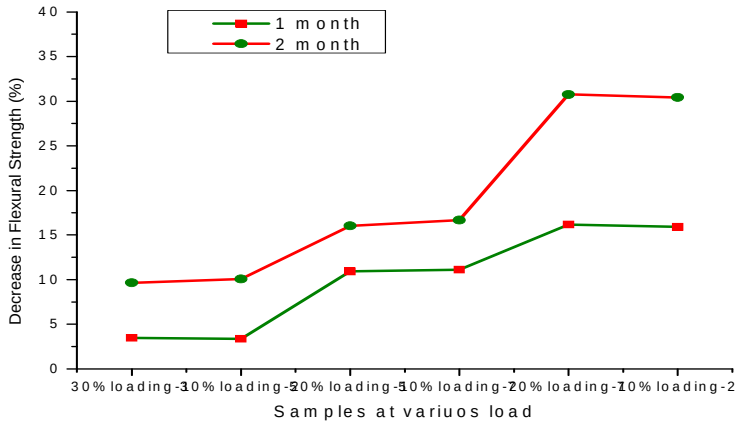

Fig.5.48 Comparison of percentage decrease in flexural strength with respect to time in 8mm core thickness specimen.

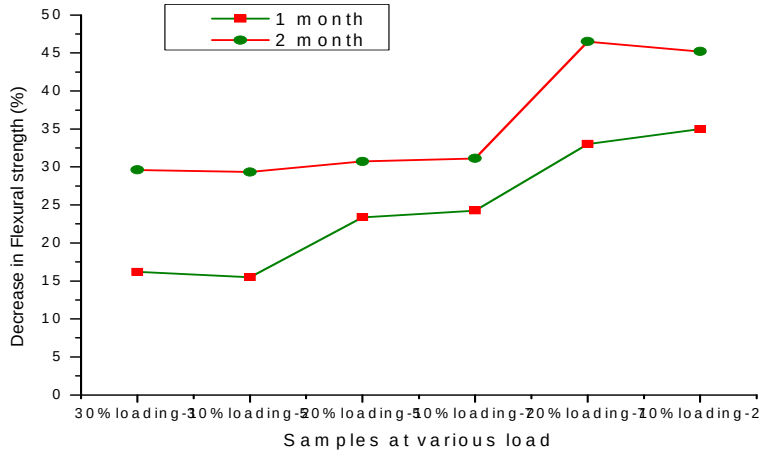

Fig.5.49 Comparison of percentage decrease in flexural strength with respect to time in 16mm core thickness specimen

The trend in decrease in flexural strength is shown in table (T 5.5, T 5.6) and graph (Fig 5.48, Fig 5.49). The flexural strength reduction is more in 16mm core thickness specimen as compared to 8mm core thickness specimen and also in 2 month when compared to 1 month.

It was also noticed that drop in strength in specimen 70% bending pre-load was more in both core thicknesses as compared to other bending pre-load specimen. Maximum decrease in strength in 8mm core thickness specimen is 30% in two months whereas in 16mm core thickness specimen it is 46.49%.

The reason for decrease in ultimate flexural strength and change in percentage flexural strength seems to be the continuous degradation done by hygrothermal load which affected the matrix and fibre strength.

5.1.3.3 RESULTS OF ULTIMATE FLEXURE MODULUS AND PERCENTAGE CHANGE IN FLEXURAL MODULUS

The comparison of the ultimate flexural modulus load wise with respect to time is as follows:

WATER AT 45°C

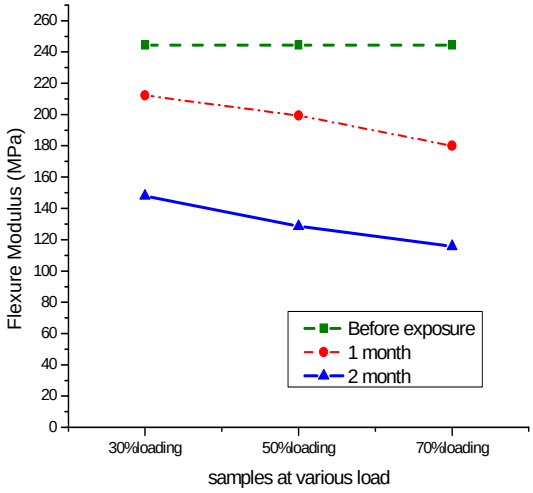

Fig.5.50 Graph showing flexure modulus of 8mm core thickness specimen after 1 month and 2 month

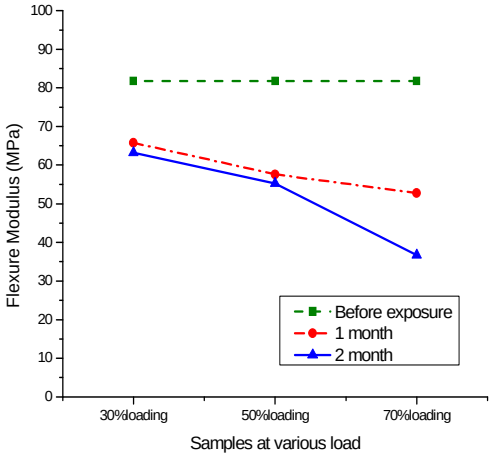

Fig.5.51 Graph showing flexure modulus of 16mm core thickness specimen after 1month and 2 month

WATER AT ROOM TEMPRETAURE

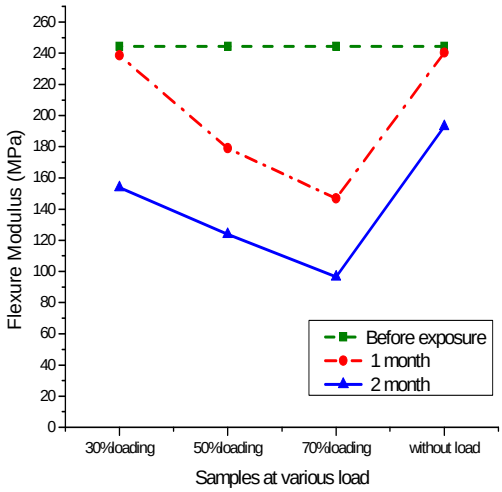

Fig.5.52 Graph showing flexure modulus of 8mm core thickness specimen after 1month and 2 month

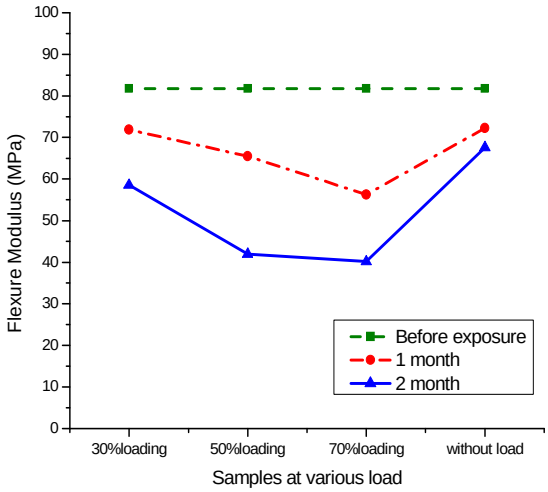

Fig.5.53 Graph showing flexure modulus of 16mm core thickness specimen after 1month and 2 month

PERCENTAGE DECREASE IN FLEXURAL MODULUS:

Table T 5.7: Decrease in flexure modulus in 8mm core specimen at 45°C

8mm core thickness specimen					
Loading	**Initial flexural strength (MPa)**	**Flexure modulus after 1month (MPa)**	**%decrease in flexure modulus (1month)**	**Flexure modulus after 2month (MPa)**	**%decrease in flexure modulus (2month)**
30%loading-1	244.34	212.19	13.16	147.89	39.47
30%loading-2	244.34	211.36	13.50	147.54	39.62
50%loading-1	244.34	199.33	18.42	128.60	47.37
50%loading-2	244.34	200.01	18.14	128.23	47.52
70%loading-1	244.34	180.04	26.32	115.74	52.63
70%loading-2	244.34	180.61	26.08	114.97	52.95

Table T 5.8: Decrease in flexure modulus in 16mm core specimen at 45°C

16mm core thickness specimen					
Loading	**Initial flexural strength (MPa)**	**Flexure modulus after 1month (MPa)**	**%decrease in flexure modulus (1month)**	**Flexure modulus after 2month (MPa)**	**%decrease in flexure modulus (2month)**
30%loading-1	81.75	65.75	19.57	63.25	22.63
30%loading-2	81.75	65.68	19.66	64.76	20.78
50%loading-1	81.75	57.63	29.50	64.25	21.41
50%loading-2	81.75	56.94	30.35	60.85	25.57
70%loading-1	81.75	52.75	35.47	36.70	55.11
70%loading-2	81.75	52.7	35.54	36.42	55.45

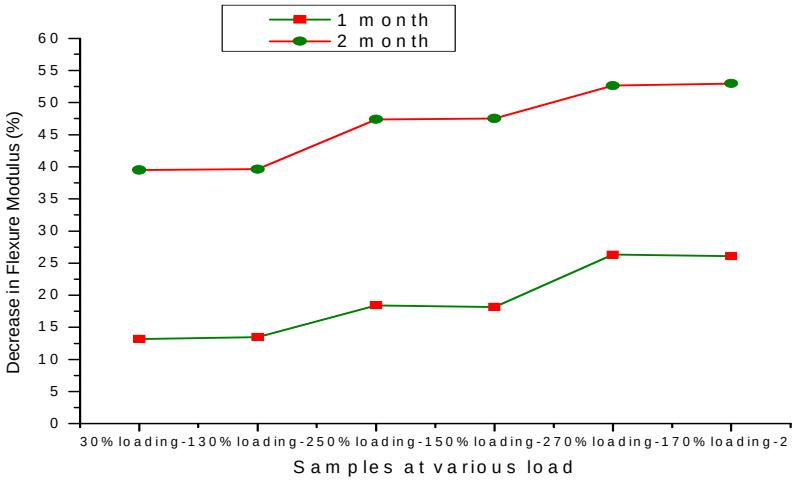

Fig.5.54 Comparison of percentage decrease in flexure modulus with respect to time in 8mm core thickness specimen.

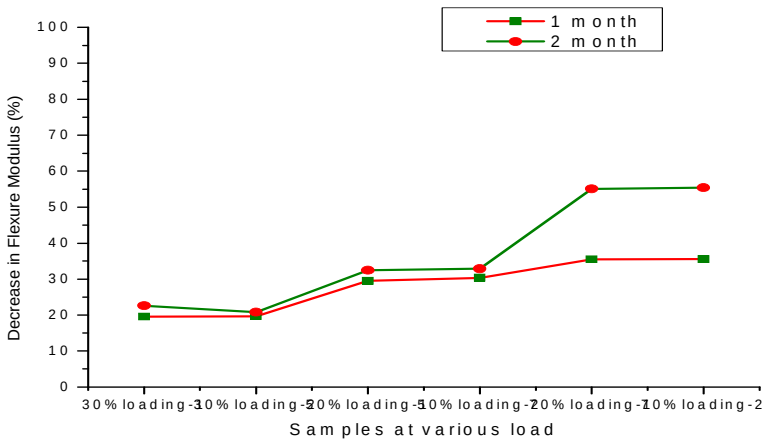

Fig.5.55 Comparison of percentage decrease in flexure modulus with respect to time in 16mm core thickness specimen.

DISCUSSION

A) Effect of core thickness on Flexure Modulus:

Above graphs (Fig 5.50 to Fig 5.53) and table (T 5.7 and T 5.8) show change in flexure modulus with respect to time of each specimen subjected to bending pre-load and those at immersed in water at 45°C and room temperature. Flexure modulus of 8mm core thickness specimen is higher as compared to 16mm core thickness. Drop in flexure modulus in 16mm core thickness specimen is increasing whereas almost constant in 8mm core thickness specimen. Average reduction in 16mm core thickness in 2nd month is 33.49% whereas in 8mm core thickness specimen it is 46.59%.

B) Effect of bending pre-loads on Flexure Modulus:

The above graphs (Fig 5.50 to Fig 5.55) and table (T 5.7, T 5.8) show that drop in flexure modulus is increasing with increasing bending pre-loads. Decrease in flexural modulus in 70% bending pre-load specimen is more when compared with other preloaded specimen of each core thickness.

C) Effect of time on Flexure Modulus:

It is observed from the above graphs (Fig 5.50 and Fig 5.55) that flexure modulus of 8mm and 16mm core thickness specimen is decreasing with respect to time. Decrease in flexure modulus in 2 month of exposure is considerably high as compared to 1 month of exposure. In 16mm core thickness specimen drop of flexure modulus is increasing with time where as in 8mm core thickness specimen drop of flexure modulus is almost constant.

Reason for decrease in flexural modulus may be softening of epoxy due to hygrothermal load because it is observed that the micro hardness of each specimen is decreasing with respect to time. Softening of matrix leads to lose stiffness of specimen which results in decrease in flexure modulus.

5.1.3.4 RESULTS OF PERCENTAGE WEIGHT GAIN IN SPECIMEN:

Change in weight gain of different core thickness and different loading specimen with respect to time are shown below in table T 5.9:

Table T 5.9: Change in weight of different specimen with respect to time

16mm core thickness				**16mm core thickness**			
Loading	**Initial weight**	**Weight after 10 days**	**%weight gain**	**Loading**	**Initial weight**	**Weight after 20 days**	**%weight gain**
30%	39.7478	39.7556	**0.019624**	30%	40.3432	43.2576	**7.224018**
50%	38.7188	38.7423	**0.060694**	50%	40.582	42.6144	**5.008132**
70%	38.4838	38.5743	**0.235164**	70%	41.4758	42.9593	**3.576785**
without load	43.1522	43.1974	**0.104746**	without load	38.882	41.4032	**6.484234**
8mm core thickness				**8mm core thickness**			
30%	41.4854	41.5702	**0.204409**	30%	37.9112	40.318	**6.34852**
50%	39.0505	39.1375	**0.222788**	50%	40.1919	43.1223	**7.291021**
70%	41.9201	41.9836	**0.151479**	70%	42.7236	43.6163	**2.089477**
without load	41.3685	41.4044	**0.086781**	without load	39.8202	42.7942	**7.468571**
16mm core thickness				**16mm core thickness**			
Loading	**Initial weight**	**Weight after 30 days**	**%weight gain**	**Loading**	**Initial weight**	**Weight after 40 days**	**%weight gain**
30%	40.0769	43.227	**7.860139**	30%	37.6559	40.78	**8.296442**
50%	40.1515	42.434	**5.684719**	50%	37.9974	40.313	**6.094101**
70%	37.0835	38.542	**3.933016**	70%	40.0162	42.077	**5.149914**
without load	40.0658	42.829	**6.896655**	without load	39.8634	42.896	**7.60748**
8mm core thickness				**8mm core thickness**			
30%	37.5048	40.1712	**7.10949**	30%	38.6383	41.793	**8.164697**
50%	38.1198	41.0513	**7.690229**	50%	39.4889	42.643	**7.987308**
70%	38.9645	39.807	**2.162225**	70%	43.5892	45.791	**5.051251**
without load	37.6813	40.5994	**7.74416**	without load	44.1948	48.056	**8.736774**
16mm core thickness				**8mm core thickness**			
Loading	**Initial weight**	**Weight after 50 days**	**%weight gain**	**Loading**	**Initial weight**	**Weight after 50 days**	**%weight gain**
30%	39.6715	43.796	**10.39663**	30%	42.5595	46.711	**9.754579**
50%	38.9907	42.153	**8.110396**	50%	39.8923	44.018	**10.3421**
70%	40.3836	43.508	**7.736804**	70%	37.5835	41.0736	**9.286256**
without load	34.5469	37.87	**9.619098**	without load	39.8686	43.738	**9.705382**

One specimen of each core thickness and each loading was kept in water at 45°C to check percentage weight gain and moisture diffusivity of same specimen after interval of each 3 days. Table T 5.8 is showing percentage weight gain of different specimen with respect to increment of 3 days time period. Moisture diffusivity of these specimen is shown in table T 5.11 and T 5.12.

Table T 5.10: Change in weight of different specimen after each 3 day

8 mm core thickness(Percentage weight gain)									
Loading	**Initial weight**	**Weight after 3 day**	**% weight gain (3day)**	**Weight after 6 day**	**% weight gain (6day)**	**Weight after 9 day**	**% weight gain (9day)**	**Weight after 12 day**	**% weight gain (12day)**
30%	41.4850	41.59	0.2531	42.7910	3.1481	44.1360	6.3903	44.2640	6.69
50%	39.0500	39.14	0.2228	40.9290	4.8118	42.1990	8.0640	42.5910	9.07
70%	41.9200	41.98	0.1431	43.0880	2.7863	44.0610	5.1073	44.5870	6.36
Without Load	41.3680	41.40	0.0870	42.7380	3.3117	43.8000	5.8789	43.8430	5.98
16mm core thickness (Percentage weight gain)									
Loading	**Initial weight**	**Weight after 3 days**	**% weight gain (3days)**	**Weight after 6 days**	**% weight gain (6days)**	**Weight after 9 days**	**% weight gain (9days)**	**Weight after 12 days**	**% weight gain (12day)**
30%	39.7478	39.957	0.5263	41.031	3.2284	42.414	6.7078	42.892	7.91
50%	38.719	38.741	0.0568	39.344	1.6142	40.573	4.7883	42.207	9.01
70%	38.484	38.574	0.2339	40.185	4.4200	41.404	7.5876	42.676	10.89
Without Load	43.152	43.197	0.1043	44.505	3.1354	47.394	9.8304	47.652	10.43

***** The time variation of percentage weight gain (w_t) can be measured as:

$$w_t = \frac{W(t) - W_0}{W_0} \times 100 \qquad \text{..... (5.5)}$$

Here $W(t)$ is the total weight after time t

W_0 is the reference dry weight of the specimen before immersion in medium.

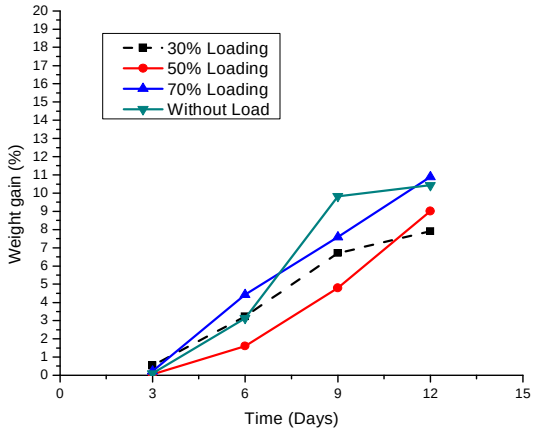

Fig.5.56 Graph showing % weight gain in 8mm core thickness specimen after interval of 3 days

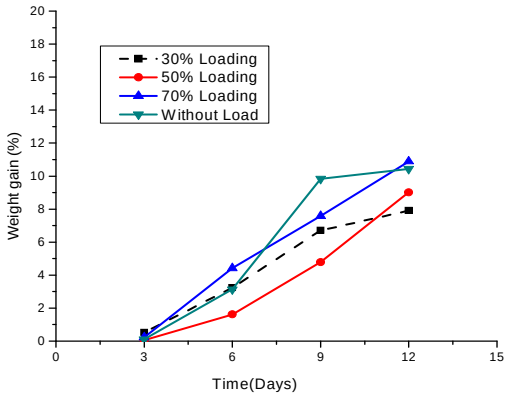

Fig.5.57 Graph showing % weight gain in 16mm core thickness specimen after interval of 3 days

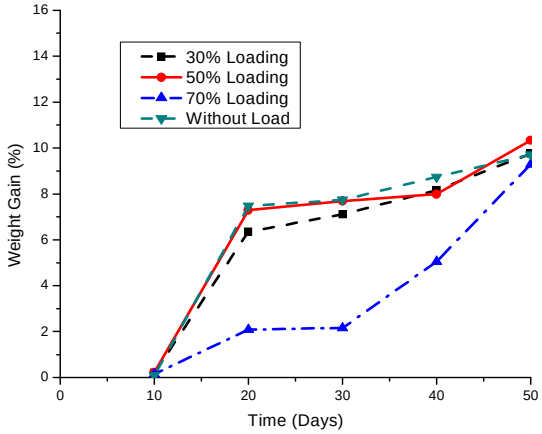

Fig.5.58 Graph showing %weight gain in specimen of 8mm core thickness after interval of 10 days

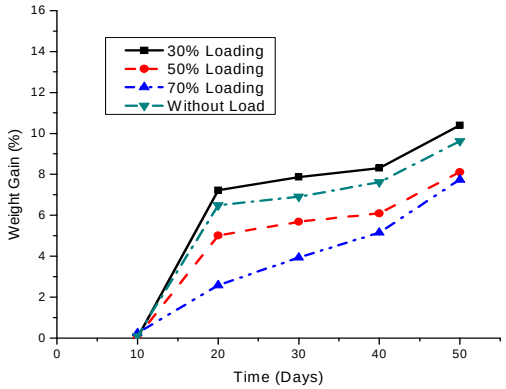

Fig.5.59 Graph showing %weight gain in specimen of 16mm core thickness after interval of 10 days

DISCUSSION

A) Effect of core thickness on weight gain:

Above graphs (Fig 5.56 to Fig 5.59) and table (T 5.9, T5.10) show percentage weight gain in both the core thickness specimen with respect to time. The percentage weight gain (of moisture) was compared for different thickness and different bending pre-load. It could be easily noticed that the trend of percentage weight gain in both the core thickness is almost similar with time.

B) Effect of bending pre-loads on weight gain:

It is observed from above figures and tables that the weight gain in 30% bending pre-load specimen is higher as compared to 50% and 70% bending pre-load specimen with some exceptions in 8mm core thickness specimen. Maximum percentage gain in 30% bending pre-load specimen is 9.55% after 50 days. Change in percentage weight gain in

8mm core thickness is varying for different bending pre-loads whereas in 16mm core thickness it is almost constant for all bending pre-load specimen.

C) Effect of time on weight gain:

It is observed from above graphs that percentage weight gain is increasing with time. It was also observed from the graphs that more moisture absorbed as the number of days increased in almost all the specimen with few exceptions. It was also observed that in both the core thicknesses up to 10 days percentage weight gain was not very high but within 10 to 20 days the percentage weight gain was higher.

The above behaviour could be explained by the following reasons:

One of the reasons for the weight gain may be absorption. Absorption occurs through capillary uptake through voids, micro cracks and interface gaps, resulting in the filling of free space with water and increasing its weight. The other could be adsorption, because temperature of water was 45°C due to which as time passes swelling in epoxy takes place because of heat and with time the pores of epoxy will loosen, giving way to moisture.

Other reason could be the weight gain in thermocol core, with time as the cracks and pours in thermocol could be filled by water.

5.1.3.5 RESULTS OF APPARENT MOISTURE DIFFUSIVITY

Moisture diffusivity depends upon the mass flow rate of moisture in specimen with respect to time. To know better results one specimen of each core thickness and each loading was taken and kept into water at 45°C and the response of weight gain and moisture diffusivity of each specimen in every 3 alternative days was observed. Table showing change in moisture diffusivity is following:

Table T 5.11: Change in moisture diffusivity of 8mm core thickness specimen with time

8 mm core thickness(moisture Diffusivity in mm^2/s)								
Loading	**3 days**	**6 days**	**10 days**	**12 days**	**20 days**	**30 days**	**40 days**	**50 days**
30%loading	0.47909	0.23955	0.14373	0.11998	0.06002	0.03916	0.03119	0.02551
50%loading	0.4245	0.21225	0.14735	0.10631	0.06745	0.04045	0.03256	0.02241
70%loading	0.48919	0.24459	0.14676	0.12252	0.07622	0.04226	0.03967	0.01989
Without load	0.47639	0.23819	0.14292	0.11931	0.06621	0.03953	0.04078	0.02238

Table T 5.12: Change in moisture diffusivity of 16mm core thickness specimen with time

16 mm core thickness(Moisture Diffusivity in mm^2/s)								
Loading	**3 days**	**6 days**	**10 days**	**12 days**	**20 days**	**30 days**	**40 days**	**50 days**
30%loading	1.25327	0.62663	0.37597	0.31388	0.19367	0.12741	0.08414	0.06315
50%loading	1.8923	0.59462	0.35677	0.29784	0.19524	0.12789	0.08589	0.06100
70%loading	1.74838	0.58742	0.35245	0.29423	0.12047	0.10909	0.09527	0.06544
Without load	1.47713	0.73857	0.42414	0.36994	0.17989	0.12734	0.09457	0.04789

Apparent moisture diffusivity D can be determined as [48]:

$$D = \pi \left(\frac{h}{4M_m}\right)^2 \left(\frac{M_2 - M_1}{\sqrt{t_2} - \sqrt{t_1}}\right)^2 \left(1 + \frac{h}{L_e} + \frac{h}{w}\right)^{-2} \quad \text{..... (5.6)}$$

Where;

h- Thickness of the specimen which is 12mm and 20mm
L_e-Length of the specimen i.e. 300mm
w- Width of the specimen i.e. 40mm
M_m- Percentage weight gain,
M_1- Moisture content after time t_1,
M_2- moisture content after time t_2

For M_m, M_1 and M_2 refer table T5.7 and T 5.8

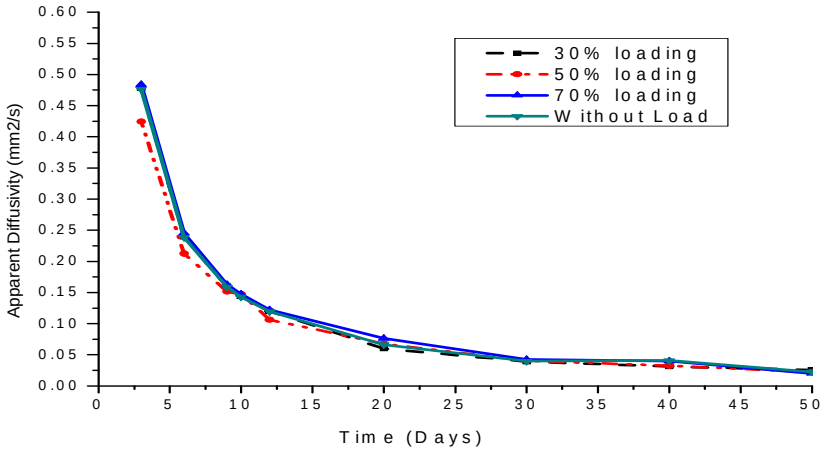

Fig.5.60 Graph showing change in apparent moisture diffusivity in 8mm core specimen w.r.t. time

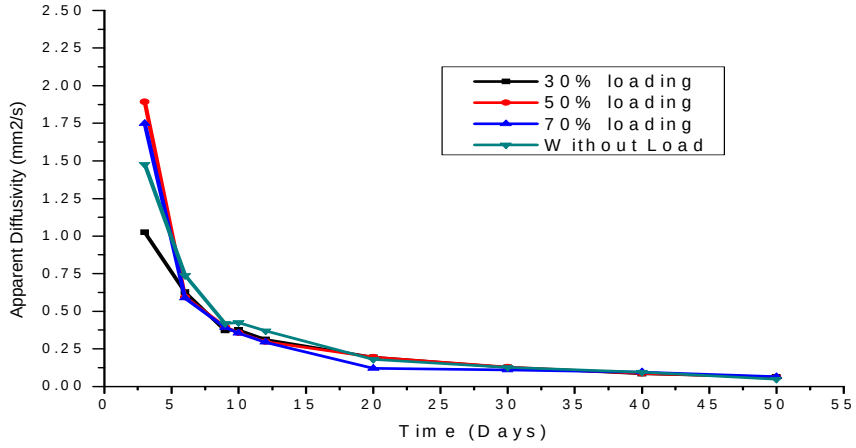

Fig.5.61 Graph showing change in apparent moisture diffusivity in 16mm core specimen w.r.t. time

DISCUSSION

A) Effect of core thickness on apparent moisture diffusivity:

Above graphs (Fig 5.60, Fig 5.61) and table (T 5.11, T 5.12) show trend of change in moisture diffusivity with respect to time. Graphs show that difusivity of 16mm core thickness specimen is more as compared to 8mm core thickness specimen. Change in moisture diffusivity in both the core thickness is almost same.

B) Effect of bending pre-loads on apparent moisture diffusivity:

Bending pre-load does not effect more in drop in apparent moisture diffusivity with respect to time. Change in moisture diffusivity is almost same in all bending pre-load specimen of both core thicknesses.

C) Effect of bending pre-load on apparent moisture diffusivity: Graphs show that moisture diffusivity is decreasing with respect to time in both the core thickness specimen and it is almost constant after 30 days. Decrease in diffusity is decreasing as time passes. It is relatively high during 3 to 6 days.

Reason for decrease in moisture diffusivity is due to increase in percentage weight gain with time.

5.2 MICROSCOPIC BEHAVIOUR

5. 2.1 RESULTS OF MICRO HARDNESS:

The Vickers hardness test or the 136 degree diamond pyramid hardness test is a micro-indentation method. The indenter produces a square indentation, the diagonals of which are measured. Vickers's Hardness Number (VHN) can be found directly from the Vickers's Hardness Testing machine. In that machine first of all an indent was made on the surface of specimen by applying force of 200gm with the help of indenter for dwell time of 20s. Average of 3 readings in each specimen at different places was taken.

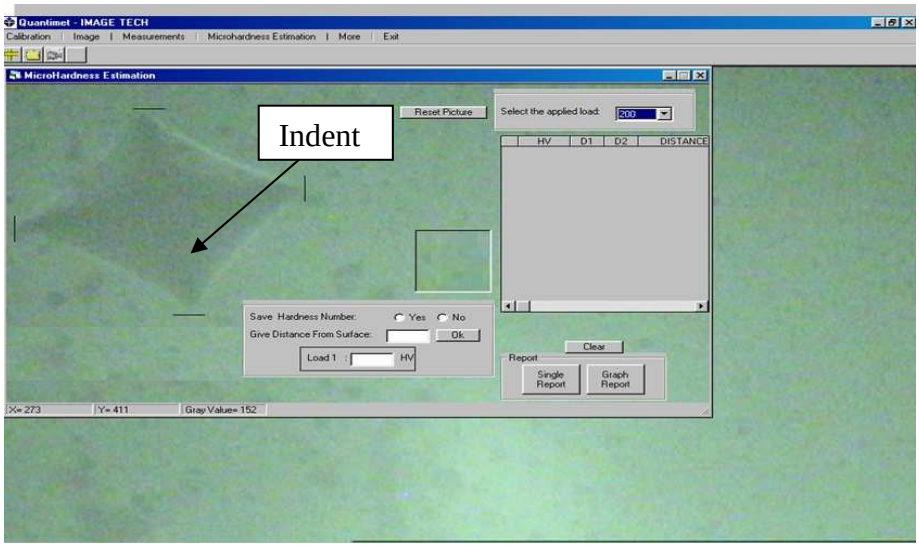

Fig. 5.62 VHN directly found from QUANTIMET micro hardness analysis software

Table T 5.13: Average and Vickers's Hardness Number of 8mm core thickness specimen

Average Vickers's Hardness Number (8mm core)										
Loading	**Initial**	**3 days**	**6 days**	**9 days**	**10 days**	**12 days**	**20 days**	**30 days**	**40 days**	**50 days**
30% loading	16.518	14.937	11.123	9.819	11.526	9.268	11.291	9.399	8.634	7.525
50% loading	17.432	13.811	11.097	10.346	11.737	9.823	11.060	10.604	10.141	9.071
70% loading	18.042	15.974	13.630	10.749	13.626	9.816	12.485	10.186	10.094	10.063
without load	18.009	12.418	10.691	10.852	13.487	10.169	12.123	8.444	7.806	7.932

Table T 5.14: Average Vickers's Hardness Number of 16mm core thickness specimen

Average Vickers's Hardness Number (16mm core)										
Loading	**Initial**	**3 days**	**6 days**	**9 days**	**10 days**	**12 days**	**20 days**	**30 days**	**40 days**	**50 days**
30% loading	16.073	14.973	12.814	9.455	11.273	9.231	10.762	10.217	10.138	9.517
50% loading	17.425	13.758	10.883	9.129	11.448	8.820	10.789	10.778	9.365	9.110
70% loading	18.196	15.424	12.968	9.486	11.758	8.972	10.514	10.216	9.570	9.503
without load	17.608	14.927	12.580	9.736	11.454	8.873	10.768	9.875	9.657	9.596

Graphs of average value of Vickers's mirco hardness number of both the core thickness specimen are following:

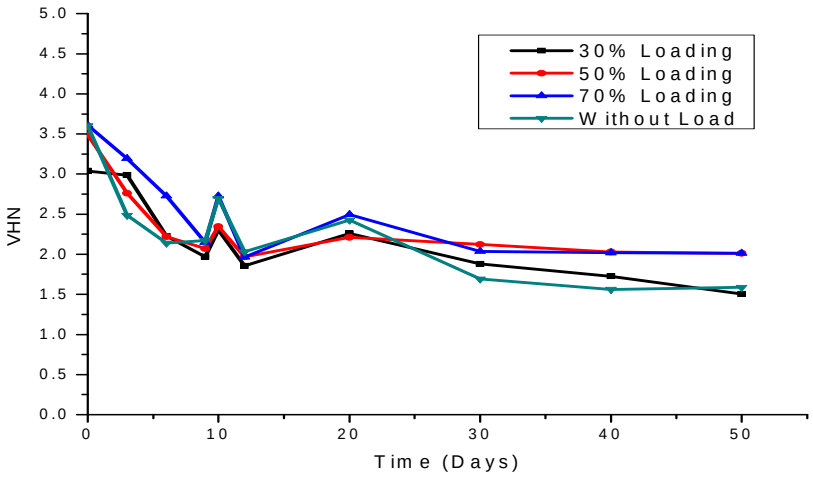

Fig.5.63 Graph showing change in average micro hardness (VHN) with respect to time in 8mm core thickness specimen

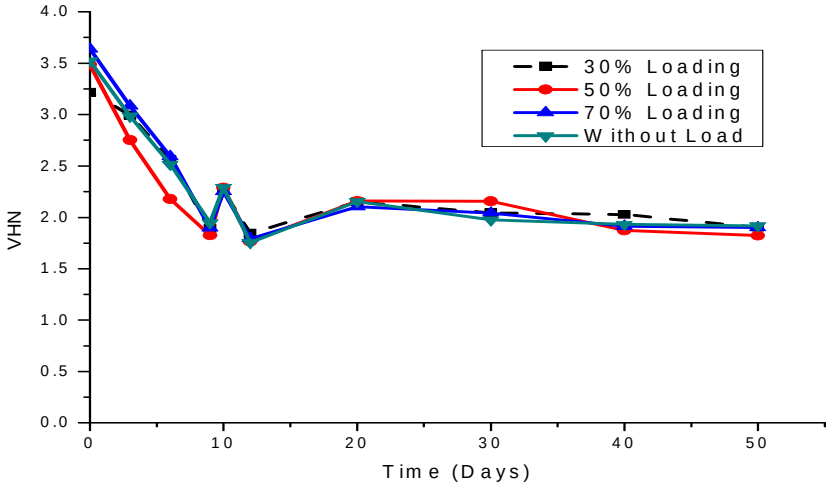

Fig.5.64 Graph showing change in average micro hardness (VHN) with respect to time in 16mm core thickness specimen

DISCUSSION

A) Effect of core thickness on Vickers's Hardness Number (VHN):

Above graphs (Fig 5.63 and Fig 5.64) show changes in VHN for specimen of different core thicknesses. It is observed that the core thickness does not affect so much in change in micro hardness (VHN) with respect to time. It is also observed that drop in micro hardness (VHN) in 16mm core thickness specimen is almost constant after 30 days with some exceptions whereas drop in micro hardness (VHN) in 8mm core thickness after 30 days is less.

B) Effect of bending pre-loads on Vickers's Hardness Number (VHN):

Change in micro hardness (VHN) in different bending pre-loads specimen is not very high with respect to time. These are almost similar with some variations for both the core thickness specimen.

C) Effect of time on Vickers's Hardness Number (VHN):

Above graphs (Fig 5.63, Fig 5.64) and table (T 5.13, T 5.14) are showing trend of change in Vickers's Hardness Number with respect to time. It is observed from the graphs that the micro hardness (VHN) is constantly decreasing with time. Up to 20 days the drop in VHN is comparatively more.

Reason for the decrease in micro hardness (VHN) with time may be the hygrothermal environment. The epoxy immerged in the water at 45°C may get soften due to temperature and moisture. Pores of epoxy will loosen which gives way to moisture due to which the sandwich structure getting softer day by day and hardness decreases.

5.2.2 DETAILS OF S.E.M. IMAGES RESULTS OF ALL SPECIMEN (EACH CORE THICKNESS AND EACH LOADING) WITH RESPECT TO TIME

The SEM images (Fig.5.65 and Fig 5.66) for the GFRP sandwich composite specimen taken at 2000 X magnification from their cut-cross-section and cut-longitudinal-section at the start of testing, before exposure to hygrothermal loads show a fibre epoxy composite with fibres densely embedded in epoxy matrix with epoxy surrounding completely the fibres which maintain their circularity and suggest good strength. The SEM image (Fig. 5.65(b) and 5.66(b)) of cut-longitudinal-section show cylindrical unbroken long fibres with no damage.

5.2.2.1 S.E.M. BEFORE EXPOSURE:

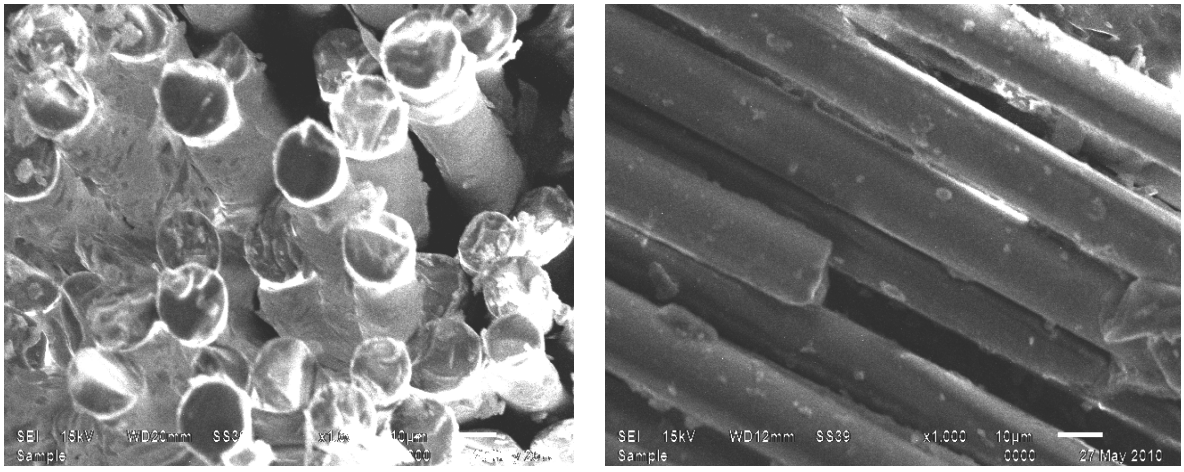

(a) (b)

Fig. 5.65 SEM of cross-section (a) and longitudinal (b) of 8mm core thickness specimen

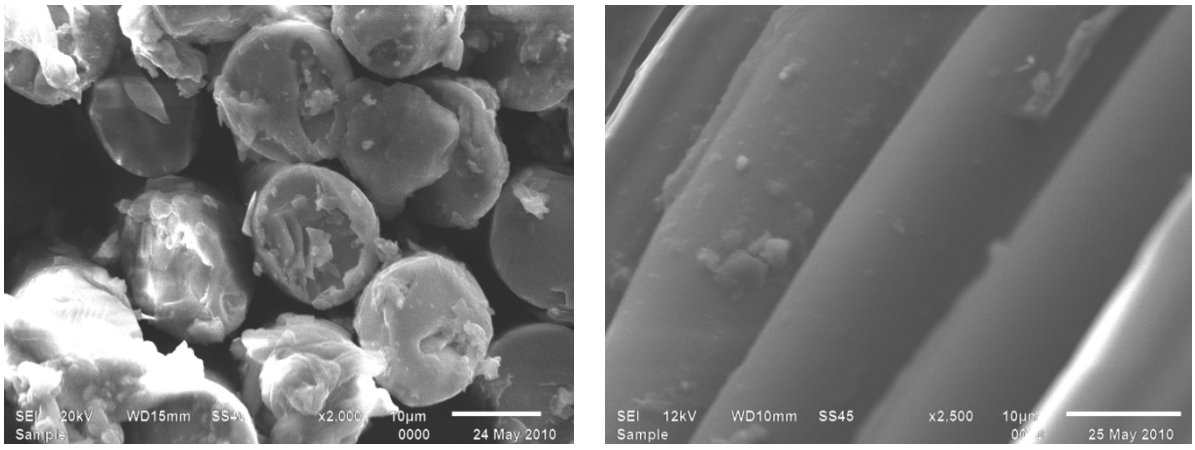

(a) (b)

Fig. 5.66 SEM of cross-section (a) and longitudinal (b) of 16mm core thickness specimen

5.2.2.2 S.E.M. RESULTS AFTER ONE MONTH OF EXPOSURE

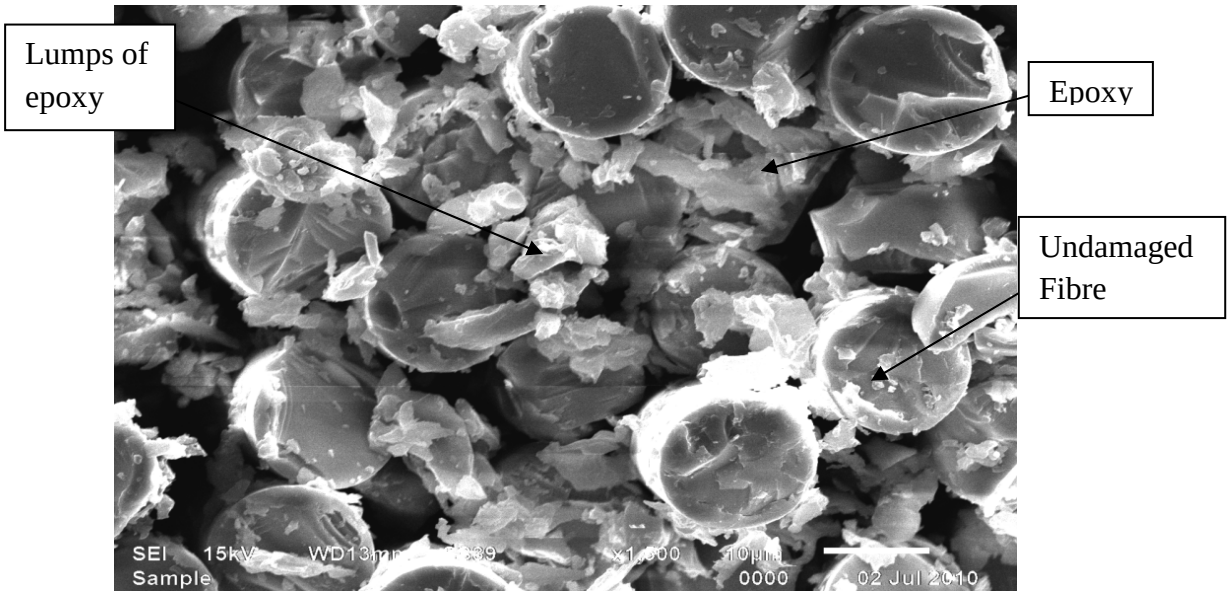

Fig.5.67 SEM image of specimen at 30% UFL after 1 month (8mm core)

The SEM images of sandwich specimen which were subjected to **30% loading** (8mm core, 1 month) shown above in Fig 5.67 show undamaged circular fibres and epoxy smearing the surface of the fibres completely in big irregular lumps probably due to absorption of water by epoxy.

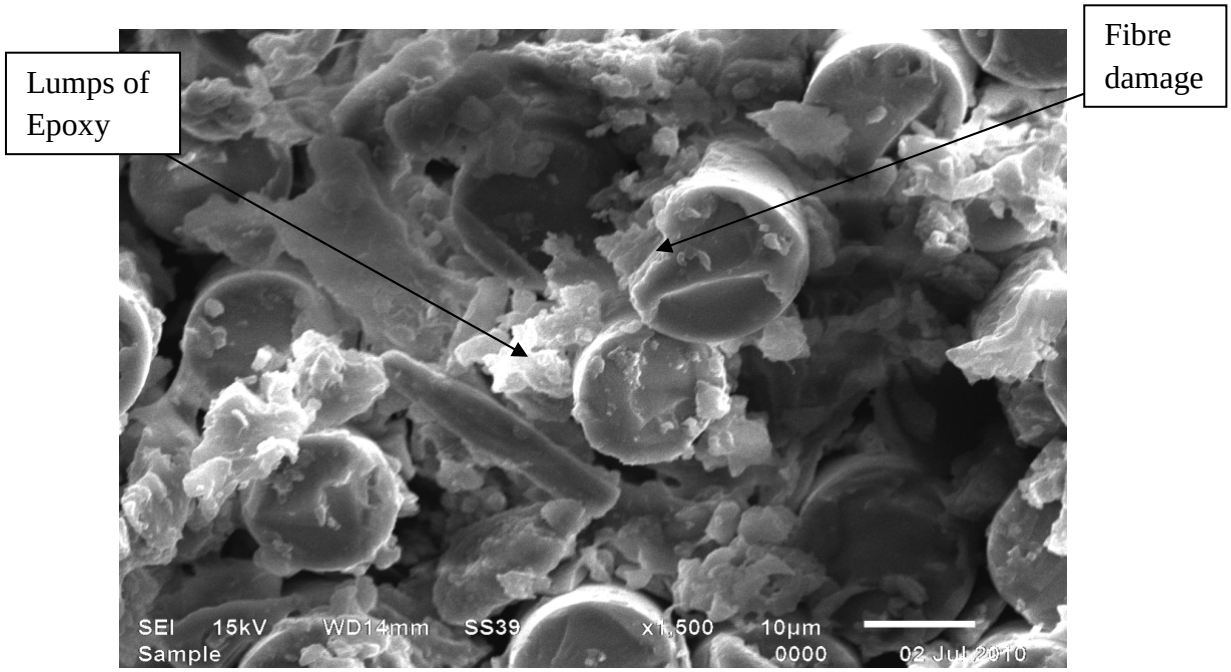

Fig.5.68 SEM image of specimen at 50% UFL after 1 month (8mm core)

The SEM images of specimen which were subjected to **50% loading** (8mm core, 1month) is shown above in Fig 5.68, the less damaged fibre and high lumping of the epoxy is clearly visible, the lumping of epoxy is due to hardening by absorption of water.

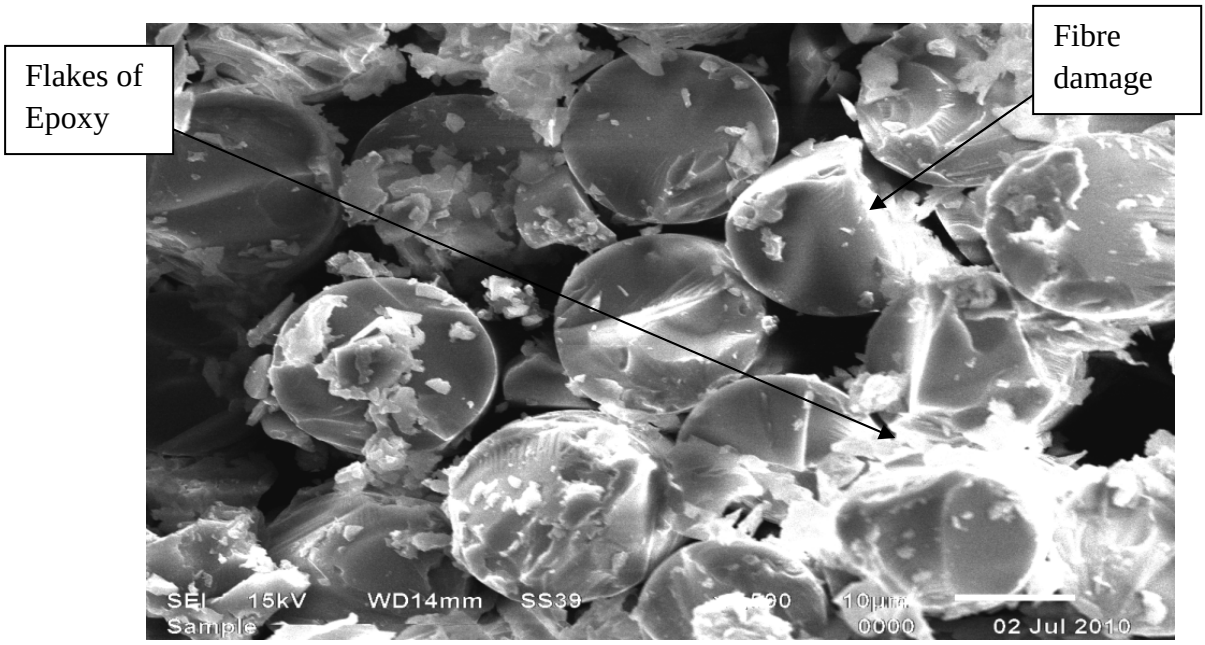

Fig.5.69 SEM image of specimen at 70% UFL after 1 month (16mm core)

The SEM images of specimen which were subjected to **70% loading** (16mm core, 1month) shown above in Fig 5.69 indicate small amount of damage to the circular fibre, whereas some amount of flaking of epoxy is evident due to its hardening by absorption of water, also voids are evident in the epoxy matrix in some places indicating a loss of strength in the composite.

5.2.2.3 S.E.M. RESULTS AFTER TWO MONTH OF EXPOSURE

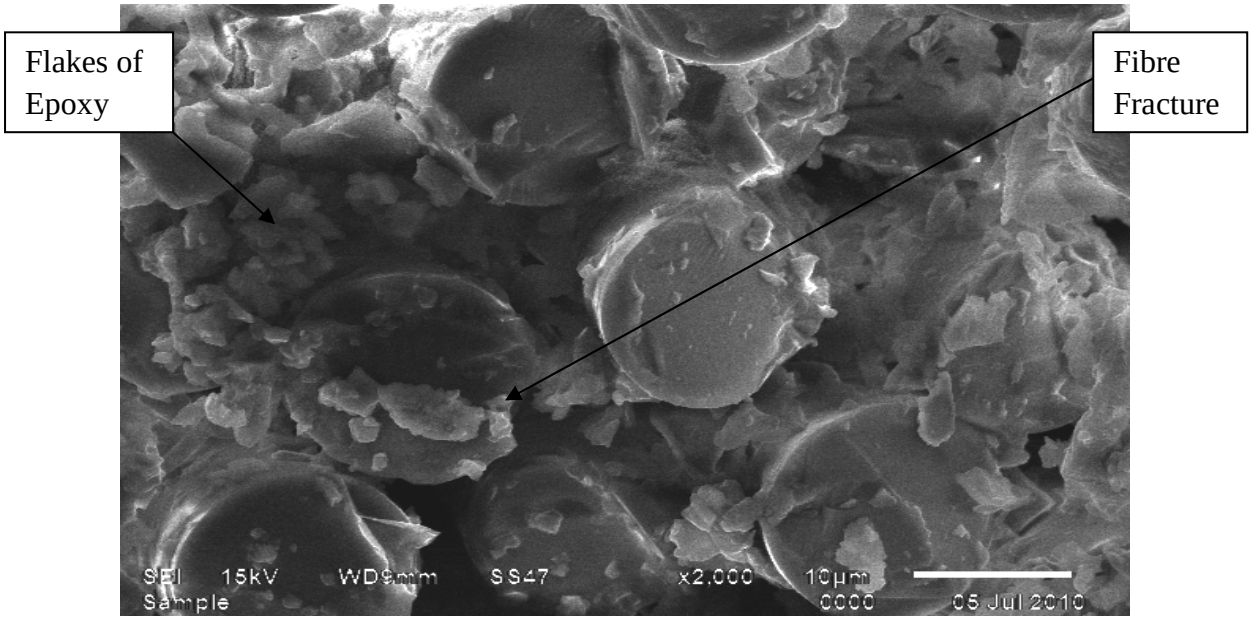

Fig.5.70 SEM image of specimen at 30% UFL after 2 month (8mm core)

The SEM images of specimen which were subjected to **30% loading** (8mm core, 2months) shown above in Fig 5.70 indicate degeneration of epoxy matrix and small amount of flaking of epoxy , it appears as though epoxy has dissolved away from the surface, as protruding less damaged fibres are visible. Less circularity change and less fibre fracture is visible.

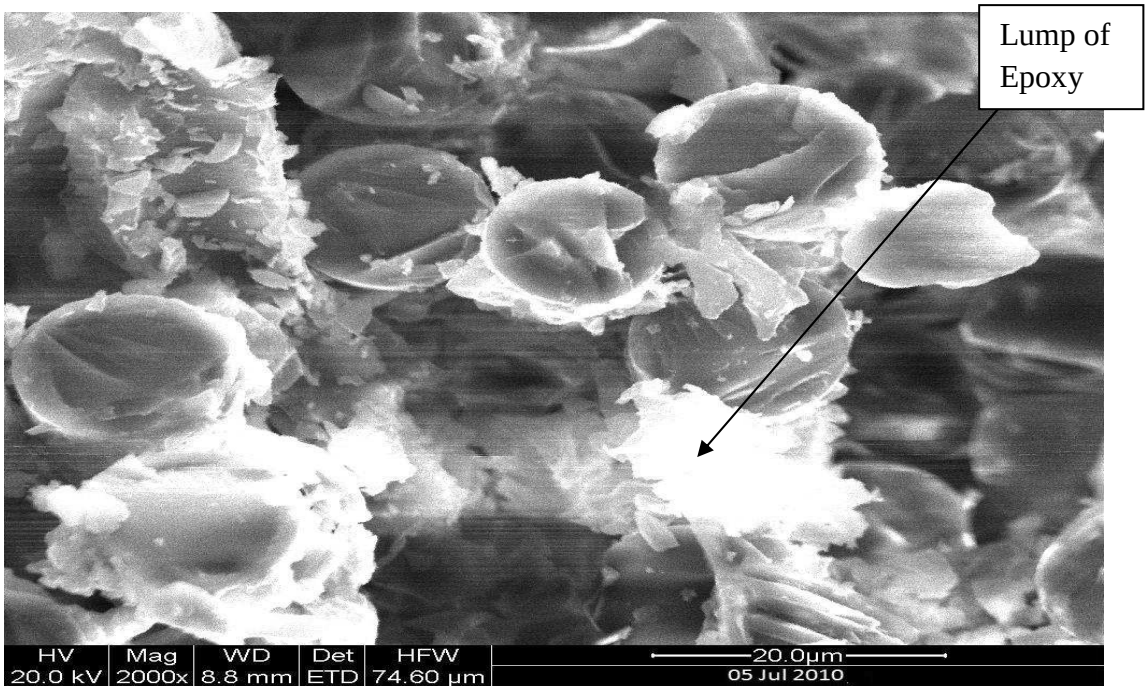

Fig.5.71 SEM image of specimen at 50% UFL after 2 month (16mm core)

The SEM images of specimen which were subjected to **50% loading** (16mm core, 2months) shown above in Fig 5.71 clearly show flaking of epoxy in some portions, which smears the fibre surface forming lumps, the degeneration of epoxy matrix is clearly visible, though less damage to fibres (less change in circularity) is observed.

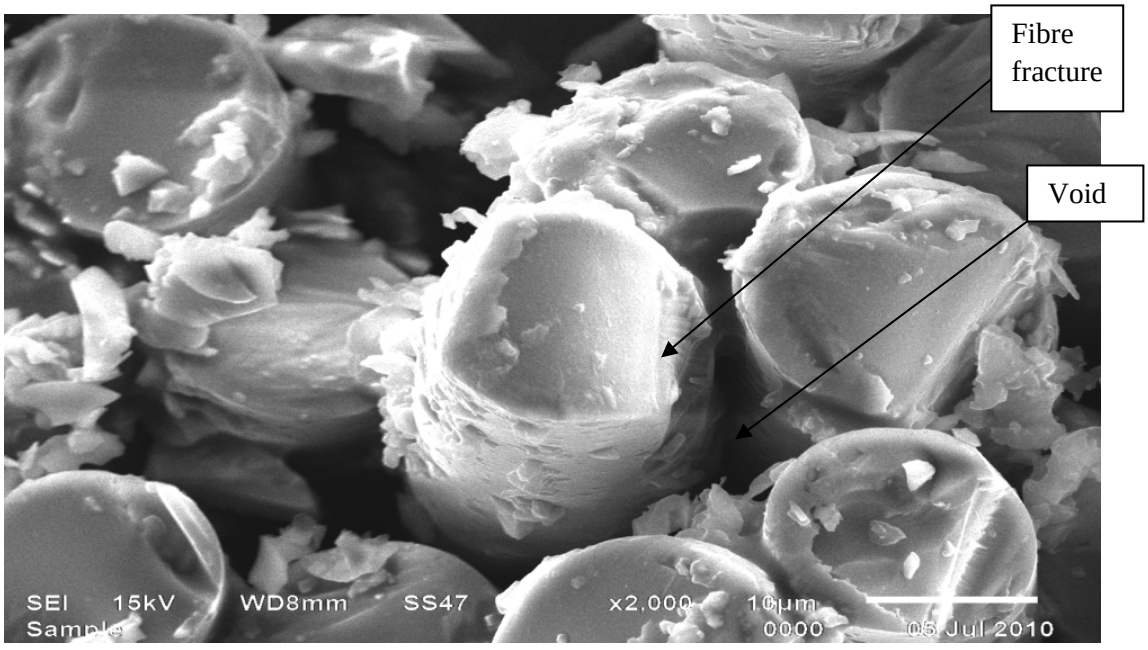

Fig.5.72 SEM image of specimen at 70% UFL after 2 month (8mm core)

The SEM images of specimen which were subjected to 7**0% loading** (8mm core, 2months) shown above in Fig 5.72 indicate degeneration of epoxy matrix, void formation between fibres in some places and fibre fracture in more quantity. Change in circularity of the fibre is also observed.

5.2.3 IMAGE ANALYSIS BY "IMAGE-J" ANALYSER SOFTWARE:

The analysis of all the SEM images was done in order to compare the area fraction of both epoxy as well as of the fibre. The commercially available software Image J was used for analysis of images. Image J is open source software developed by National Institute of Health and considered as powerful for image analysis. Few representative images after analysis by software are shown from Fig.5.73 to Fig.5.85. The red area represents the fibre, the green is taken as epoxy, and some black region observed is taken as voids.

Procedure followed for analysis of the SEM images is explained below:

1) The image to be analysed was opened in the software.

2) A line was drawn parallel to the 20µm line (shown on SEM images) using the Set Scale option. That distance was set equivalent to number of pixel (automatically counted by software).

3) Now as the scale was set a line was drawn across fibre edges to measure the length of fibre.

4) To calculate the area fraction, first of all image was converted into RGB colour (Various colour options could be chooses, here Red/Green colour was used to fill the areas of SEM image)

5) After applying above option the colour of image would change (from the grey scale to chosen Red/Green), in which red colour indicated the fibre area, green indicated epoxy and black was for voids. These areas were selected automatically by software according to the image contrast.

6) Using the Split Channel option the software would split the three colours into three different windows representing the fibre area, epoxy area and void area.

7) To calculate the area fraction first tick the option of measure area fraction in Set Measurement menu. To measure the area fraction, the option Analyze →Measure was used. Area to be measured was selected by making a window around it and above mentioned Analyze option showed the results in a tabular form.

BEFORE EXPOSURE:

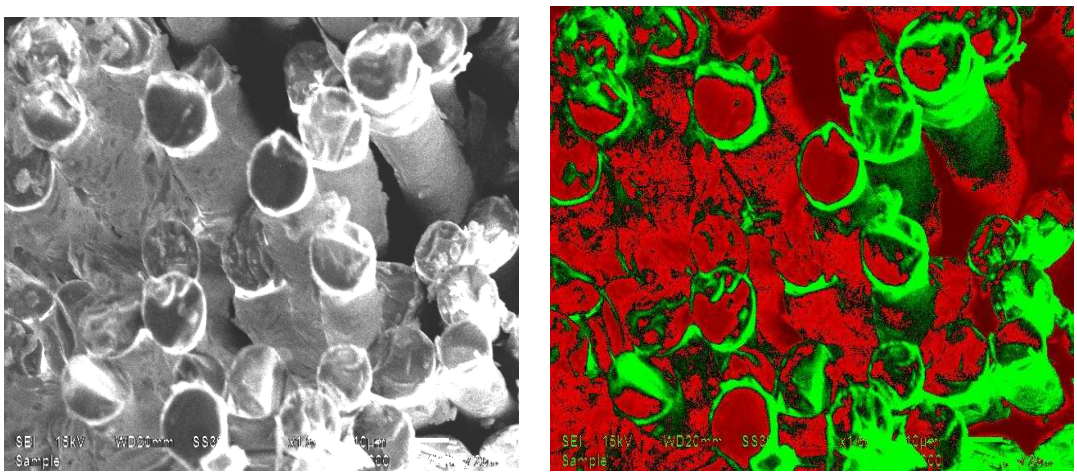

Red- Fibre

Green- Epoxy

Black- Voids

Fig.5.73 (Left) SEM image without exposure, (Right) same SEM image by Image Analyser

AFTER ONE MONTH OF EXPOSURE

8mm core thickness specimen

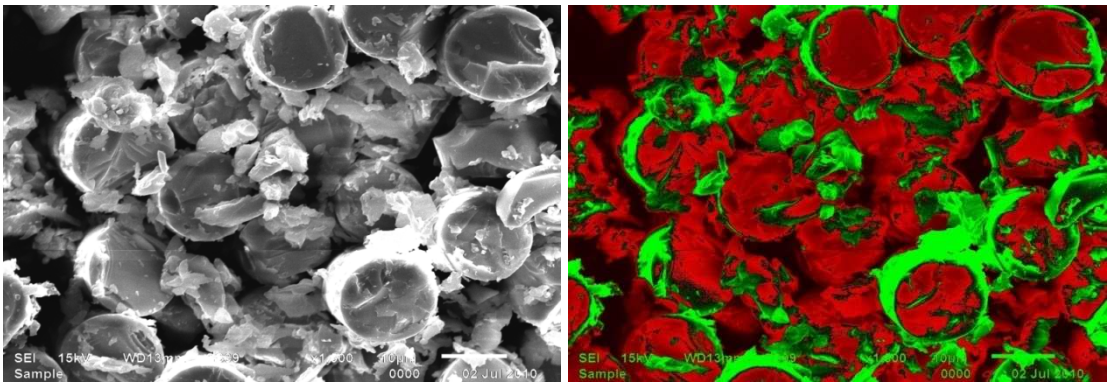

Fig.5.74 (Left) SEM image of 8mm core thickness specimen at 30% UFL, (Right) same SEM image by Image Analyser

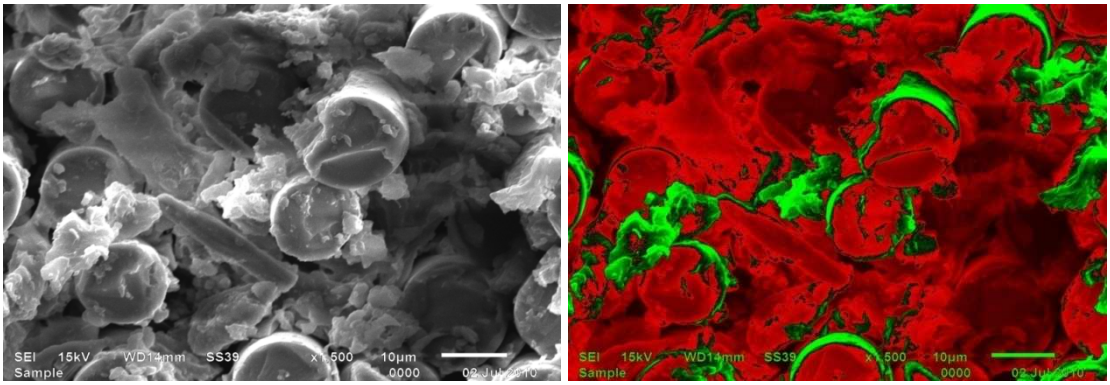

Fig.5.75 (Left) SEM image of 8mm core thickness specimenat 50% UFL, (Right) same SEM image by Image Analyser

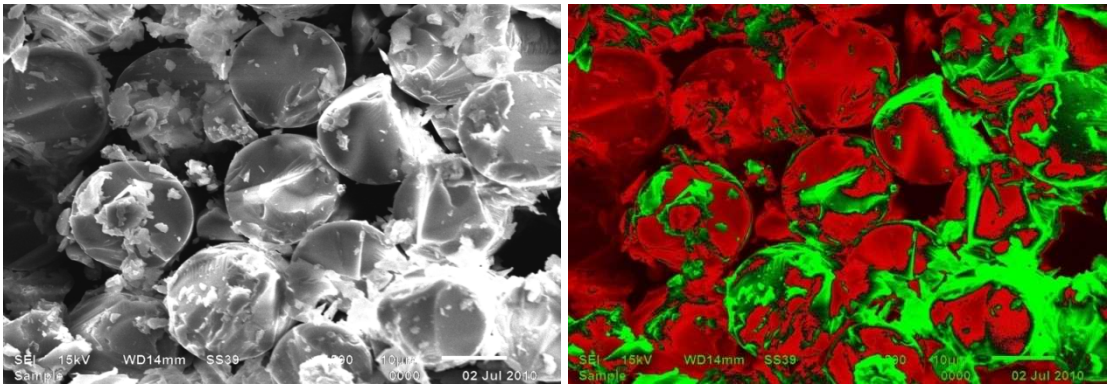

Fig.5.76 (Left) SEM image of 8mm core thickness specimen at 70% UFL, (Right) same SEM image by Image Analyser

The SEM images and SEM images by Image analyser of sandwich composite specimen which were subjected to **30%, 50% and 70% loading of UFL** (8mm core, 1 month) shown above in Fig 5.74 to Fig 5.76 show undamaged circular fibres and epoxy smearing the surface of the fibres completely in small irregular lumps probably due to absorption of water by epoxy. There are no voids visible and also the circularity of fibres is not changing.

16mm core thickness specimen

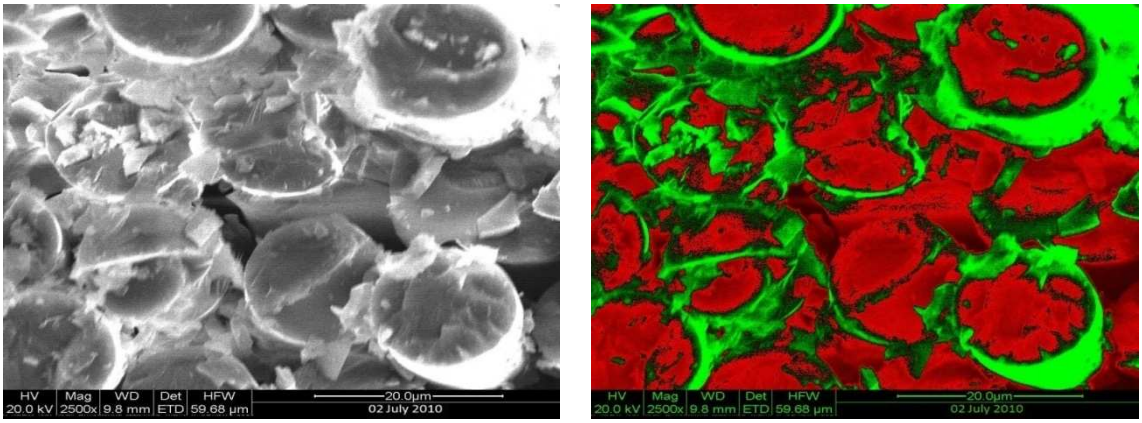

Fig.5.77 (Left) SEM image of 16mm core thickness specimen at 30% UFL, (Right) same SEM image by Image Analyser

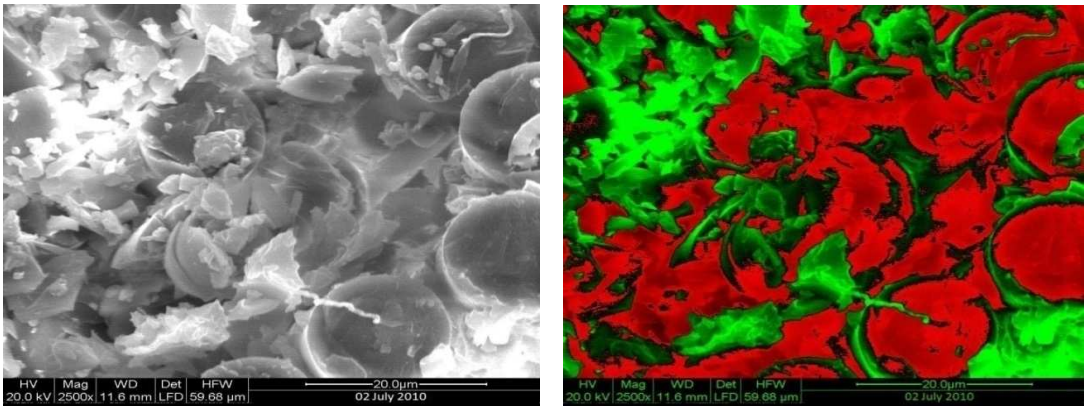

Fig.5.78 (Left) SEM image of 16mm core thickness specimen at 50% UFL, (Right) same SEM image by Image Analyser

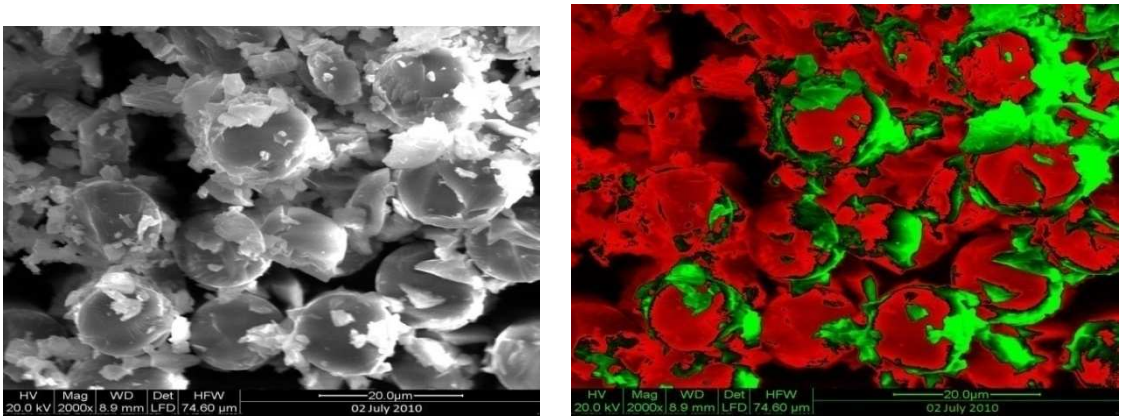

Fig.5.79 (Left) SEM image of 16mm core thickness specimen at 70% UFL, (Right) same SEM image by Image Analyser

The SEM images and SEM images by Image Analyser of sandwich composite specimen which were subjected to **30%, 50% and 70% loading** of UFL (16mm core, 1month) shown above (Fig 5.77 to Fig 5.79) indicate no damage to the circular fibre, whereas lumping of epoxy is clearly evident due to its hardening by absorption of water, also voids in 70% loading specimen are evident in the epoxy matrix indicating a loss of strength in the composite. It is also shown that lumping of epoxy is less in 30% loading as compared to 50% and 70% loading. A little bit change in circularity of the fibres is also visible.

AFTER TWO MONTH OF EXPOSURE

8mm core thickness specimen

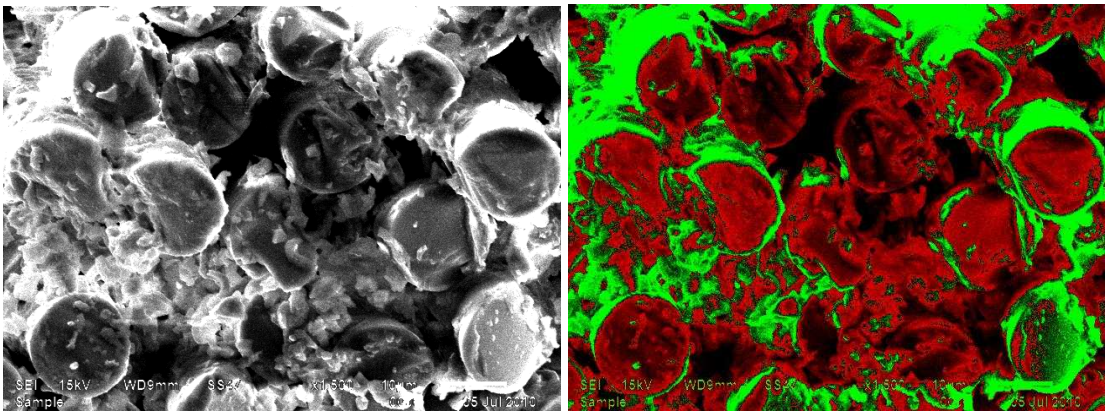

Fig.5.80 (Left) SEM image of 8mm core thickness specimen at 30% UFL, (Right) same SEM image by Image Analyser

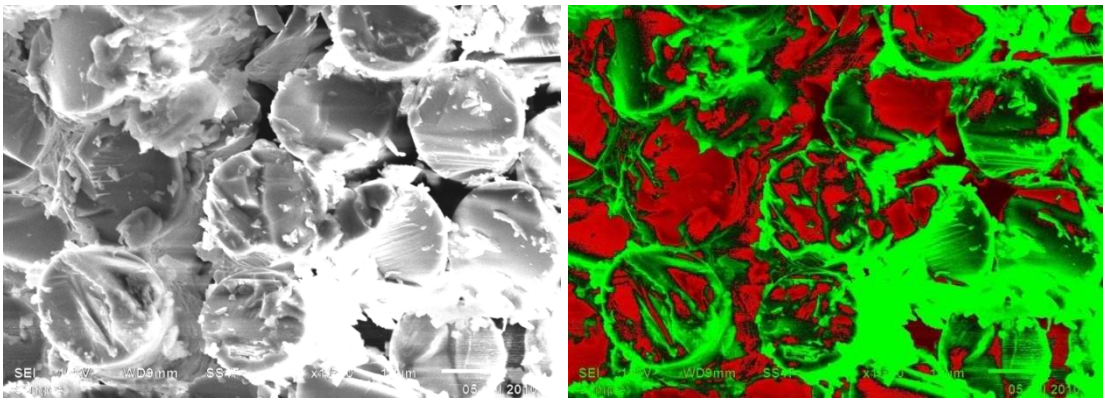

Fig.5.81 (Left) SEM image of 8mm core thickness specimen at 50% UFL, (Right) same SEM image by Image Analyser

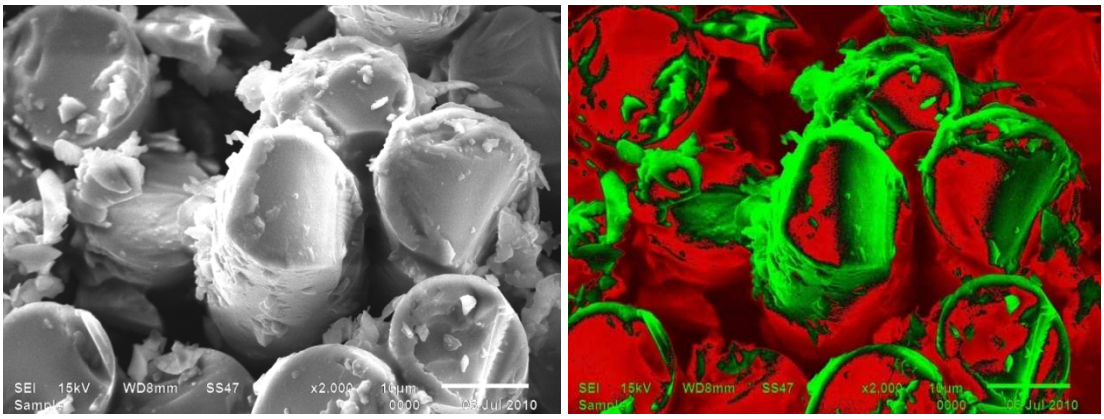

Fig.5.82 (Left) SEM image of 8mm core thickness specimen at 70% UFL, (Right) same SEM image by Image Analyser

The SEM images and SEM images by SEM Analyser of sandwich specimen which were subjected to **30%, 50% and 70% loading of UFL** (8mm core, 2months) shown above (Fig 5.80 to Fig 5.82) indicate degeneration of epoxy matrix, extensive void formation in 30% loading specimen between fibres, flaking of epoxy is clearly evident, it appears as though epoxy has dissolved away from the surface, as protruding damaged fibres are visible. Small change in circularity of fibres is also visible. Fibre fracture is also visible in 70% loading specimen in high amount.

16mm core thickness specimen

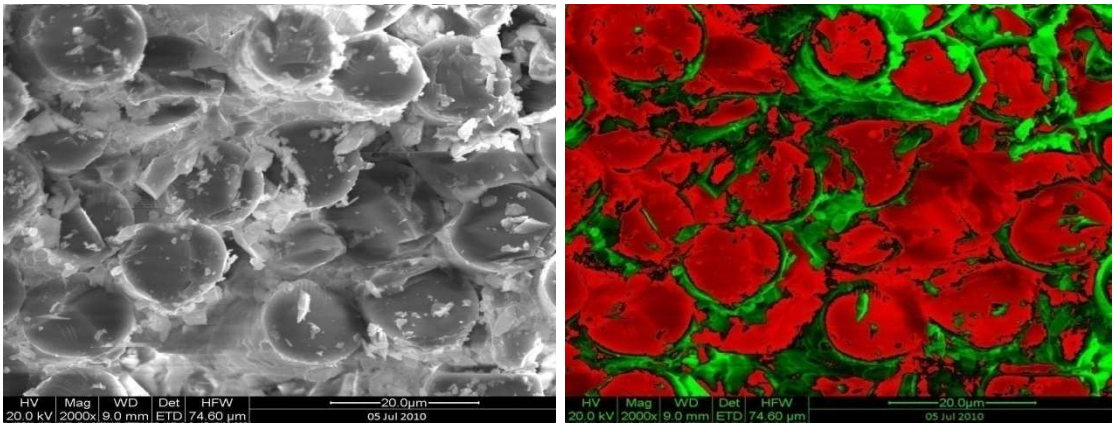

Fig.5.83 (Left) SEM image of 16mm core thickness specimen at 30% UFL, (Right) same SEM image by Image Analyser

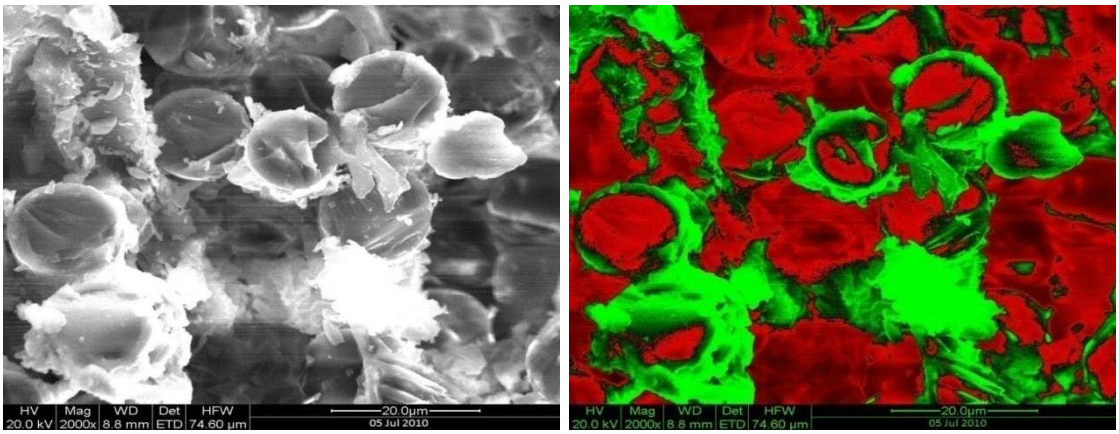

Fig.5.84 (Left) SEM image of 16mm core thickness specimen at 50% UFL, (Right) same SEM image by Image Analyser

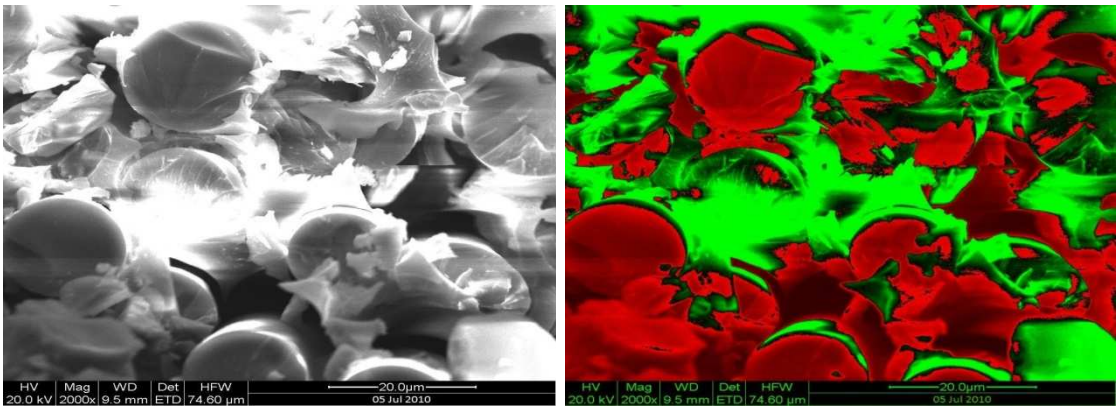

Fig.5.85 (Left) SEM image of 16mm core thickness specimen at 70% UFL, (Right) same SEM image by Image Analyser

The SEM images and SEM images by Image Analyser of sandwich specimen which were subjected to **30%, 50% and 70% loading of UFL**(16mm core, 2months) shown above (Fig 5.83 to Fig 5.85) clearly show flaking of epoxy, which smears the fibre surface forming lumps, the degeneration of epoxy matrix is clearly visible. Some damage to fibres (less change in circularity and no change in fibre fracture) is observed. Some void formation in 30% loaded specimen between fibres is also present there. Lump forming in 70% loading is more as compared to other loading.

5.2.4 RESULT OF AREA FRACTION AND CIRCULARITY BY IMAGE ANALYSIS

The Table T 5.15 shows the percentage area fraction in fibre and epoxy in both the core thickness specimen with respect to time

Table T 5.15 Comparison of percentage area fraction of fibre and epoxy with respect to time

8mm core thickness specimen						
Sample name	Initial		After 1 month		After 2 months	
	% Area fraction		% Area fraction		% Area fraction	
	fibre	epoxy	fibre	epoxy	fibre	epoxy
30% loading	78.2	21.8	66.7	33.3	60.2	39.8
50% loading			70.7	29.3	65.3	34.7
70% loading			69.5	30.5	56.4	43.6
without load			71.5	28.5	65.8	34.2
16mm core thickness specimen						
Sample name	Initial		After 1 month		After 2 months	
	% Area fraction		% Area fraction		% Area fraction	
	fibre	Epoxy	fibre	epoxy	fibre	epoxy
30% loading	69.1	30.9	60.3	39.7	56.7	43.3
50% loading			67.8	32.2	58.4	41.6
70% loading			57.3	42.7	55.1	44.9
without load			58.5	41.5	55.2	44.8

The graphical comparisons of the results obtained from the analysis of the above tables are following:

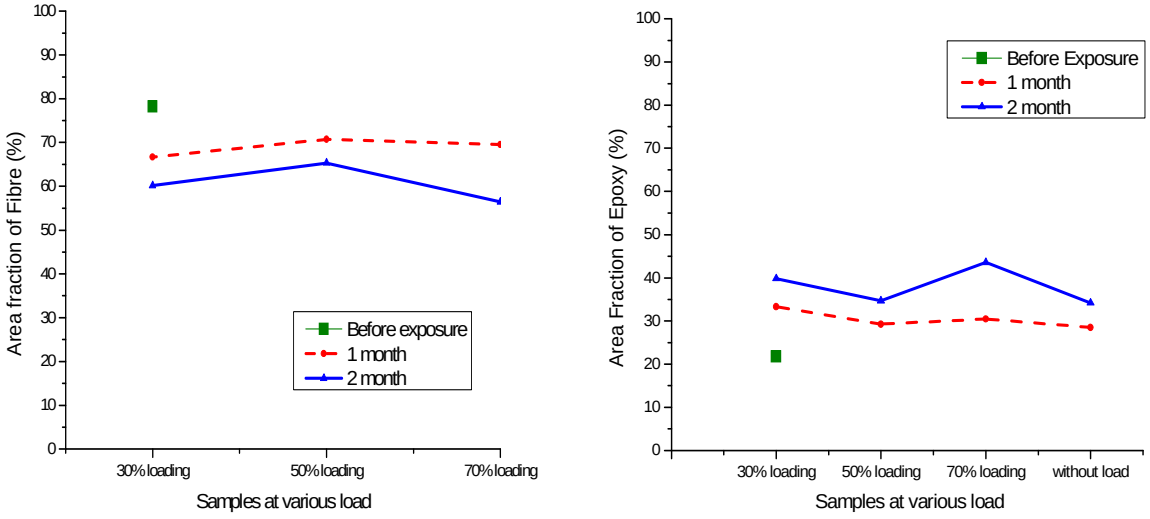

Fig.5.86 Comparison of Fibre and Epoxy area fraction with respect to time (8mm core)

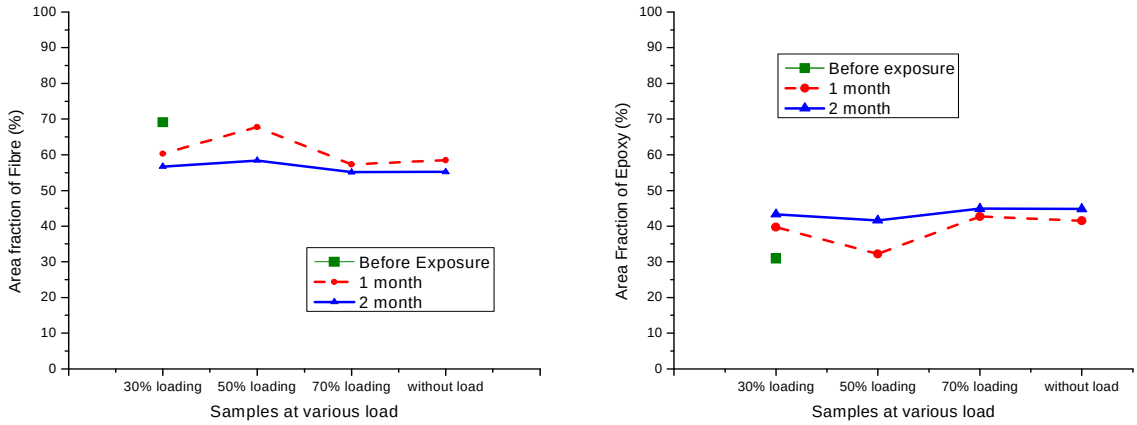

Fig.5.87 Comparison of Fibre and Epoxy area fraction with respect to time (16mm core)

DISCUSSION

The area fraction of fire and epoxy of different specimen subjected to bending pre-loads is compared in graphs (Fig 5.86, Fig 5.87) and table T 5.15. It is clearly seen that area fraction of epoxy is increasing with time as there is considerable increase after two month compared to one month. But the trend is seen to be opposite in fibre area fraction. Here the fibre area fraction is decreasing with time. In 8mm core thickness specimen drop of fibre area fraction is more as compared to 16mm core thickness specimen. All specimen subjected to different bending preloads show almost the same trend with some exceptions when compared between one and two month.

The reason for such a trend seems to be that fibre in total area is degrading with heat and moisture attack and epoxy seems to have expanded with above effect which leaves more area for epoxy as compared to fibre.

CIRCULARITY RATIO

The Table T 5.16 shows the maximum and minimum diameter of fibre and circularity ratio in both the core thickness specimen with respect to time.

Table T 5.16 Comparison diameter of fibre and circularity ratio with respect to time

Sample Name	1 month			2 month		
	Smaller dia of fibre (mm)	Max dia of fibre (mm)	Circularity ratio	Smaller dia of fibre (mm)	Max dia of fibre (mm)	Circularity ratio
16mm core						
30% loading	0.0179	0.0179	1.000	0.0149	0.015	0.993
50% loading	0.0197	0.0198	1.005	0.0168	0.0168	1.000
70% loading	0.0208	0.0206	0.990	0.0154	0.0158	0.975
Without load	0.0242	0.0242	1.000	0.0165	0.0165	1.000
8mm core						
30% loading	0.0162	0.0162	1.000	0.0164	0.0165	0.994
50% loading	0.0174	0.0174	1.000	0.0177	0.0177	1.000
70% loading	0.0194	0.0194	1.000	0.0198	0.02	0.990
Without load	0.0186	0.0186	1.000	0.019	0.0191	0.995

Circularity ratio = $\frac{\text{Minimum fibre diameter}}{\text{Maximum fibre diameter}}$ ..... (5.7)

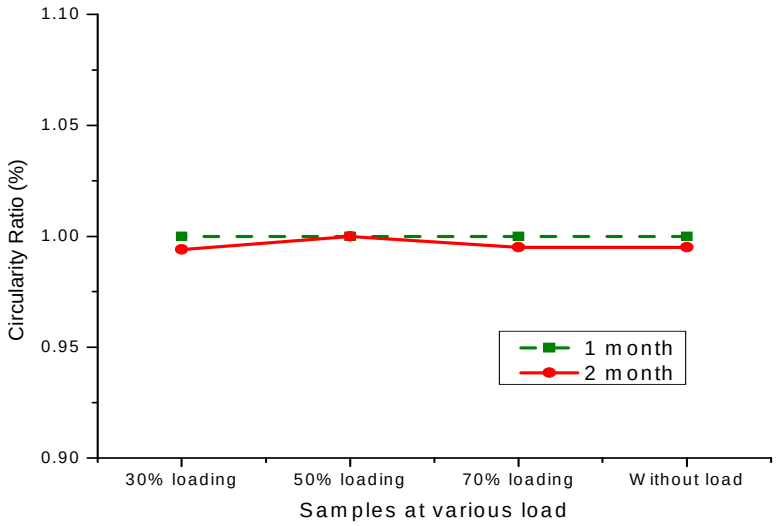

Fig.5.88 Comparison of Circularity Ratio with respect to time (8mm core)

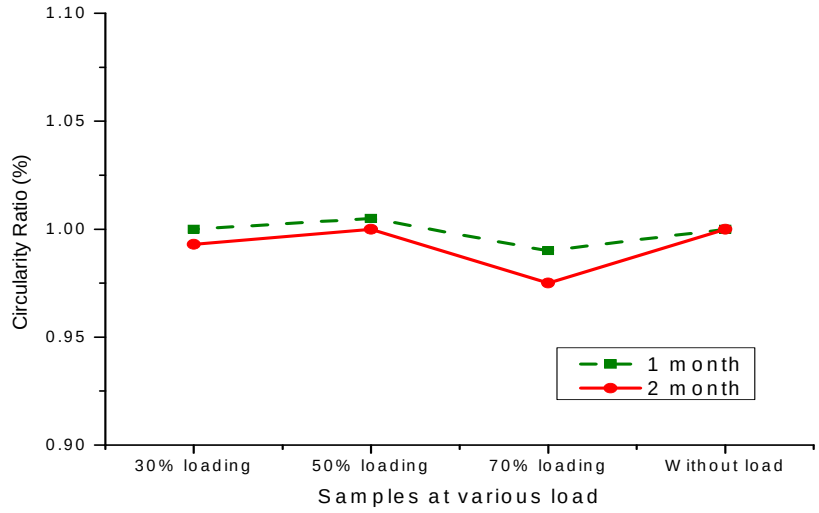

Fig.5.89 Comparison of Circularity Ratio with respect to time (16mm core)

The Circularity ratio (Fig.5.88, Fig.5.89 and table T 5.16) values seem to have gone downwards from a ratio of 1.0 with some exceptions, with time. The reason for such a trend is hygrothermal load which leads to change in shape with most damage on outer circumference of fibre.

5.3 RESULT OF PURE EPOXY SPECIMEN

For finding out the different characteristics only in matrix, 1 specimen of only epoxy was kept in each bath for different time period and observed. The results for epoxy specimen are shown in graphs following:

A) Weight gain

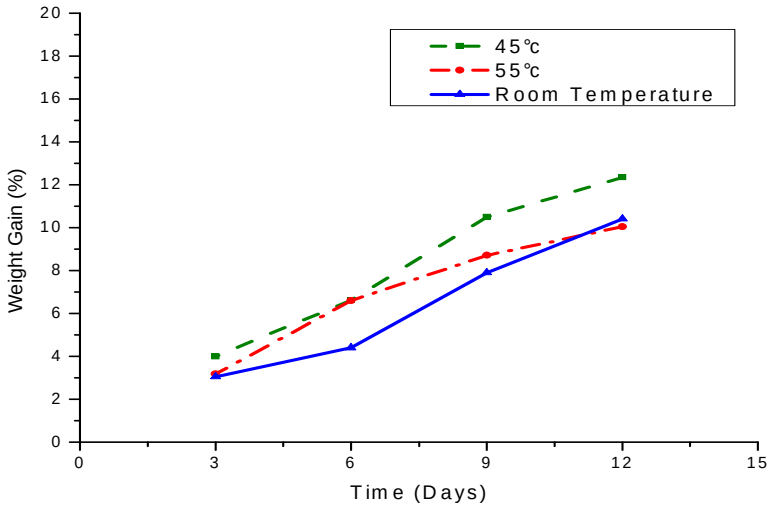

Fig.5.90 Graph showing percentage weight gain in epoxy specimen at different temperature with respect to time

B) Micro hardness (Vickers's Harndness Number)

In epoxy specimen load of 300g was applied for dwell time of 20s to make an indent on the surface.

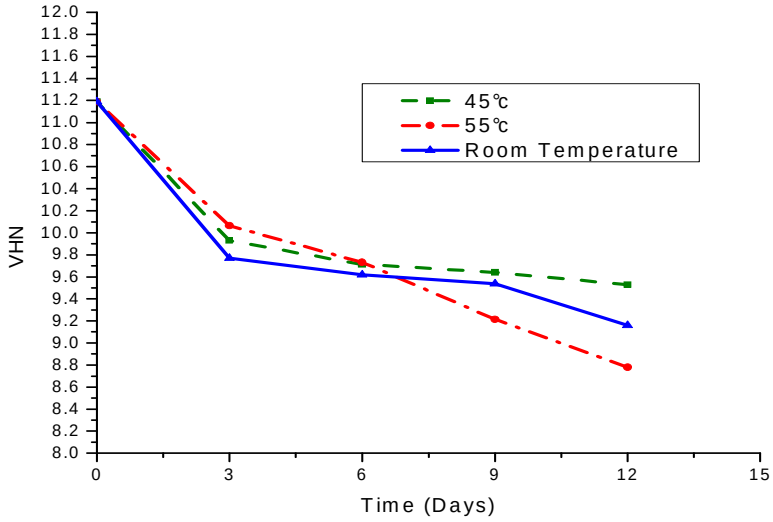

Fig.5.91 Graph showing decrease in VHN in epoxy specimen with respect to time

C) Apparent Moisture Diffusivity

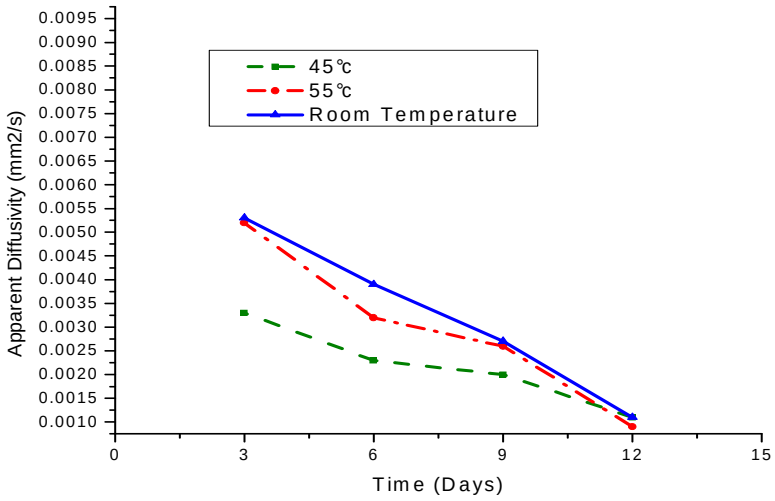

Fig.5.92 Graph showing change in Apparent Moisture Diffusivity in epoxy specimen with respect to time

DISCUSSION

The trend in change in weight gain, Vickers's Hardness Number and apparent moisture diffusivity is same in epoxy specimen as it was in sandwich specimen i.e. weight gain is increasing with time whereas microhardness and apparent moisture diffusivity is decreasing with time as shown in above (Fig. 5.90 to Fig 5.92). The reason for increase in weight gain is swelling of epoxy due to hygrothermal load giving way to moisture to inter into the specimen. Weight gain in epoxy specimen at 45°C is higher as compared to 55°C and room temperature.

Microhardness (VHN) is decreasing in epoxy specimen. The reason for this may be weight gain and swelling in epoxy because due to weight gain and swelling epoxy get soften. Decrease in micro hardness of specimen immersed at 55°C is higher as compared to 45°C and room temperature with respect to time.

Apparent moisture diffusivity is related to weight gain. Weight gain in epoxy specimen is increasing with time due to which apparent moisture diffusivity is decreasing .

It was observed that the matrix sample is following almost same trend as the sandwich specimen in all the cases.

5.4 Result of thermocol specimen

To observe the behaviour of thermocol sample one sample of thermocole have been kept into water. Initial weight of thermocol sample was 0.8292g and after 3 days weight was 0.8296g. It was observed that weight gain in thermocol specimen was very low and after 4 or 5 days it used to break so further behaviour could not be measured.

5.5 RELATION BETWEEN MICROSCOPIC AND MACROSCOPIC BEHAVIOUR

5.5.1 Relation between Microscopic and Macroscopic behaviour for *8mm core thickness specimen*

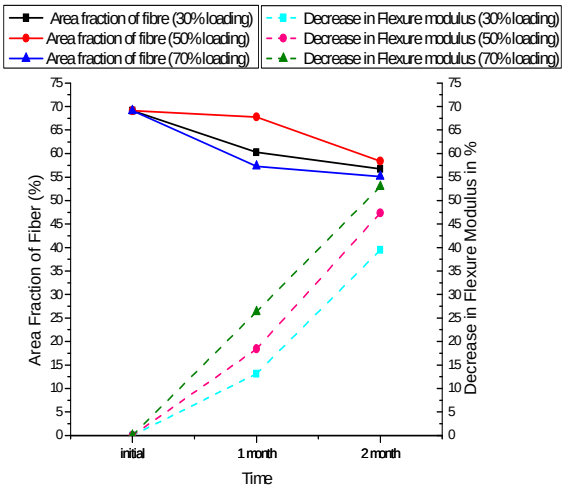

Fig.5.93 Relation of area fraction of fibre and percentage dercease in Flexure Modulus

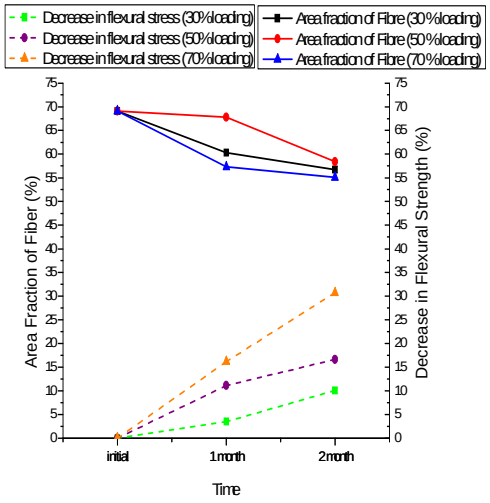

Fig.5.94 Relation of area fraction of fibre and percentage dercease in Flexural Strength

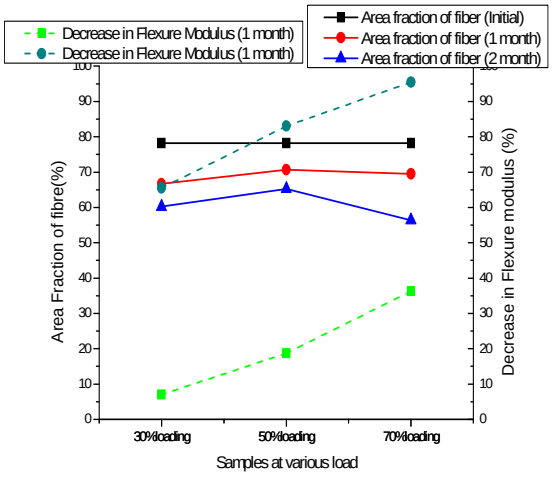

Fig.5.95 Relation of area fraction of fibre and percentage dercease in Flexure Modulus

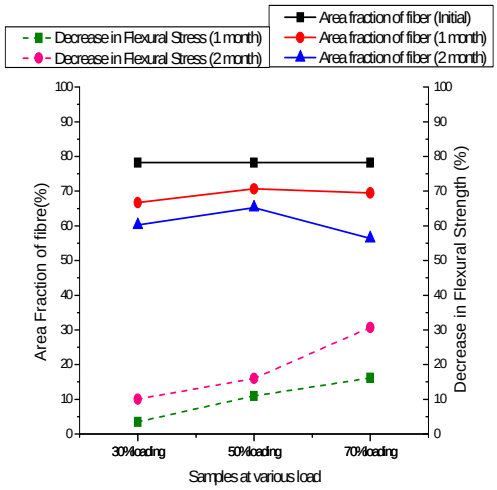

Fig.5.96 Relation of area fraction of fibre and percentage dercease in Flexural Strength

The above graphs (Fig 5.93 and Fig 5.94) are showing relation of area fraction of fibre and decrease in flexure modulus and decrease in flexural strength after one month and two month for 8 mm core thickness specimen. Trend in graphs are showing that with time area fraction of fibre is decreasing whereas decrease in flexure modulus is increasing.

Figure 5.95 and Fig 5.96 is showing relation of area fraction of fibre and decrease in flexure modulus and decrease in flexural strength for 30%, 50% and 70% bending pre-load specimen. Graphs are showing that there is more decrease in flexure modulus and flexural strength in 70% bending pre-load specimen as compared to 30% and 50% bending pre-load

specimen with time. Decrease in area fraction of fibre is also more in 70% bending pre-load specimen after two month. Graphs show that area fraction of fibre is directly related to flexure modulus and flexural strength. As time increases area fraction of fibre decreases due to hygrothermal loads which causes decrease in flexure modulus and flexural strength.

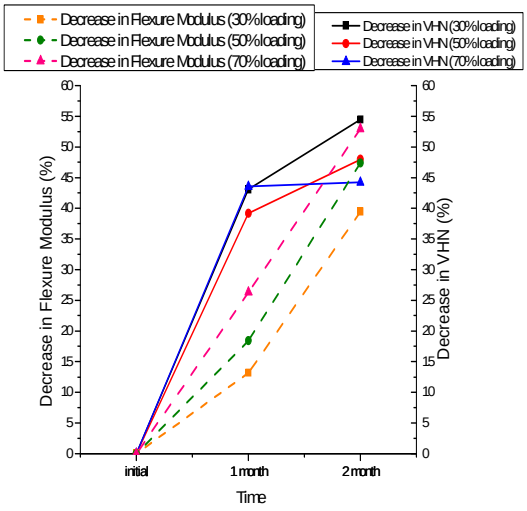

Fig.5.97 Relation of percentage decrease in VHN and percentage decrease in Flexure Modulus

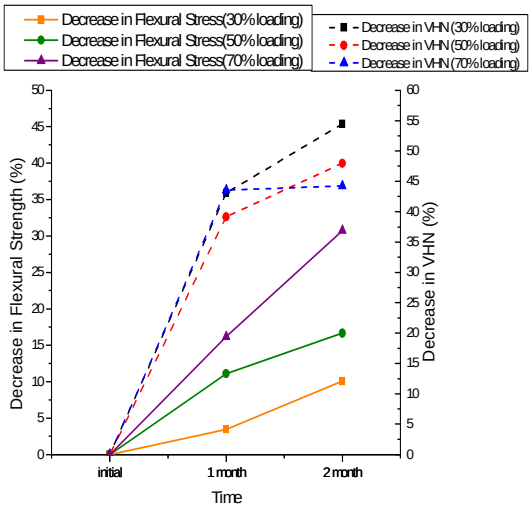

Fig.5.98 Relation of percentage decrease in VHN and percentage decrease in Flexural Strength

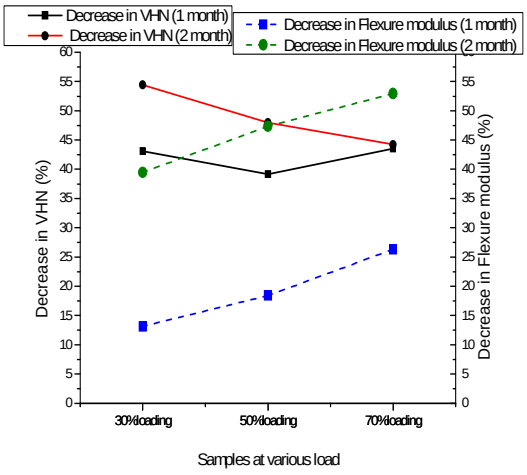

Fig.5.99 Relation of percentage decrease in VHN and percentage decrease in Flexure Modulus

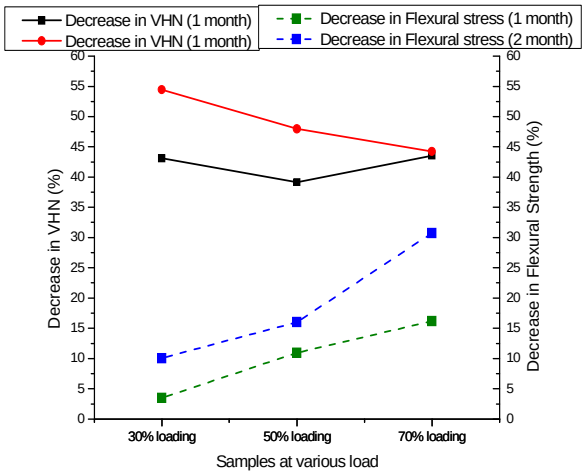

Fig.5.100 Relation of percentage decrease in VHN and percentage decrease in Flexural Strength

Figure 5.97 is representing relation of percentage decrease in micro hardness (VHN) and percentage decrease in flexure modulus of 8mm core thickness specimen after 1 month and 2 month. It is observed from the graph that with time hardness as well as flexure modulus of different bending pre-load specimen decreases. Percentage decrease in micro hardness is less than percentage decrease in flexure modulus in 1 month where as in 2 month both are almost similar.

Relation of percentage decrease in micro hardness and percentage decrease in flexural strength is shown in Fig 5.98 after 1 month and 2 month, and in Fig 5.100 for different bending pre-load. Graphs show that both micro hardness (VHN) and flexural strength is decreasing with time and also with increase in bending pre-load percentage with some exceptions.

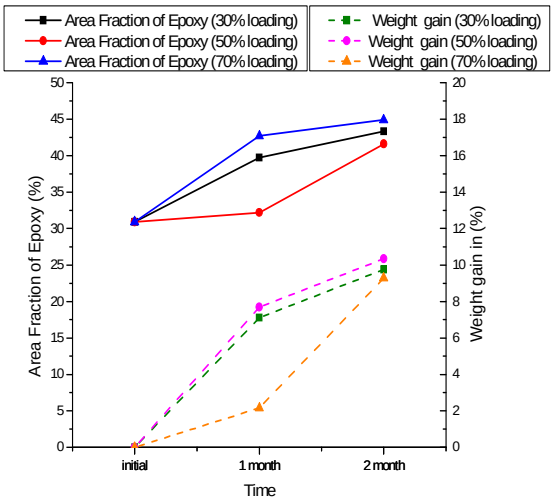

Fig.5.101 Relation of area fraction of epoxy and percentage weight with time

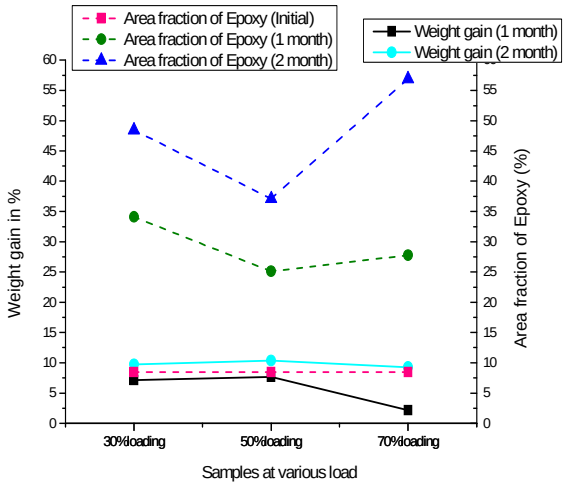

Fig.5.102 Relation of area fraction of epoxy and percentage weight with laoding

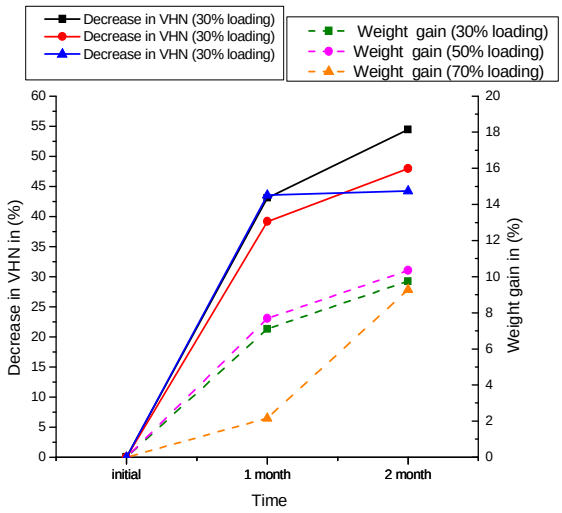

Fig.5.103 Relation of percentage decrease in VHN and percentage weight gain with time

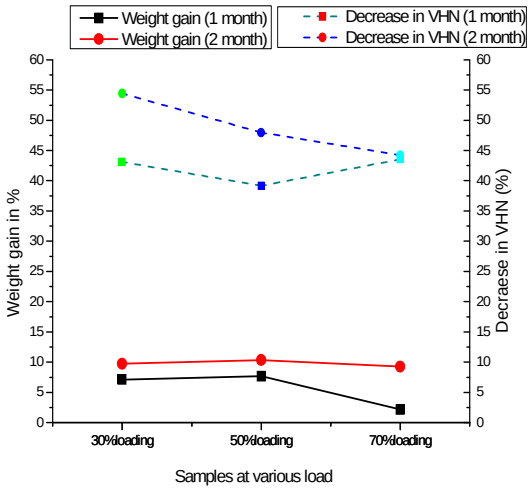

Fig.5.104 Relation of percentage decrease in VHN and percentage weight gain with loading

Figure 5.101 and 5.102 shows relation of area fraction of epoxy and weight gain after 1 month and 2 month and for different bending pre-loads. Graphs show that with time both area fraction of epoxy and weight gain increases for each loading. Area fraction of epoxy in 2 month for every percentage loading is more than 1 month. This may be due to swelling of epoxy.

Figure 5.103 and 5.104 is showing relation of percentage decrease in microhardness (VHN) and percentage weight gain for each specimen subjected to bending pre-load of 8mm core thickness after 1 month and 2 month. Graphs show that for every percentage of loading specimen with time percentage weigh gain increases whereas micro hardness (VHN) decreases. With increase in weight gain epoxy becomes softer which leads to decrease in micro hardness (VHN).

5.5.2 Relation between Microscopic and Macroscopic behaviour for *16mm core thickness specimen*

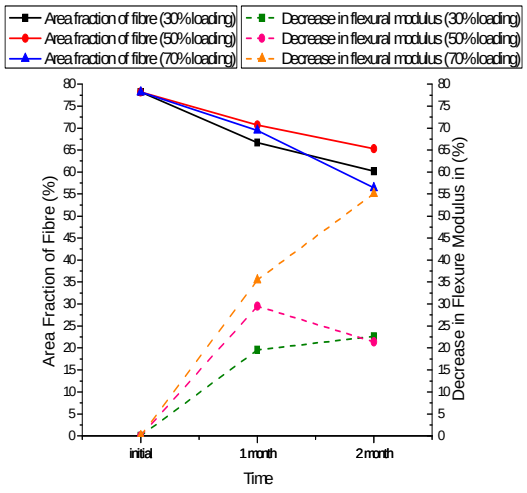

Fig.5.105 Relation of area fraction of fibre and percentage dercease in Flexure Modulus

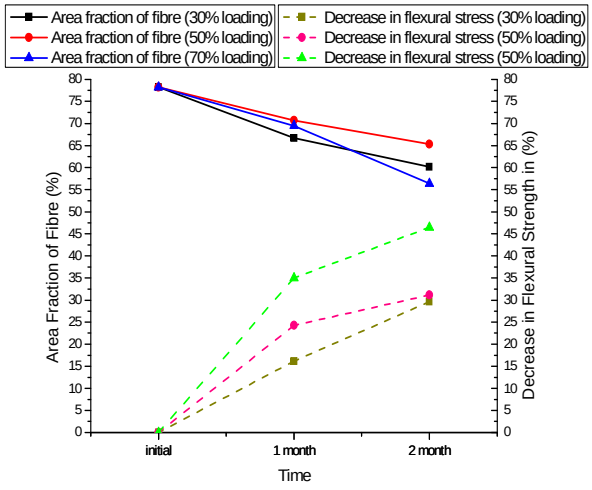

Fig.5.106 Relation of area fraction of fibre and percentage dercease in Flexural Strength

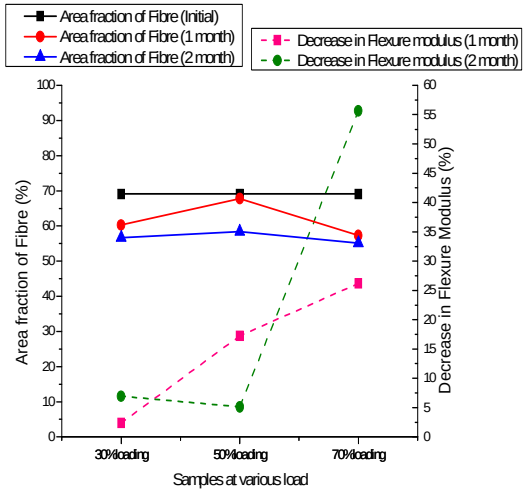

Fig.5.107 Relation of area fraction of fibre and percentage dercease in Flexure Modulus

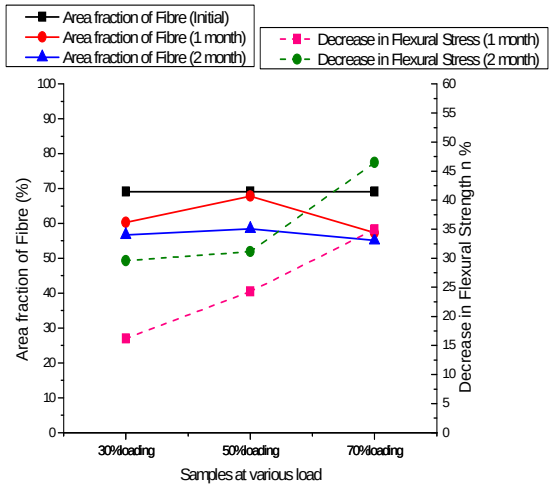

Fig.5.108 Relation of area fraction of fibre and percentage dercease in Flexural Strength

The above graphs (Fig 5.105and Fig 5.106) show relation of area fraction of fibre and decrease in flexure modulus and decrease in flexural strength after one month and two month for 16 mm core thickness specimen. From figures it is clearly visible that with time all, area fraction of fibre, flexure modulus and flexural strength decreases.

Decrease in flexural modulus of 70% bending pre-load specimen is too large after two months as compared to other preloaded specimen. Graphs are also showing that with less decrease in fibre area fraction, decrease in flexure modulus and flexural strength is more for each bending pre-loaded specimen.

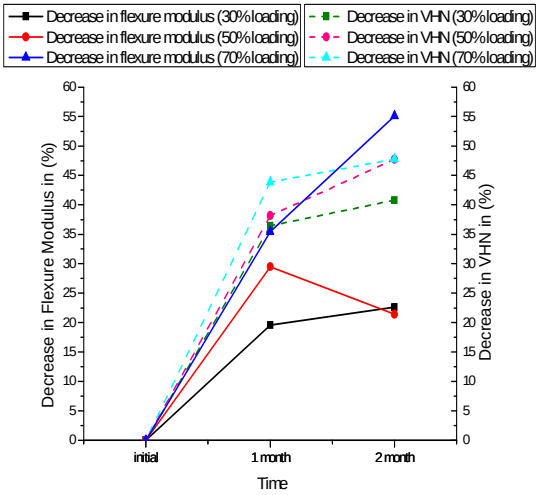

Fig.5.109 Relation of percentage decrease in VHN and percentage decrease in Flexure Modulus

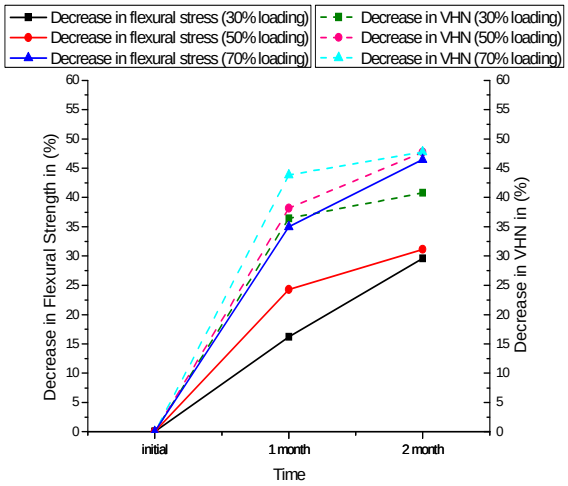

Fig.5.110 Relation of percentage decrease in VHN and percentage decrease in Flexural Strength

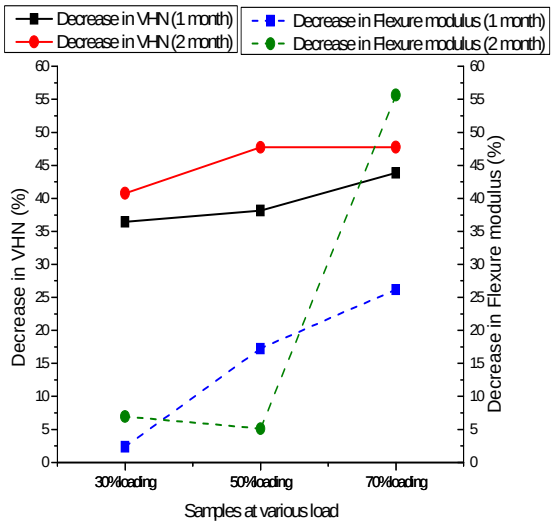

Fig.5.111 Relation of percentage decrease in VHN and percentage decrease in Flexure Modulus

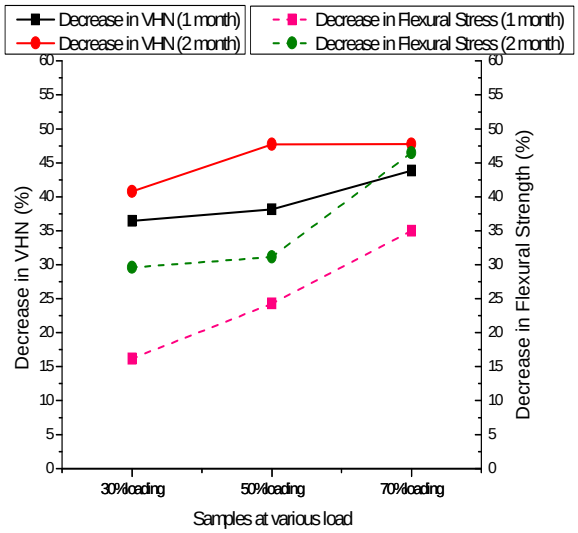

Fig.5.112 Relation of percentage decrease in VHN and percentage decrease in Flexural Strength

Figure 5.109 is showing relation of percentage decrease in micro hardess (VHN) and percentage decrease in flexure modulus of 16mm core thickness specimen after 1 month and 2 month for different loading specimen. It is obsreved from the graph that both are directly related with time. Decrease in micro hardness (VHN) leads to decrease in flexure moduls.
Figure 5.111 and 5.112 show relation of decrease in VHN and decrease in flexural strength after 1 month and two month for different loading. Graphs are showing that both micro

hardness (VHN) and flexural strength is decreasing with time and also with increase in bending pre-load percentage.

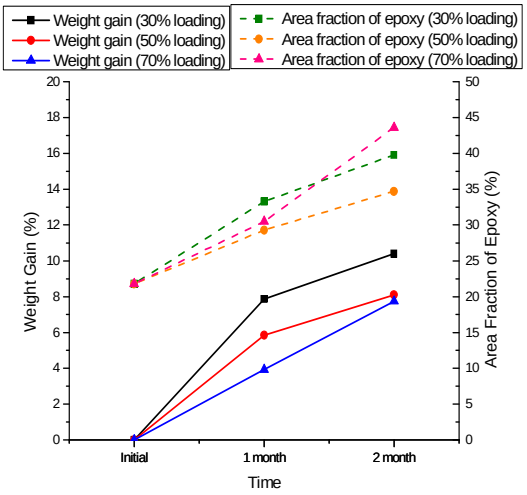

Fig.5.113 Relation of area fraction of epoxy and percentage weight with time

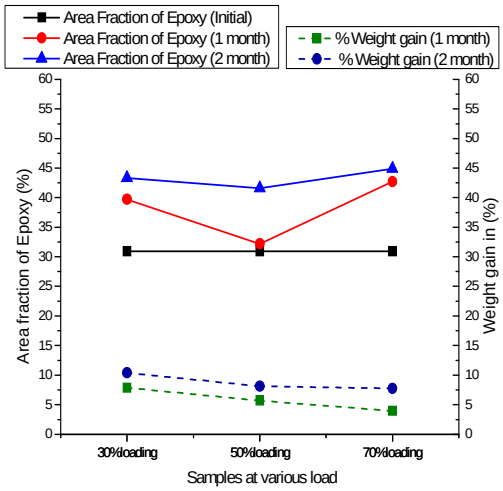

Fig.5.114 Relation of area fraction of epoxy and percentage weight with laoding

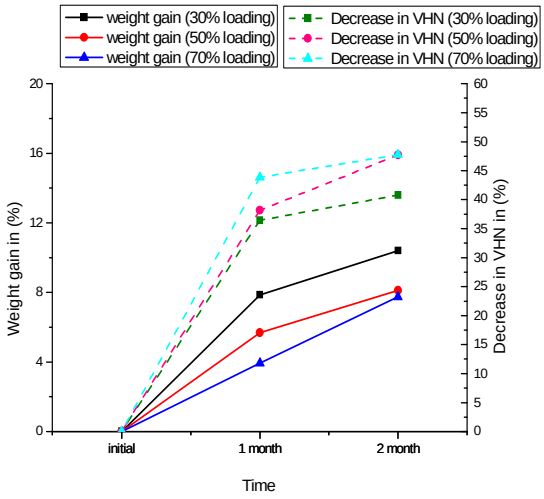

Fig.5.115 Relation of percentage decrease in VHN and percentage weight gain with time

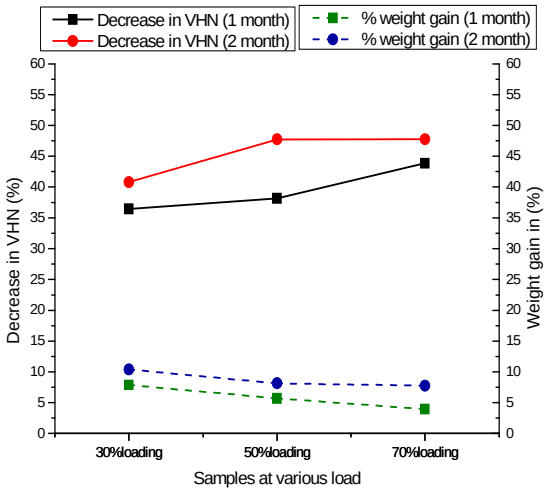

Fig.5.116 Relation of percentage decrease in VHN and percentage weight gain with loading

Figure 5.113 and 5.114 shows relation of area fraction of epoxy and weight gain after 1 month and 2 month and for different bending pre-load. Graph shows that with time both area fraction of epoxy and weight gain increases for each specimen. Area fraction of epoxy in 2 month for every percent bending pre-load is more than 1 month. This may be due to swelling of epoxy.

Figure 5.115 and 5.116 is showing relation of percentage decrease in micro hardness (VHN) and percentage weight gain for each specimen subjected to bending pre-load of 16mm core thickness after 1 month and 2 month. Graphs show that for every percentage of bending pre-load specimen, percentage weight gain increases with time whereas micro hardness (VHN) decreases.

CHAPTER 6 CONCLUSION AND SCOPE OF FUTURE WORK

6.1 CONCLUSION:

From the experiment conducted following conclusion have been obtained:

1) The decrease in flexural strength was considerably large (about 15.9 % in 8 mm core and 34.9 % in 16 mm core after 1 month and about 30 % in 8 mm core thickness specimen and about 46.49 % in 16 mm core thickness specimen after 2 month) in the almost all the specimen immersed in water tank at 45°C as compared to the initial unexposed specimen's flexural strength. This reduction trend was on higher side in specimen subjected to bending pre-loads at 50 % and 70 % of Ultimate Flexural Load. Decrease in flexural strength in the specimen immersed in the water tank (at room temperature) in both the month was less than the specimen immersed in the water tank (at 45°C). The SEM images also show some damage to fibre in specimen immersed in water at 45°C.
The decrease in flexure modulus was considerably high in both the core thicknesse with in one month only in almost all the specimen as compared to inital (before exposure) specimen. Difference in flexure modulus between first and second month specimen was comparatively less. The decrease in flexure modulus was more in 16 mm core thickness specimen as compared to 8mm core thickness specimen after one month but decrease in flexure modulus in 8mm core thickness specimen was more than 16mm core thickness specimen after 2 month. Average decrease flexure modulus in 16mm core thickness in first month was 28.21 % and in second month was 33.49 % whereas in 8mm core thickness specimen average decrease in flexure modulus in first month was 16.4 % and in second month was 46.49 %. Decrease in flexure modulus in both the water tanks (at 45°C and at room temperature) in both the month was almost same.

2) The percentage weight gain showed an increasing trend with time as expected in both core thickness specimen. The percentage weight gain in 16mm core thicknesses specimen was slightly higher than 8mm core thickness specimen. Percentage weight gain in GFRP sandwich structure subjected 30 % of ultimate flexure load specimen was higher as compared specimen subjected to 50 % and 70 % of ultimate flexure load in both core thickness.

3) Micro hardness values (VHN) were constantly decreasing with time for both core thickness specimen. Upto 20 days the decrease in micro hardness (VHN) was comparatively more. There was slight change in micro hardness (VHN) in 16mm core thickness specimen after 30 days with some exceptions whereas change in micro hardness (VHN) in 8mm core thickness after 30 days was less. Change in micro hardness (VHN) in different specimen subjected to flexure pre-loads was very less with respect to time. These were almost similar

4) Apparent moisture diffusivity was decreasing with time in both the core thickness (8mm and 16mm) specimen. Slope of change in moisture diffusivity was almost constant after 30 days in both core thickness specimen. Decrease in moisture diffusivity was relatively high during 3 to 6 days. For each specimen subjected to flexure pre-load apparent moisture diffusivity of 16mm core thickness specimen was larger as compared to 8mm core thickness specimen.

5) The area fraction of the fibre and epoxy were analysed using image analysis. The results show an increase in area fraction of the epoxy. Increase in area fraction of epoxy was more in second month when compared to first month for all specimen subjected to bending pre-load. Similarly the result of fibre area fraction shows a decreasing trend with time with marked decrease in second month as compared to one month in all specimen. All specimen loaded at different value show the same trend of decrease in fibre area fraction and increase in epoxy area fraction. This indicates that epoxy was expanding covering more area with fibre degradation and pullout leading to decrease in fibre in same area. Fibre area fraction of 8mm core thickness specimen was slightly higher as compared to 16mm core thickness specimen.

6) The slight change in circularity was observed in the fibre after two months which was easily noticed in SEM image of specimen. There was slight change in circularity of fibres after one month in both the core thickness specimen. Change in circularity of fibres was slightly higher in 16mm core thickness samples after two month as compared to 8mm core thickness samples. There is not much effect of bending pre-load on circularity of fibre.

7) Relation between macroscopic and microscopic behaviour was observed. It was observed that with increase in percentage weight gain, micro hardness (VHN) of all specimen decreases. It was also observed that with time the percentage area fraction of fibre decreases which leads to decrease in flexural strength and flexure modulus of both core thickness specimen. As percentage weight gain increases there was increase in percentage area fraction of epoxy with time and small change in circularity also identified for both the core thickness specimen.

6.2 SCOPE OF FUTURE WORK:

1) The sandwich structure with different types of core for example honeycomb and PVC foam with different thicknesses can be studied at different environmental conditions.

2) The duration of current experiment can be increased to see the effect in long term environment.

3) Alkaline aqueous solution can be taken in spite of water environment for study.

4) The experimental results of sandwich structure can be validated by using modelling and analysis.

5) The effect of hygrothermal (temperature and water) environment on sandwich structure specimen with a crack present can also be studied.

CHAPTER 7 REFERENCES

[1] www.whitebuffalobeadsandstones.com & www.ia.ucsb.ed

[2] www.wikipedia.com/Composite material.html

[3] www.structsource.com/pdf/composite.pdf

[4] www.emba.uvm.edu/iatridis/me257/Introduction.html

[5] www.engr.sjsu.edu/sgleixner/PRIME/FRP.pdf

[6] www.autospeed.com/composites.html/complete guide

[7] www.wickipedia.com/frp/category

[8] www.bikudo.com/images/glass fibre

[9] www.bowers-wilkins.cn/images/kelvar fibre

[10] www.eng.uab.edu/compositesLab/F_sandwch3.htm (University of Alabama)

[11] www.sciencedirect.com

[12] www.basf-cc.co.in

[13]www.engineer.tamuk.edu/departments/ieen/faculty/DrLPeel/Courses/Meen3344/Powerpoint_Files/ Chapter_16_avi.ppt.

[14] www.selecindia.com/products.php?category=30

[15]www.ab.com/industrialcontrols/products/relays_timers_and_temp_controllers/solid-state_relays.html

[16] American standard for testing materials (ASTM) C-393, ASTM- D790

[17] HexWeb Honeycomb Attributes and Properties.

[18] S. Heimbs, P. Middendorf, M. Maier- Honeycomb Sandwich Material Modelling for Dynamic Simulations of Aircraft Interior Components

[19] U.S. Department of Transportation Federal Aviation Administration - Damage tolerance of composite sandwich structure [2000] .

[20] www.asme.org- Modelling the Transport of Low-Molecular-Weight penetrates within Polymer Matrix Composites (David A. Bond, Paul A. Smith).

[21] www.catamarans.com/GFRP sandwich structure application

[22] http://en.wikipedia.org/wiki/Three_point_flexural_test#Testing_method

[23] A.Mukherjee, S.J. Arwikar- Performance of externally bonded GFRP sheets on concrete in tropical environments Part I: Structural scale tests (ACI Structural Journal) Title No. 102-S76 [2006].

[24] A.Mukherjee, S.J. Arwikar- Performance of externally bonded GFRP sheets on concrete in tropical environments Part II: Micro structural tests (ACI Structural Journal) Title No. 102-S82 [2006].

[25] Abhijit Mukherjee and S. J. Arwikar-Performance of Glass Fibre-Reinforced Polymer Reinforcing Bars in Tropical Environments-Part I: Structural Scale Tests (Composite Structures 81 (2007) 21–32) [2007].

[26] Abhijit Mukherjee and S. J. Arwikar-Performance of Glass Fibre-Reinforced Polymer Reinforcing Bars in Tropical Environments-Part II: Micro structural Tests **(**Composite Structures 81 (2007) 33–40) [2007].

[27] A. Bezazi, A. El Mahi, J.-M. Berthelot and B. Bezzazi- Experimental analysis of behaviour and damage of sandwich composite materials in three-point bending Part 1-Static tests and stiffness degradation at failure studies Volume 39, Number 2 / March, 2007 pages 170-177 [2007].

[28] A. Bezazi, A. El Mahi, J.-M. Berthelot and B. Bezzazi- Experimental analysis of behaviour and damage of sandwich composite materials in three-point bending Part 2 Fatigue test results and damage mechanisms Volume 41, Number 3 / May, 2009 , pages 257-267 [2009].

[30] Asp, L. E. -The effects of moisture and temperature on the interlaminar delamination toughness of a carbon/ epoxy composite (Volume 24, Issues 2-4, February-April 2002, Pages 179-184) [1998].

[31] Akawut Siriruk, Y. Jack Weitsman and Dayakar Penumadu- Environmental effect on Polymeric foams and sandwich composites (Volume 69, Issue 6, May 2009, Pages 814-820) [2008].

[32] Akawut Siriruk, Y. Jack Weitsman and Dayakar Penumadu- Effect of sea environment on interfacial delamination behaviour of polymeric sandwich structures (Volume 69, Issue 6, May 2009, Pages 821-828) [2008].

[33] Amir Shahdin, Laurent Mezeix, Christophe Bouvet, Joseph Morlier ' and Yves Gourina- Fabrication and mechanical testing of glass fibre entangled sandwich beams: A comparison with honeycomb and foam sandwich beams, Volume 90, Issue 4, October 2009, Pages 404-412 [2009].

[34] A. R. Bezazi, A. El Mahi, J.M. Berthelot and B. Bezzazi- Flexural fatigue behaviour of cross-ply laminates, Volume 35, Number 2 , Pages 149-161 [2003].

[35] Baley, C., Davies, P., Grohens, Y., and Dolto, G. -Application of interlaminar tests to marine composites (Volume 11, Number 2 / March, 2004, pages 77-98) [2004].

[36] Benkhedda, A., Tounsi, A., and Adda bedia, E. A.-Effect of temperature and humidity on transient hygrothermal stresses during moisture desorption in laminated composite plates [2007].

[37] Botelho, E. C., Pardini, L. C., and Rezende, M. C. -Hygrothermal effects on the shear properties of carbon fibre/epoxy composites, Volume 41, Number 21 / November, 2006, pages 7111-7118 [2006].

[38] Craig A. Steeves and Norman A. Fleck- Collapse mechanisms of sandwich beams with composite faces and a foam core, loaded in three-point bending. Part II: experimental investigation and numerical modelling, Volume 46, Issue 4, April 2004, Pages 585-608 [2004]

[39] D. Bond, A. Nesbitt, E. Gardon -Effect of cure cycle heat transfer rates on the physical and mechanical properties of an epoxy matrix composite (Volume 67, Issue 9, July 2007, Pages 1892-1899) [2006].

[40] David R. Veazie, Kito R. Robinson and Kunigal Shivakumar- Effects of the marine environment on the interfacial fracture toughness of PVC core sandwich composites (Volume 35, Issues 6-8, September-December 2004, Pages 461-466) [2004].

[41] Egidio Rizzi, Enrico Papa and Alberto Corigliano- Mechanical behaviour of a syntactic foam: experiments and modelling, Volume 37, Issue 40, 4 October 2000, Pages 5773-5794 [2000].

[42] F. Aviles and M. Augilar-Montero- Mechanical degradation of foam-cored sandwich materials exposed to high temperature (Volume 92, Issue 1, January 2010, Pages 122-129) [2009].

[43] Fibre Reinforced Composites (Materials, manufacturing and design), third edition- by PK Mallick, Publisher- CRC Press.

[44] G. Caprino, P. Iaccarino , and A. Lamboglia- The effect of shear on the rigidity in three-point bending of unidirectional CFRP laminates made of T800H/3900-2 Volume 88, Issue 3, May 2009, Pages 360-366 [2008]

[45] Hyeung-Yun Kim and Woonbong Hwang- Effect of debonding on natural frequencies and frequency response functions of honeycomb sandwich beams, Volume 55, Issue 1, January 2002, Pages 51-62 [2001].

[46] Jilin Yu , Erheng Wang, Jianrong Li and Zhijun Zheng- Static and low-velocity impact behaviour of sandwich beams with closed-cell aluminium-foam core in three-point bending Volume 35, Issue 8, August 2008, Pages 885-894 [2008].

[47] J. S. Earl, J. M. Dulieu-Barton and R. A. Shenoi- Determination of hygrothermal ageing effects in sandwich construction joints using thermoelastic stress analysis (Volume 63, Issue 2, February 2003, Pages 211-223) [2002].

[48] M. Dawood, E. Taylor and S. Rizkalla- Two-way bending behavior of 3-D GFRP sandwich panels with through-thickness fibre insertions. (Volume 92, Issue 4, pages950-963) [2010]

[49] Pavankiran Vaddadi, Raman P. Singh, Journal of Composite Materials-Inverse analysis for transient moisture diffusion through fibre-reinforced composites (Volume 41, No. 3, pages 309-334) [2002].

[50] Pavankiran Vaddadi, Raman P. Singh-Transient hygrothermal stresses in fibre reinforced composites a heterogeneous characterization approach (Volume 34, No.8, pp. 719-730 [12 page(s) (article)] (22 ref.)) [2003].

[51] Pavankiran Vaddadi, Raman P. Singh - Interlaminar fatigue crack growth of cross-ply composites under thermal cycles (Volume 85, Issue 2, September 2008, Pages 175-187) [2007].

[52] V. Crupi and R. Montanini- Aluminium foam sandwiches collapse modes under static and dynamic three-point bending, Volume 34, Issue 3, March 2007, Pages 509-521 [2005].

[53] V.Alvarez & A.Vazquez -Effect of Hygrothermal History on Water and Mechanical Properties of Glass/Vinylester Composite [2005].

[54] W. Steven Johnson and C. Kyle Berkowitz- Fracture and Fatigue Tests and Analysis of composite Sandwich Structure, volume 39, No. 16, Pages 1417-1431 [2005].

[55] Ghorbel, I. and Valentin, D.-Hydrothermal Effects on the Physico-Chemical Properties of Pure and Glass-Fibre Reinforced Polyester and Vinylester Resins, Volume 14, Issue 4, Pages 324-334 [1993]